DESIGN OF POLARISATION CONVERTING METASURFACE

A Project report submitted in partial fulfilment of the requirements for

the award of the degree of

BACHELOR OF TECHNOLOGY

IN

ELECTRONICS AND COMMUNICATION ENGINEERING

Submitted by

K. JANANI (318126512143) K. ROHIT (318126512147)

D. ANIL (318126512132) M. CHAND (319126512L13)

Under the guidance of

Mr. Vijay Kumar Sahu **MTech (Ph.D.)**

(Assistant professor)

Dept. Of ECE

DEPARTMENT OF ELECTRONICS AND COMMUNICATION ENGINEERING

ANIL NEERUKONDA INSTITUTE OF TECHNOLOGY AND SCIENCES

(UGC AUTONOMOUS)

(Permanently Affiliated to AU, Approved by AICTE and Accredited by NBA & NAAC with 'A' Grade)

Sangivalasa, Bheemili Mandal, Visakhapatnam dist. A.P(2021-2022)

ANIL NEERUKONDA INSTITUTE OF TECHNOLOGY AND SCIENCES

(UGC AUTONOMOUS)

(Permanently Affiliated to AU, Approved by AICTE and Accredited by NBA & NAAC with 'A' Grade)

Sangivalasa, Bheemili Mandal, Visakhapatnam dist.(A.P)

PRAGNANAM BRAHMA

ANITS

CERTIFICATE

This is to certify that the project report entitled "**DESIGN OF POLARISATION CONVERTING METASURFACE**" submitted by in partial fulfilment of the requirements for the award of the degree of **Bachelor of Engineering, K.JANANI (318126512143), K.ROHIT (318126512147), D.ANIL (318126512132), M.CHAND (319126512L13)** in **Electronics and Communication Engineering** of Andhra University, Visakhapatnam is a record of bonafide work carried out under my guidance and supervision.

Project Guide

Mr. Vijay Kumar Sahu

Assistant Professor

Department of E.C. E

ANITS

Assistant Professor
Department of E.C.E.
Anil Neerukonda
Institute of Technology & Sciences
Sangivalasa, Visakhapatnam-531 162

Head of the Department

Dr. V. Rajyalakshmi

Professor and HOD

Department of E.C.E

ANITS

Head of the Department
Department of E C E
Anil Neerukonda Institute of Technology & Sciences
Sangivalasa-531 162

ACKNOWLEDGEMENT

We would like to express our deep gratitude to our project guide **Mr. Vijay Kumar Sahu,** Assistant Professor, Department of Electronics and Communication Engineering, ANITS, for his guidance with unsurpassed knowledge and immense encouragement. We are grateful to **Dr. V. Rajyalakshmi**, Head of the Department, Electronics and Communication Engineering, for providing us with the required facilities for the completion of the project work.

We are very much thankful to the **Principal and Management, ANITS, Sangivalasa,** for their encouragement and cooperation to carry out this work.

We express our thanks to all **teaching faculty** of Department of ECE, whose suggestions during reviews helped us in accomplishment of our project. We would like to thank **all non-teaching staff** of the Department of ECE, ANITS for providing great assistance in accomplishment of our project.

We would like to thank our parents, friends, and classmates for their encouragement throughout our project period. At last, but not the least, we thank everyone for supporting us directly or indirectly in completing this project successfully.

PROJECT STUDENTS

K. JANANI (318126512143)

K. ROHIT (318126512147)

D.ANIL (318126512132)

M.CHAND (319126512L13)

CONTENTS

ABSTRACT

In this paper, we propose, design of ultrathin and high-efficiency linear cross-polarization converter based on artificially engineered surfaces in the reflection mode. The converter is composed of single layer and double-layer periodic surface structures with orthogonal complementary slots. The top and bottom layers are printed on both sides of the Polytef substrate with a dielectric loss of 0.002 and εr 2.65. The proposed converter can transform the linearly polarized incident electromagnetic (EM) wave to a linearly cross-polarized one with near-unity efficiency in the reflection mode.

We explain the conversion mechanism based on numerical simulations and the broadband behaviour of FSS and the ground plane is better understood by looking at surface current patterns at resonant frequencies. Such ultrathin polarization converters can be used in wireless microwave communication, remote sensing, and EM imaging where linearly polarization diversity is needed.

LIST OF FIGURES

Page no

1.Antenna

2. Metamaterials

5 Double layer unit cell design

LIST OF TABLES

CHAPTER-1

ANTENNA

1.1 Introduction:

Communication has become the key to momentous changes in the organization of business and industries as they themselves adjust to the shift to an information economy. Information is indeed the lifeblood of modern economies and antennas provide mother earth a solution to a wireless communication system.

An antenna is a transducer designed to transmit or receive electromagnetic waves. In other words, antennas convert electromagnetic waves into electrical currents and vice versa. They are used with waves in the radio part of the electromagnetic spectrum, that is, radio waves, and are a necessary part of all radio equipment. Antennas have many uses: communication, radar, telemetry navigation, etc. The figure shows the output from a coherent source is directed out into free space using an antenna. The signal source is linked to the antenna by some kind of waveguide. The antenna acts as a sort of transformer. It takes the electromagnetic field pattern, moving along the guide and transforms it into some other pattern, which is radiated out into free space.

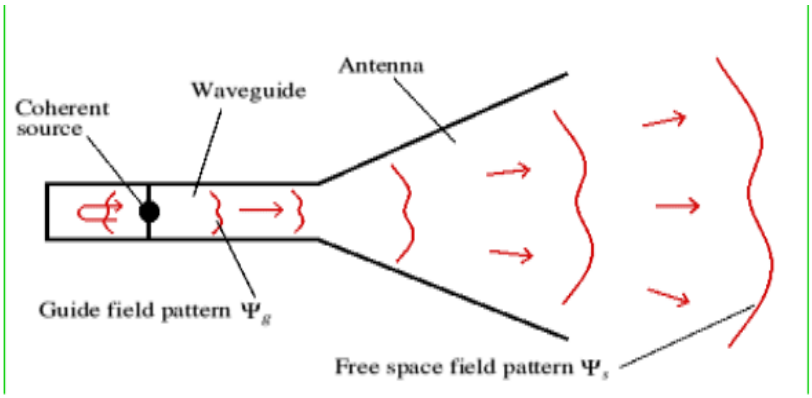

Fig 1.1 Schematic of an antenna system

Using this simple picture, we can establish two basic properties of any antenna

● An antenna itself does not generate any power. So, unless the antenna is imperfect and dissipates some power the total power carried by the guide and free space fields must be the same. Practically, all antennas tend to be slightly resistive. So, some power is normally lost, but for now, we can assume any loss is small enough to ignore.

● An antenna is a reciprocal device i.e.; it behaves in the same way irrespective of the way we pass signal power through it. This reciprocal behaviour is a useful feature of a coherent antenna. It means that in principle, the only difference between a transmitting and a receiving antenna is the direction we've chosen to pass signals through it.

1.2 Types of Antennas:

There are two fundamental types of antenna directional patterns, which with reference to a specific two-dimensional plane. They are:

1.Omni-directional (radiates equally in all directions), such as a vertical rod (in the horizontal plane)

2.Directional (radiates more in one direction than in the other) .

In colloquial usage "omnidirectional" usually refers to all horizontal directions with reception above and below the antenna being reduced in favour of better reception near the horizon. A directional antenna usually refers to one focusing a narrow beam in a single specific direction such as a telescope or satellite dish, or, at least, focusing in a sector such as a 120° horizontal fan pattern in the case of a panel antenna at a cell site. The present antenna in the thesis i.e. Microstrip antenna is an omnidirectional antenna which radiates normal to the patch surface into the upper hemisphere (180° in elevation plane) and 360 in the azimuth plane.

1.3 Basic Models of Antennas:

There are many variations of antennas. Below are a few basic models.

● The Isotropic radiator is a purely theoretical antenna that radiates equally in all directions. It is considered to be a point in space with no dimensions and no mass. This antenna cannot physically exist but is useful as a theoretical model for comparison with all other antennas.

Most antennas‟ gains are measured with reference to an isotropic radiator and are rated in dBs (decibels with respect to an isotropic radiator).

● The Dipole antenna is simply two wires pointed in opposite directions arranged either horizontally or vertically, with one end of each wire connected to the radio and the other end hanging free in space. Since this is the simplest practical antenna.

● The Yagi-Uda antenna is a directional variation of the dipole with parasitic elements added which are functionally similar to adding a reflector and lenses (directors) to focus a filament light bulb.

● The random wire antenna is simply a very long (at least one-quarter wavelength) wire with one end connected to the radio and the other in free space, arranged in any way most convenient for the space available. Folding will reduce effectiveness and make theoretical analysis extremely difficult.

● The Parabolic antenna consists of an active element at the focus of a parabolic reflector to reflect the waves into a plane wave. Like the horn, it is used for high gain, microwave applications, such as satellite dishes.

● The Patch antenna consists mainly of a square conductor mounted over a ground plane. Another example of a planar antenna is the tapered slot antenna (TSA), as the Vivaldi-antenna.

1.4 Basic Antenna Parameters:

1.4.1 Radiation Pattern:

An Antenna radiation pattern is defined as “a mathematical function or a graphical representation of the radiation properties of the antenna as a function of space coordinates. In most cases, the radiation pattern is determined in the far-field region and is represented as a function of directional coordinates. The figure shows a symmetrical three-dimensional polar pattern with a number of radiation lobes**.**

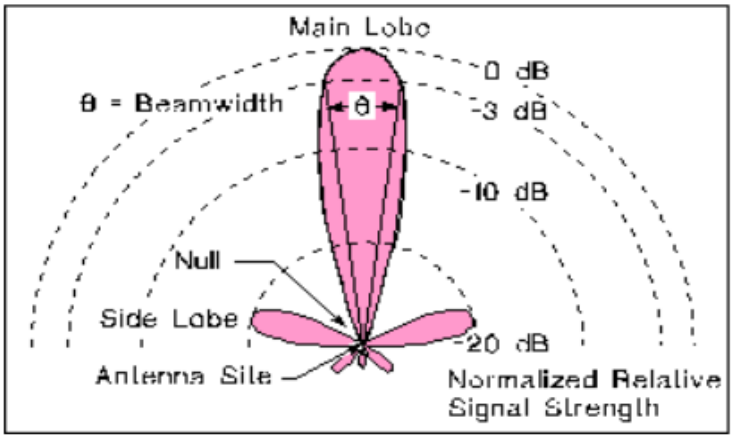

Fig1.2 Radiation lobes of an antenna pattern

1.4.2 Beam Width:

The beam width of a pattern is defined as the angular separation between two identical points on the opposite side of the pattern maximum. One of the most widely used beam widths is the Half-Power Beam width (HPBW). Another important Beam width is the angular separation between the first nulls of the pattern, and it is referred to as the First Null Beam width (FNBW). Both HPBW and FNBW are shown in below figure 1.3

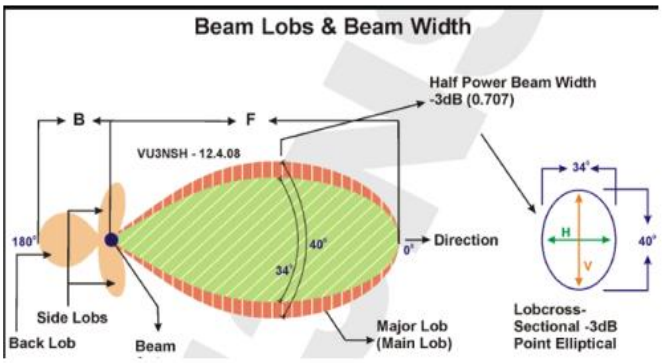

Fig 1.3 Beam width of an antenna

1.4.3 Directivity:

The directivity of an antenna is “the ratio of the radiation intensity in a given direction from the antenna to the radiation intensity averaged over all directions". The average radiation intensity is equal to the total power radiated by the antenna divided by 4 π.

1.4.4 Gain:

The gain of the antenna is closely related to the directivity, it is a measure that takes into account the efficiency of the antenna as well as its directional capabilities. A gain of an antenna is defined as “the ratio of intensity in a given direction to the radiation intensity that would be obtained if the power accepted by the antenna were radiated isotropically”. The radiation intensity corresponding to the isotopically radiated power is equal to the power accepted by the antenna divided by 4π.

1.4.5 Effective Length:

The effective length represents the antenna in its transmitting and receiving modes and it is particularly useful in relating the open-circuit voltage Voc of receiving antennas. This relation can be expressed as Voc= Ei x Le (1.3)

Where Voc=open-circuit voltage at antenna terminals,

Ei - incident electric field

Le = vector effective length

1.4.6 Antenna Equivalent Areas:

These equivalent areas are used to describe the power capturing characteristics of the antenna when a wave impinges on it. The different antenna equivalent areas are scattering area, loss area, capture area. The scattering area is defined as the equivalent area when multiplied by the incident power density is equal to the scattered or reradiated power. The loss area is defined as the equivalent area when multiplied by the incident power density leads to the power dissipated as heat through a load. The capture area is defined as the equivalent area when multiplied by the incident power density leads to the total captured, collected, or intercepted by the antenna. In general,

Capture area =effective area of scattering area + loss area

1.4.7 Antenna Efficiency:

The total efficiency E0 is used to take into account losses at the input terminals and within the structure of the antenna. Such losses may be due to reflections because of the mismatch

between the transmission line and the antenna and IR losses due to the conductors and dielectric. In general overall efficiency can be written as E0=Er. Ec. Ed

Where E0 = Total efficiency.

Er = Reflection efficiency.

Ec = Conduction efficiency.

Ed = Dielectric efficiency

1.4.8 Input impedance:

The input impedance of an antenna is impedance presented by an antenna at its terminals. The antenna impedance ZA can be expressed as,

$$ZA = RA + j\,XA$$

Where RA is the antenna resistance in ohms and XA is the antenna reactance in Ohms. The radiation Resistance is expressed as

$$RA = Rr + RL$$

Where Rr is the radiation resistance and RL is the loss resistance. The radiation resistance is associated with the radiation of real power. For a lossless antenna, the input resistance reduces the radiation resistance. The input impedance is also the ratio of the voltage to current at its terminal or the ratio of the appropriate electric and magnetic fields at a point.

1.4.9 Bandwidth:

The bandwidth of an antenna is that frequency range over which it will perform within certain specified limits. These limits are with respect to impedance match, gain, and radiation pattern characteristics. Typical specification limits are

● An impedance mismatch of less than 2:1 relative to some standard impedance such as 50 ohms

● A loss in gain or efficiency of no more than 3 db.

● A directivity pattern whose main beam is 13 dB greater than any of the side lobes, and a back lobe at least 15 dB below the main beam

● Bandwidth is measured by changing the frequency of a constant strength test n above and below centre frequency and measuring power output. The high and low frequencies, where power is one-half (-3 dB) of what it was at the centre, define the bandwidth. It is expressed as frequency (high minus low) or in percentage (high-low/centre*100%). The below figure 1.4 shows the typical bandwidth plot of the microstrip antenna.

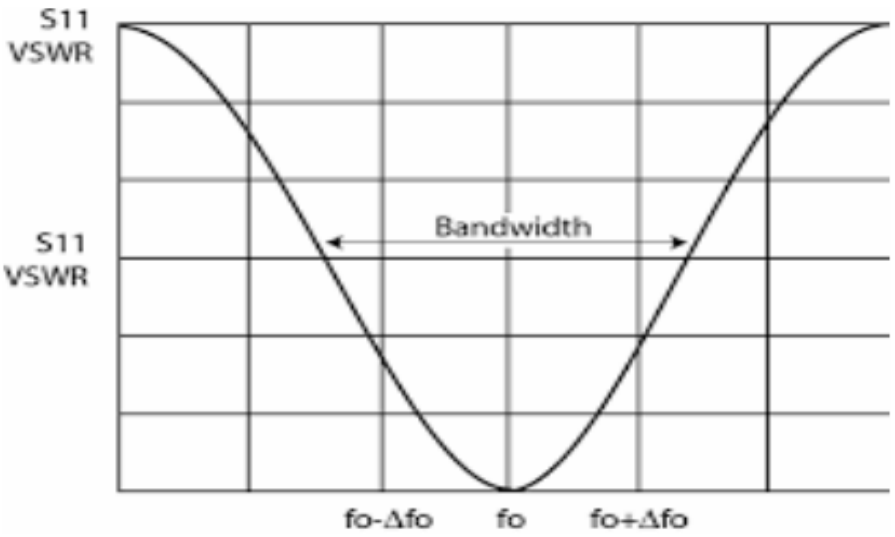

Fig 1.4 Bandwidth of the Antenna

1.4.10 Reflection coefficient and Return loss:

Reflection Coefficient shows what fraction of an incident signal is reflected when a source drives a load. A reflection coefficient magnitude of zero is a perfect match; a value of one is a perfect reflection. The symbol for the reflection coefficient is uppercase Greek Letter gamma(T) Note that the reflection coefficient is a vector, so it includes an angle. Unlike VSWR, the reflection coefficient can distinguish between short and open circuits. A short circuit has a value of -1(1 at an angle of 180 degrees), while an open circuit is one at an angle of 0 degrees. Quite often we refer to only the magnitude of the reflection coefficient.

Return Loss shows the level of the reflected signal with respect to the incident signal in dB. The negative sign is dropped from the return loss value, so a large value for return loss indicates a small reflected signal. The return loss of a load is merely the magnitude of the reflection coefficient expressed in decibels.

The correct equation for return loss is:

Return Loss=-20Log (┌) , where ┌ is reflection coefficient.

Thus in its correct form, return loss will usually be a positive number. If it's not, you can usually blame measurement error. The exception to the rule is something with negative resistance, which implies that it is an active device (external DC power is converted to RF) and it is potentially unstable it could oscillate).

1.4.11 Voltage Standing Wave Ratio (VSWR):

VSWR describes how much energy is reflected from the antenna because of impedance mismatching. A perfectly impedance matched antenna would have VSWR equal to one. Return loss (RL) is often used as it illustrates the gain reduction that would be introduced due to the mismatch of the antenna. VSWR is very important for wireless communications because the received signals from the satellites are usually very weak (on the order of -160 dB) and reflections are undesired on the transmission line connecting the antenna and the receiver. VSWR less than 2:1 (equivalent to a return loss of -9.5dB) is considered to be acceptable for most wireless applications because the time delay of any reflections is typically small, thus providing small amounts of error within the receiver. A lower VSWR may be required for particularly high-performance applications and unique installations

1.4.12 Polarization:

A radiated wave's polarization is determined by the direction of the lines of force making up the electric field. If the lines of electric force are at right angles to the Earth's surface, the wave is vertically polarized. If the lines of electric force are parallel to the Earth's surface, the wave is horizontally polarized as shown in below figure 1.5. When a single-wire antenna extracts (receives) energy from a passing radio wave, maximum pickup results if the antenna is oriented in the same direction as the electric field component.

A vertical antenna receives vertically polarized waves, and a horizontal antenna receives horizontally polarized waves. If the field rotates as the waves travel through space, both horizontal and vertical components of the field exist, and the wave is elliptically polarized. Generally, the antenna radiates an elliptical polarization, which is defined by three parameters: axial ratio, tilt angle, and sense of rotation. When the axial ratio is infinite or zero, the polarization becomes linear with the tilt agile defining the orientation. The quality of linear

polarization is usually indicated by the level of the cross-polarization. For the unity axial ratio, a perfect circular polarization results and the tilt angle is not applicable.

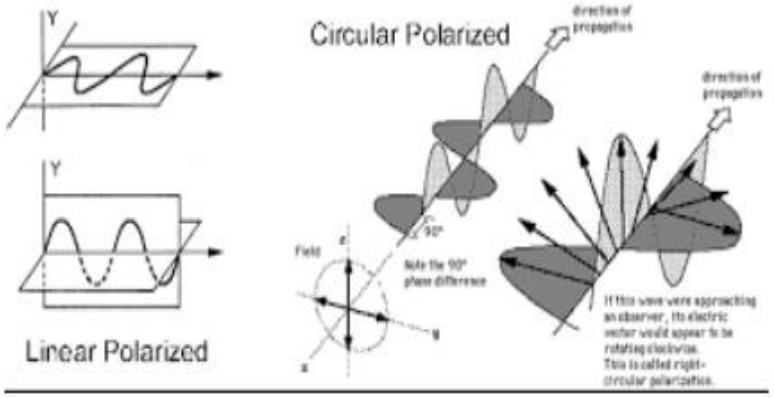

Fig 1.5 Linear and circular polarization of an Antenna

In general, the axial ratio is used to specify the quality of circularly polarized waves as shown. Antennas produce circularly polarized waves when two orthogonal field components with equal amplitude but in phase quadrature are radiated.

1.4.13 Axial ratio:

The Axial Ratio is the ratio of orthogonal components of an E-field. A circularly polarized field is made up of two orthogonal E-field components of equal amplitudes and 90 degrees out of phase). Because the components are equal magnitude, the Axial Ratio is 1 (or 0 dB).In order to check the polarization of the designed antenna, the axial ratio (AR) was calculated and analyzed. The axial ratio, as defined, is the ratio of the major axis to the minor axis of the tilted ellipse formed by the electric field of elliptically polarized waves.

1.5 EQUIVALENT DIAGRAM OF AN ANTENNA:

A transmission-line Thevenin equivalent of the antenna system is shown in figure Source is represented by an ideal generator, the transmission line is represented by a line with characteristics impedance Zs, and the antenna is represented by a load ZL where,

$$ZL=RL + j\ XL$$

The load resistance RL is used to represent the conduction and dielectric losses associated with antenna structure while Rr referred to as the radiation resistance, is used to represent radiation

by the antenna. The reactance XL is used to represent the imaginary part of the impedance associated with radiation by the antenna. Taking into account the internal impedance of the source and neglecting line and reflection (mismatch) losses, maximum power is delivered to the antenna under conjugate matching.

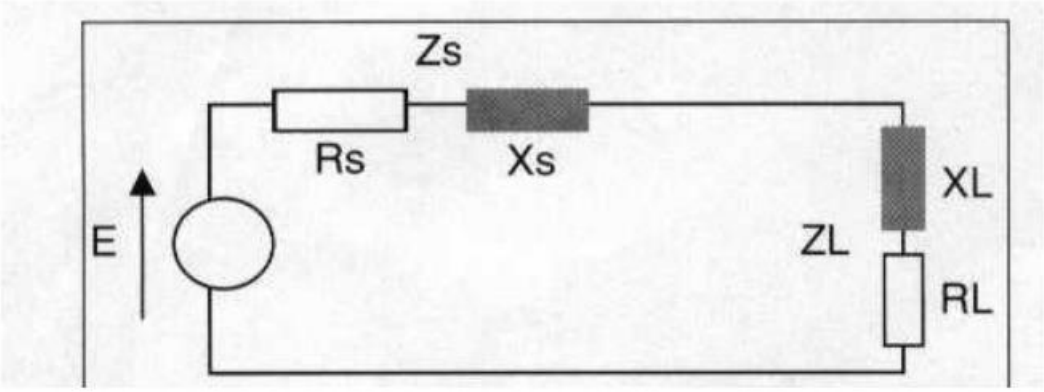

Fig 1.6 Equivalent diagram of an Antenna

CHAPTER 2

METAMATERIALS

Metamaterials are artificially engineered materials with exotic electromagnetic properties that do not commonly exist in natural materials. This chapter introduces the basic concept of metamaterials and their implementation in planar circuits. Their operation principle is explained from the circuit model prospective. The applications of the resonance-based metamaterial components in designing microwave filters and sensors are discussed. In addition, the miniaturised elements inspired by metamaterials are presented as alternative components in designing frequency selective surfaces.

2.1 INTRODUCTION:

Metamaterials are commonly considered as the homogeneous structures with exotic electromagnetic properties. A metamaterial is composed of resonant inclusions with sizes much smaller than the wave length λg. The average unit cell size of λg/4 required for homogeneity. In this condition, the structure shows a uniform electromagnetic behavior that is dependent on the unit cell properties and their near-field coupling behaviors. The electromagnetic properties refer to the relative permittivity relative permeability, and the refractive index. Therefore, according to the permittivity and permeability values, electromagnetic materials can be categorized in four domains demonstrated in Fig(a). Dielectric materials are all categorized as double positive (DPS) materials. Materials with negative permittivity can be found in nature including plasmas with low losses and metals at optical and infrared frequencies. Materials with negative permeability are less common in nature since the magnetic interactions in most materials are too weak. Magnetized ferrites in saturation can show negative magnetic permeability. Materials with simultaneously negative permittivity and permeability usually known as 'double negative materials' do not naturally exist. Despite that, the propagation of electromagnetic waves in a medium with simultaneously negative permittivity and permeability was theoretically studied. The first realization of this kind of medium was conducted in the early 2000s. Media with simultaneously negative permittivity and permeability are implemented using metallic inclusions with dimensions much smaller than the wavelength. Double negative materials exhibit interesting electromagnetic phenomena and add a new degrees of freedom for designing new devices with improved performances. Although initially, the term 'metamaterial' was used mostly for DNG structures, nowadays metamaterials

refer to any artificially engineered materials with subwavelength inclusions for manipulating electromagnetic waves

In this chapter, first the wave propagation in double negative materials is explained through electromagnetic theory. Then the realization of metamaterials in planar trans mission lines and circuits is explained with a focus on resonant structures. The application of the metamaterial-based resonant unit cells in the design of microwave filters and sensors are briefly discussed. Eventually, metamaterial-based miniaturized elements are introduced as an effective approach to designing frequency selective sur faces (PSS).

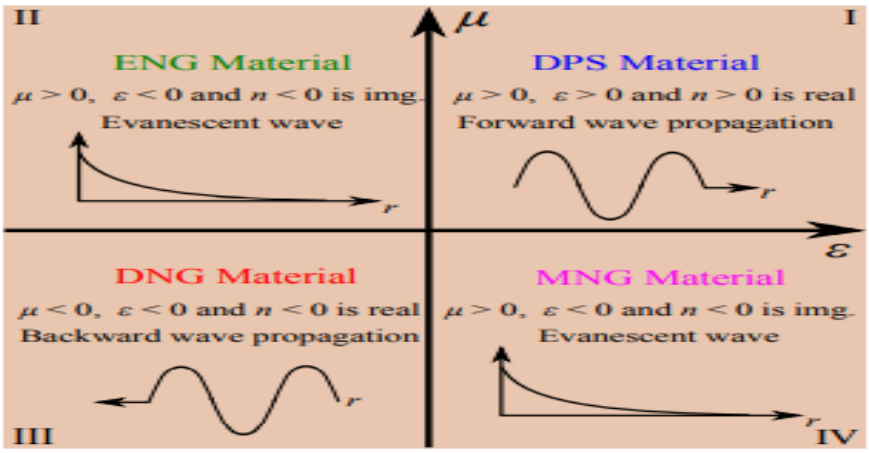

Fig 2.1 Classification of metamaterials

Material categories based on the permittivity and permeability. materials can be categorised in four major groups double positive materials (DPS), epsilon negative materials (ENG), mu negative materials (MNG), and double negative materials (DNG).

2.2 WAVE PROPAGATION IN DOUBLE NEGATIVE MATERIALS

To understand the electromagnetic wave propagation in a double negative medium, we should start with Maxwell's equations. By assuming a linear and isotropic medium, the Maxwell's equations in a source-free region can be written as

It can be inferred that if both e and μ are positive, the electric field vector E, the magnetic field vector H, and the wave vector k constitute a right-handed triplet. Conversely, if both e and μ are negative, the three vectors E, H, and k make a left-handed triplet. In addition, the power flow through the electromagnetic waves is related to the Pointing vector, which is defined as

$$S=E\times H^*$$

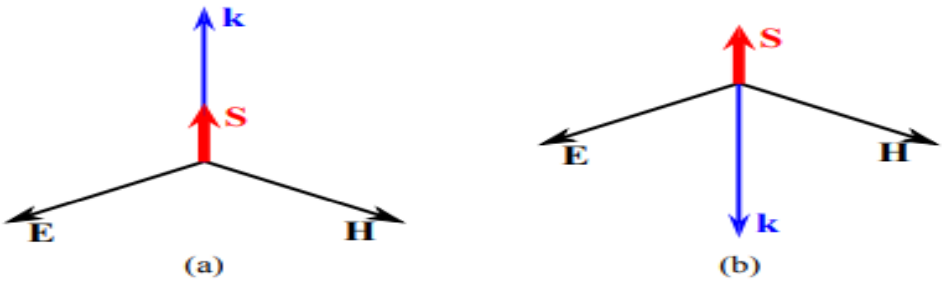

Fig 2.2

Wavevector and Pointing vector. Description of the electric field. magnetic field and wavevector triad obtained from Maxwells equations together with the Pointing vector obtained from the Pointing theorem. (a) Double positive medium and (b) Double negative medium.

This relation clearly demonstrates that the S, E, and H vectors will always make a right-handed triplet. So, in a double negative medium, the S and k vectors are in the opposite directions, whereas they are pointing to the same direction in a double positive medium. where the above Fig(a) demonstrates the double positive medium and Fig(b) describes the double negative medium.

The Pointing vector shows the direction of the energy propagation over the time, and so is parallel to the group velocity v. On the other hand, the wavevector k is in a same direction as the phase velocity. Therefore, in a double negative medium, the phase and group velocities are in the opposite directions. This type of wave propagation is known as backward wave propagation .

A homogeneous double negative medium by incorporating periodic tangement of sub wavelength split-ring resonators (SRRs) and wires . In order to achieve simultaneously negative permittivity and permeability, it should be excited with the electric field along the wire axis and the magnetic field perpendicular to the SRR plane. The solid line shows the transmitted power through the SRR array whereas the dashed line represents the power transmitted through the array of combined SRRs and wires. As seen, there is a band stop region for the SRR array.

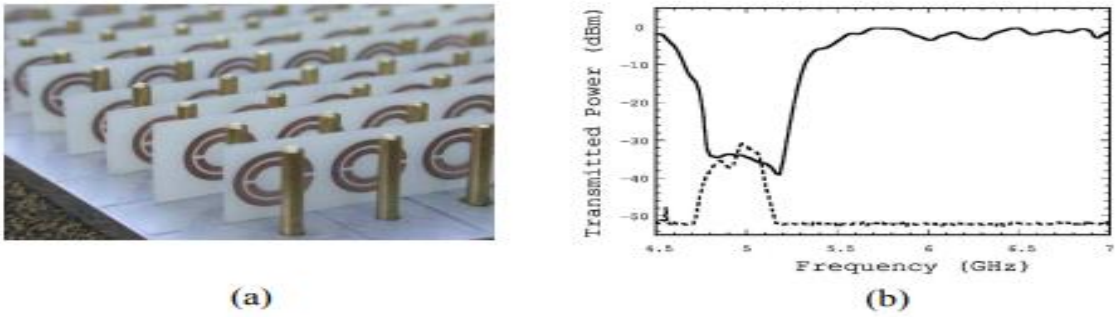

Fig 2.3 First implementation of double negative medium.

(a) First realisation of left-handed media by combination of SRRs. (b) Power transmission response of the structure, where solid line shows the response of SRR array and the dashed line for the composite array of SRRs and wires.

However, the dashed curve indicates a passband that is due to the double negative behaviour around these frequencies.

Soon after the first experimental demonstration of the double negative media, several new electromagnetic structures have been developed based on the same concept. In what follows, we will discuss the implementation of artificial transmission lines and then introduce some of their applications.

2.3 Metamaterials transmission lines

Soon after implementing a three-dimensional double negative medium, it has been realised that the transmission line implementation of left-handed media (LHM) is also possible. Here, we will discuss the theory of left-handed transmission line and their applications.

2.3.1 Purely left-handed transmission lines

The purely left-handed transmission line can be obtained by cascading the unit cell sections in the below Fig (a), which is obtained by interchanging the inductance and capacitance in the unit cell of the conversional right-handed transmission line unit cell

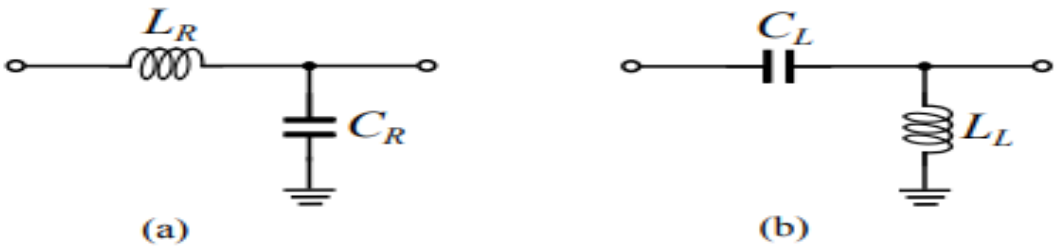

Fig 2.4 Unit cells of the purely right-handed and purely left-handed transmission lines. Lumped-element unit cell models of the (a) purely right-handed and (b) purely left-handed transmission lines.

In this figure, the subscription “R” stands for the right-handedness whereas "L" stands for the left-handedness. Based on Fig. 2.4, the propagation constant and the Bloch impedance of the right-handed transmission lines can be calculated as

$$\cos(\beta_R d) = 1 - \frac{L_R C_R}{2}\omega^2$$

$$Z_{BR} = \sqrt{\frac{L_R}{C_R}\left(1 - \frac{\omega^2}{\omega_{CR}^2}\right)}$$

where d is the unit cell length, and wcR = 2/LRCR is the angular cutoff frequency of the right-handed transmission line. In addition, the propagation constant and the Bloch impedance of the left-handed transmission line can be calculated as

$$\cos(\beta_L d) = 1 - \frac{1}{2L_L C_L \omega^2}$$

$$Z_{BL} = \sqrt{\frac{L_L}{C_L}\left(1 - \frac{\omega_{cL}^2}{\omega^2}\right)}$$

where wc = 2/√L₁C₁ is the dutoff angular frequency of the left-handed transmission line. In order to have a better insight, the propagation constant and the blotch impedances have been simulated and plotted against the frequency for a right-handed transmission line with LR = 2 nH and CR 0.5 pF and a left-handed transmission line with LL = 0.5 NH and C₁ = 0.5 pF. Fig. 2.5 presents the plots for right-handed transmission lines, whereas the propagation constant and Bloch impedance for the left-handed transmission lines are demonstrated

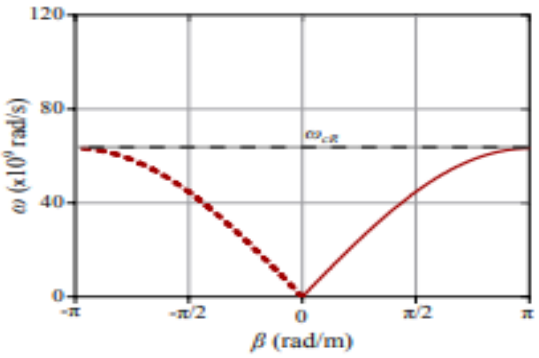

Propagation constant of a right-handed transmission line.

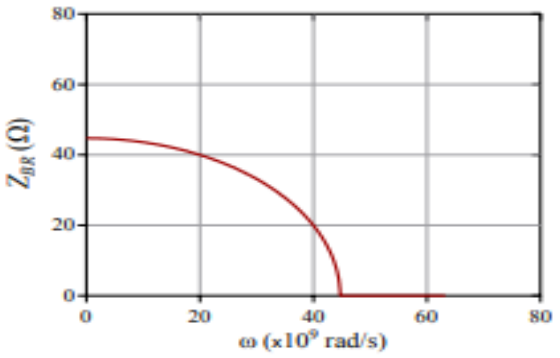

Bloch impedance of a right-handed transmission line.

Fig 2.5 Propagation constant and Bloch impedance of a right-handed transmission line

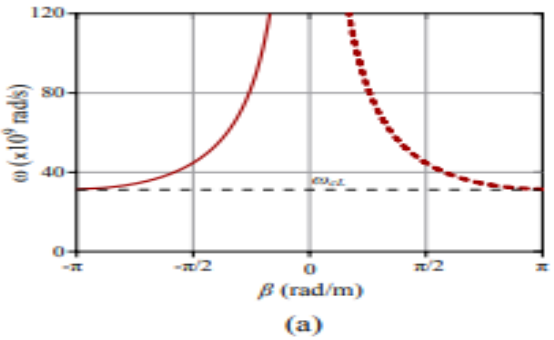

Propagation constant of a left-handed transmission line.

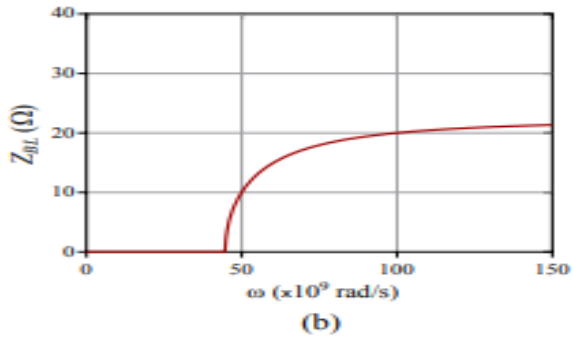

Bloch impedance of a left-handed transmission line.

Fig 2.6 Propagation constant and Bloch impedance of a left-handed transmission line.

Now, under long wavelength assumption of d << Ag, the above relations converge to homogeneous transmission line models. In this condition, the propagation constant and Bloch impedance of the right-handed transmission line can be expressed as

$$B_R = \omega\sqrt{L_R C_R}$$

$$Z_{BR} = \sqrt{\frac{L_R}{C_R}}$$

This results in parallel phase and group velocities for the right-handed transmission lines as

$$v_{pR} = v_{gR} = \frac{1}{\sqrt{L_R C_R}}$$

Under homogeneous assumption the propagation constant and block impedance of the left handed transmission lines can be expressed as

$$\beta_L = \frac{1}{\omega_I \sqrt{L_L C_L}}$$

$$Z_{BL} = \sqrt{\frac{L_L}{C_L}}$$

That results is anti parallel phase and group velocities as follows

$$-v_{pL} = v_{gL} = \omega^2 \sqrt{L_L C_L}$$

This can be also inferred from the dispersion diagrams of the right and left-handed transmission lines in fig 2.5(a) and fig(2.6) . In these , the solid line represents the waves propagating in positive direction and the dashed line represents the wave propagating in negative direction. However, by considering just one of them and choosing appropriate coordinates, only the positive group velocity (solid line) is acceptable according to causality .So, based on these figures, both ß and up are positive for the right-handed transmission, while they are negative in the left-handed case.

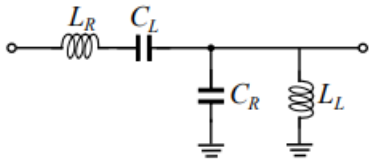

Fig 2.7 Composite left/ right handed transmission line. Lumped element model of composite left/ right transmission line unit cell.

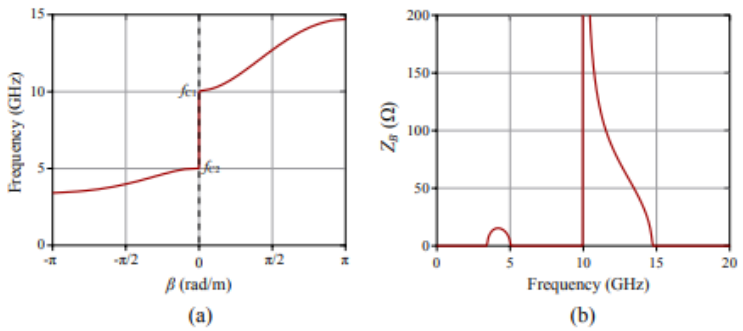

Fig 2.8 Propagation constant and block impedance of a typical composite right /left-handed transmission line (a)propagation constant of a right /left-handed transmission line (b)block impedance of a right /left-handed transmission line.

2.3.2 Composite right/left-handed transmission lines

Purely left-handed transmission lines are not practically implementable because of the inherent parasitic series inductance and parallel capacitances. These parasitic elements cause a composite left/right-handed behaviour in practical implementations. Thus, the practical artificially implemented metamaterial transmission lines are called composite left/right-handed transmission lines .LR and CR represent the parasitic inductance and capacitance of the host line respectively. In order to have a better insight about the operation principle of the CRLH TLs, the propagation constant and the Bloch impedance of a typical CRLH TL with the element values of LR 2 nH, CR = 0.5 pF, L_2 = 0.5 nH, and C_1 = 0.5 pF are simulated and plotted in Fig. 2.8. As seen, the transmission line shows two passbands with a stopband in between. In the lower passband the effects of L_1 and C, are dominant so, the trans mission line shows a left-handness behaviour. Conversely, in the higher passband, LR and CR are dominant and the transmission line shows a right-handness behaviour. In the stopband between the two passband regions, the transmission line acts as a single negative media, so it inhibits the wave propagation.The edge frequencies of the stopbad and obtained as

$$f_{c1} = \max\left(\frac{1}{2\pi\sqrt{L_R C_L}}, \frac{1}{2\pi\sqrt{L_L C_R}}\right)$$

$$fC_2 = \min\left(\frac{1}{2\pi\sqrt{L_R C_L}}, \frac{1}{2\pi\sqrt{L_L C_R}}\right)$$

The dual passband characteristics of this kind transmission lines can be incorporated in designing dual band circuits and components. In special case the stopband region will be vanished when

$$L_R C_L = L_L C_R$$

This kind of transmission line is known as balanced CRLH TL that exhibits a continuous transition between the left-handed and right-handed regions. The dispersion diagram and the Bloch impedance of a typical balanced CRLH TL with the unit cell parameters of LR = 2 nH, CR = 2 nH, LL = 0.5 nH, and CL 0.5 pF are simulated = and plotted in Fig. 2.9. As demonstrated in Fig. 2.9(a), there is continuous transition from left-hand to right-hand propagation. This property makes these transmission lines suitable for designing wide-band components

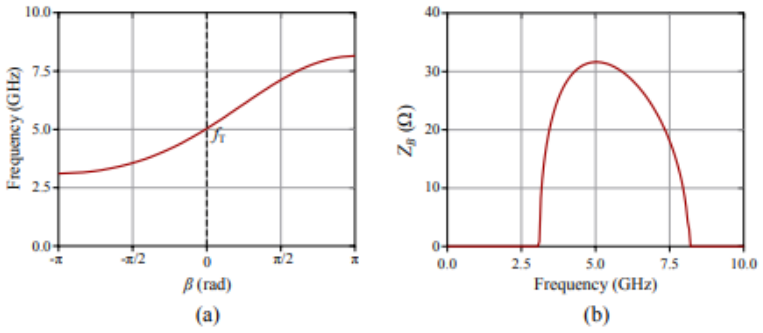

Fig (2.9)Propagation constant and block impedance of a balanced composite right/left handed transmission line. (a)Propagation constant of a balanced transmission line (b) bloch impedance of balanced transmission line

2.4 Implementation of the CLRH TLs

The CRLH TLs discussed in Section 2.3 can He implemented in different ways in various transmission line technologies. However, generally we can divide them into two major categories as: (i) LC-loaded lines. (ii) resonator loaded lines. In the following, we will briefly discuss both of the methods.

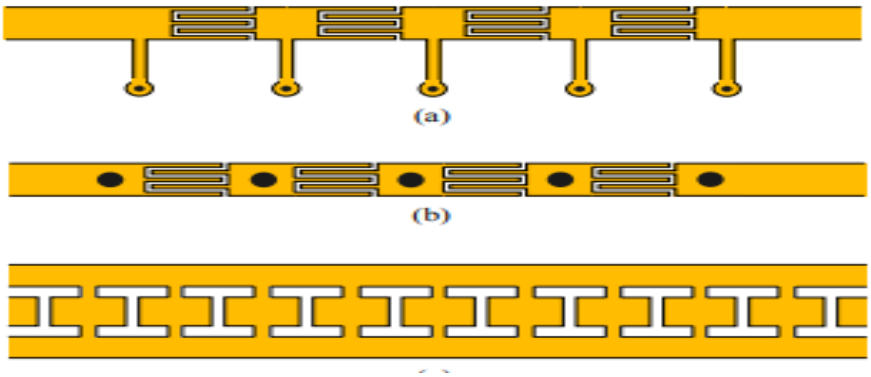

Fig 2.10 Implementation of LC-loaded CRLH TLs. (a) Implementation in microstrip line technology with series capacitive gaps and parallel short ended inductive stubs. (b) Implementation in microstrip line with via holes as parallel inductive paths to the ground. (c) Realisation in coplanar waveguide technology with series capacitive gaps and inductive paths to the ground. The metallisation is shown with yellow and via holes are indicated as black dots.

2.4.1 LC loaded lines

In this method, a conversional transmission line is periodically loaded with series capacitors and parallel inductors. These elements can be added by using discrete lumped components They can be embedded in the host transmission lines by using series capacitive gaps and parallel inductive stubs. In a CRLH TL is implemented in microstrip technology by adding inter-digital series capacitive gaps for providing series capacitance and short-ended parallel stubs for realising parallel inductances. indicates another possible implementation in microstrip technology, where the parallel inductance in implemented by making via holes to the ground plane. This approach can be used in coplanar technology as well by introducing series capacitive gapes to the signal strip line and parallel inductive paths connecting the signal strip to the ground metallisation on the two sides.

2..4.2 Resonator loaded lines

The resonant type metamaterial transmission lines can be designed by periodically loading a host transmission lines with sub-wavelength resonators. Different kinds of resonators can be used as the loading elements on the transmission lines. Among all, the split-ring resonators SRR and its complementary structure known complementary split-ring resonator CSRR are very common due to their compact size. A basic structure of a SRR together with its equivalent

circuit model is demonstrated in fig 2.11. In this figure, Co=2πtroCpul represents the total capacitance between the rings, where Cpul is the per unit length capacitance between the ring. The inductance Le can be approximated by a single ring with the average radius of ro and the ring width of t . Therefore, the resonance frequency of a SRR can be calculated as fo = 1/(2√/LsCo/4). The SRR can be excited through an axial magnetic field in the z direction. It can also be driven through an electric field along the x axis. If the effects of metal and substrate thicknesses and also the losses are neglected, an exact dual complementary behaviour can be expected from the CSRR . The circuit model of the CSRR can be deducted from the SRR circuit model, where the Ls in SRR is replaced by the capacitance Cc of a circular disc with an average radius of ro-1/2 that is surrounded by the ground plane at a distance off from its edge. On the other hand, the two Co/2 capacitances are replaced with two parallel Lo/2 inductances each representing the inductive behaviour of the metallic traces that connect the inner disc to the ground plane. The resonance frequency of a CSRR can be obtained as 1/(2√/CcLo/4). The resonance frequency of a CSRR can be obtained as 1/(2√CcLo74) and the CSRR can be excited through an axial electric field in the z direction or through a magnetic field in the y direction (Baena et al. 2005). These resonators have been widely used for designing artificial transmission lines in planar technologies. In the following, we will review some of these artificial structures.

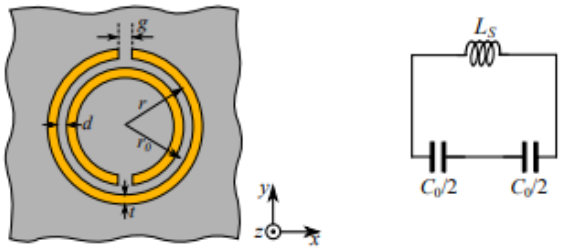

Fig 2.11 Split ring resonator (SRR).A typical topology of complementary split ring resonator (CSRR)and its equivalent circuit model. Metallisation is shown in yellow.

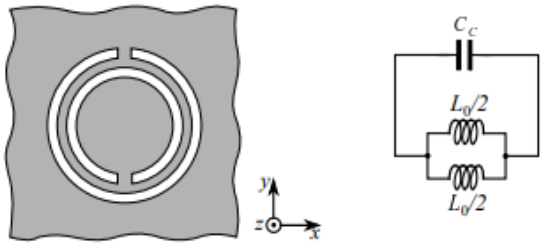

Fig 2.12 Complementary split ring resonator(SRR).A typical topology of complementary split ring resonator (CSRR)and its equivalent circuit mode .Metallisation is shown in grey.

First, we consider the structures in coplanar waveguide technology. shows a coplanar waveguide with split-ring resonators (SRRs) aligned with the slots and patterned on the back side of the substrate. In this condition, the SRRS will be excited by the magnetic fields generated by the signal strip and produce a band stop in the transmission response in the vicinity of their resonance frequency. The band stop is mainly associated with the negative permeability of the structure around the resonance of SRRs that make a single negative medium. Now, by adding parallel strips connecting the coplanar waveguide to the ground metallisation on the sides, a double negative propagation medium will be obtained that shows a bandpass behaviour in vicinity of the SRRS resonance frequency. This coplanar CLRH TLs in demonstrated2.14. The SRR-based artificial transmission lines can also be implemented in microstrip technology. Fig 2.15 shows a single negative transmission line with negative permeability around the SRRs resonance frequency. This provides a bandgap in the spectral response of the transmission line. This bandgap is depicted in the transmission response.

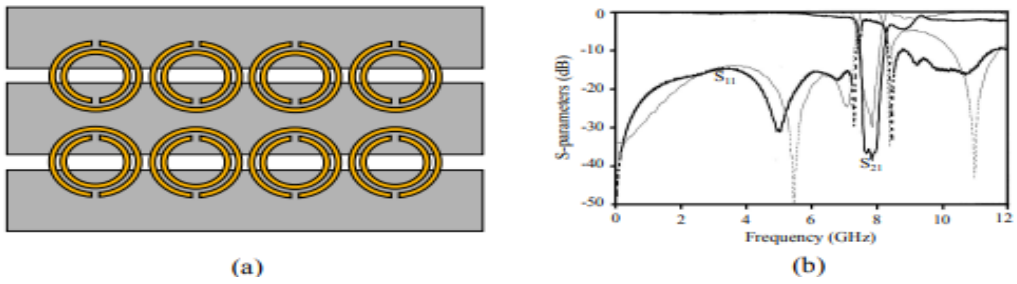

Fig 2.13 SSR based transmission line in coplanar technology (a) Layout of a typical metamaterial transmission line in coplanar waveguide technology. (b)Measured and simulated S parameters of the structure. The split ring metallization is shown in yellow and the waveguide metallization is grey.

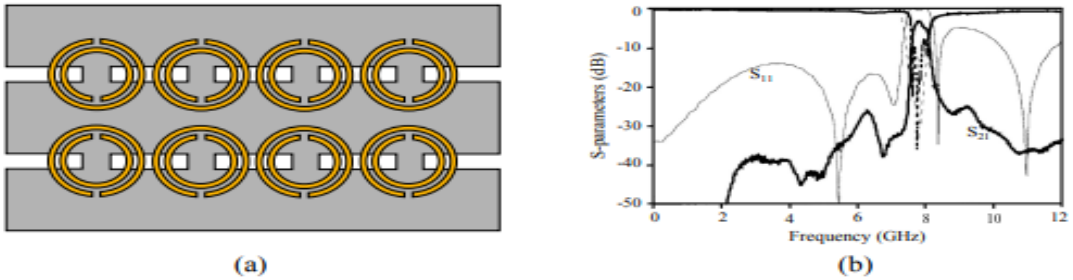

Fig 2.14 CRLH TLs in coplanar waveguide technology. (a) Layout of a typical CRLH TL in coplanar waveguide technology. (b) Measured and simulated S-parameters of the structure. The split-ring metallisation is shown in yellow and the waveguide metallisation is grey.

of the device . Again the band stop frequency behaviour can be switched to bandpass by adding parallel inductive paths to the ground that produce negative permittivity. An implementation of this idea is presented in Fig. 2.16, where the metallic via holes connecting the microstrip to the ground plane provide the parallel inductive paths. A typical S-parameters of the SRR-based CRLH microstrip line is demonstrated in Fig. 2.16. As seen, the transmission line shows a passband in which it acts a left-handed wave propagation media

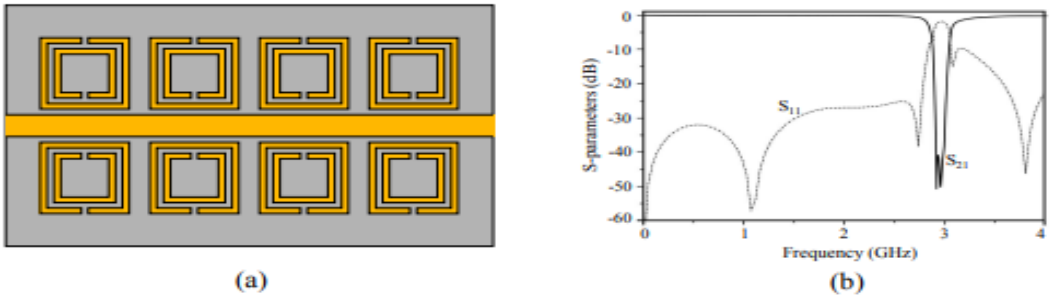

Fig 2.15 Artificial transmission line in microstrip technology. (a) Layout of à microstrip line loaded with SRRs on the sides. (b) Simulated S-parameters of the structure. The microstrip metallisation is shown in yellow.

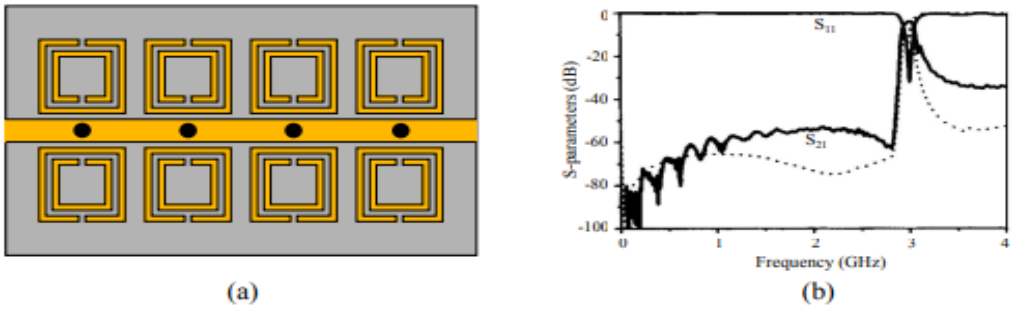

Fig 2.16 CRLH TL in microstrip technology. (a) Layout of a microstrip CREH TL (b) Simulated and measured S-parameters of the structure. The microstrip metallisation is shown in yellow and the via holes are shown as black circles.

The complementary split-ring resonators (CSRRS) can also be incorporated in design ing metamaterial transmission lines. The CSRRs should be etched out of the ground plane metallisation and can be excited by axial electric fields.

One possibility for designing CSRR-based artificial transmission line is by using the microstrip. A microstrip line loaded with CSRRS etched in the ground plane is demonstrated in Fig. 2.17. This transmission line acts as a one-dimensional effective propagation medium with negative permittivity. So, as shown in Fig. 2.17(b) it precludes the wave propagation in vicinity of the CSRRS resonance frequency.

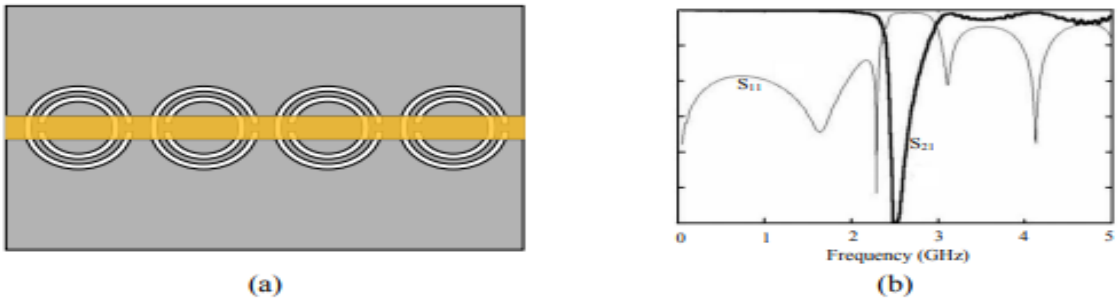

Fig 2.17 Artificial transmission line based on CSRRs. (a) Layout of a microstrip line loaded with CSRRs. (b) Measured S-parameters of the structure. The microstrip metallisation is shown with yellow and the ground plane metallisation is grey.

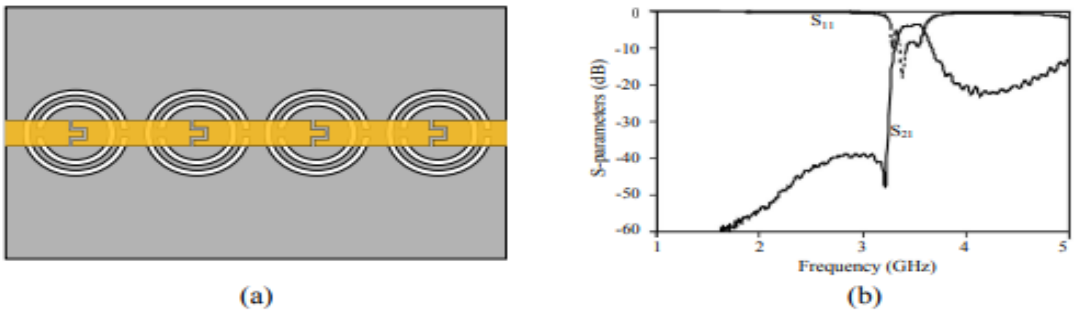

Fig 2.18 CSRR-based CRLH TL in microstrip technology. (a) Layout of a CSRR-based microstrip CRLH TL. (b) Measured S-parameters of the structure. The microstrip metallisation is shown with yellow and ground plane metallisation is grey.

order to obtain a left-handed CSRR-based transmission line, we should introduce effective negative permeability to the structure. This can be implemented by adding periodic capacitive

gaps to the conductive strip of the transmission line. These capacitive gaps will provide effective negative permeability in a specific frequency band. If this frequency band overlaps with the resonance frequency of CSRRS, a narrow left-handed transmission passband will be produced as demonstrated fig 2.18(b).

2.5 Applications of resonant type metamaterials in filter and sensor designs

In the design of resonator-loaded artificial transmission lines, the main goal was firstly to achieve a left-handed behaviour in a desired frequency band However, soon the sub-wavelength structure of the SRRs and CSRRS and their high quality factor resonances attracted RF designers to use them as building blocks in developing new circuits and devices. Two of these interesting applications are microwave filters and sensors that are the focus of this dissertation.

2.5.1 Application in microwave filters

Compact and high-performance filters compatible with integrated circuit technologies are of great interest in RF communication systems and portable devices. Key factors in the design planar microwave filters are high quality factor, and compact size. The SRRS and CSRRs opened the doors for developing new strategies of designing compact filters. In contrast to the conversional resonators used in filter designs such as parallel coupled lines, closed or open loop resonators, the SRRS provide much smaller sizes by the virtue of distributed capacitance between the two rings and the overall ring inductance. In addition, the negative image of SRR known as the CSRR offers much compacter size in comparison with conversional complementary, resonators. Many novel compact filter structures have been designed and implemented by different groups. To name just a few examples, the composite right/left-handed behaviour of unbalanced CSRR-loaded microstrip line has been used to design dual-band bandpass filter. The balanced CSRR-based CRLH TLs have been used for deign of ultra-wide-band bandpass filters. Compact differential filters with common-mode suppression are developed by combining SRRS and CSRRS. The effective size of the filters have been even decreased further by considering S-shaped SRRS and CSRRs . In this thesis, we have designed very compact bandpass and band stop filters by introducing metamaterial-based resonators with

dual-mode resonance behaviour. The dual-mode resonator acts as a doubly tuned resonant circuit element and the number of the resonator needed for a specific filter response is reduced by half resulting in more compact structure.

2.5.2 Application in microwave sensors

In addition to their potential applications in compact filters and circuit elements, the metamaterial-inspired resonators such as SRRS and CSRR can be used in the design of compact and high-resolution microwave sensors. In principle this is because of their high-quality factor resonance, their compact size, and the high-sensitivity of their resonance with respect to the geometrical parameters and surrounding constituting materials. Furthermore, it is demonstrated that the sensitivity of the conversional sensors can be improved by incorporating metamaterial-based resonators. Thus, the sensing applications of metamaterials have been a very active research area in recent years.

In this regard, of this thesis focus on the sensing applications of metamaterials. The metamaterial-inspired resonators are applied in the design of microwave microfluidic sensors explains a design of wide dynamic range metamaterial rotation sensor based on a pair of coupled meandered resonators.

2.6 Metamaterial inspired frequency selective surfaces

Frequency selective surfaces (PSS) are usually formed by two-dimensional periodic arrangement of metallic elements on a dielectric substrate. Based on the geometry and arrangement of the metallic unit cell, the array might show different functionalities such as bandpass or band stop spatial filter, absorber, reflect array, and etc. Important factors in evaluating the performance of PSS are their overall size, the sensitivity of their frequency response to the angle of the incident electromagnetic wave, the harmonic content of their frequency response, and their ability

to operate in close proximity to the radiation source. The FSS functionality is mainly determined by its unit cell geometry and dimension. In terms of the unit cell properties, the PSSS can be divided into two major subclasses as: (1) Traditional PSS based on resonant

element unit cells, (ii) miniaturised elements P56s based on non-resonant unit cells. In the following, we will briefly discuss the operation principles and the performance of each category.

2.6.1 Traditional FSS with resonant unit cell

The operation of this type FSS is based on resonant elements. The elements are excited through the electric or magnetic field of the radiated wave. The incident electromagnetic wave will induce electric current in metallic traces and electric field across the capacitive gaps in the array. The magnitude of the induced current and electric field depends on the level of coupling between the electromagnetic field and the unit cells. The maximum coupling occurs at the fundamental frequency, where the length of the unit cell is equal to A/2. So, the unit cells should be designed in a way that they resonate at the desired frequency of operation. Because of the fundamental dependence of the traditional FSSS on the unit cell length, the excitation of higher-order modes is unavoidable. As a result, the frequency response of these type of FSS usually includes several higher-order harmonic responses. This will not only degrade the out-of-band performance of the FSS, but affects the scan angle performance as well since some of the harmonic modes might be excited under oblique incidences.

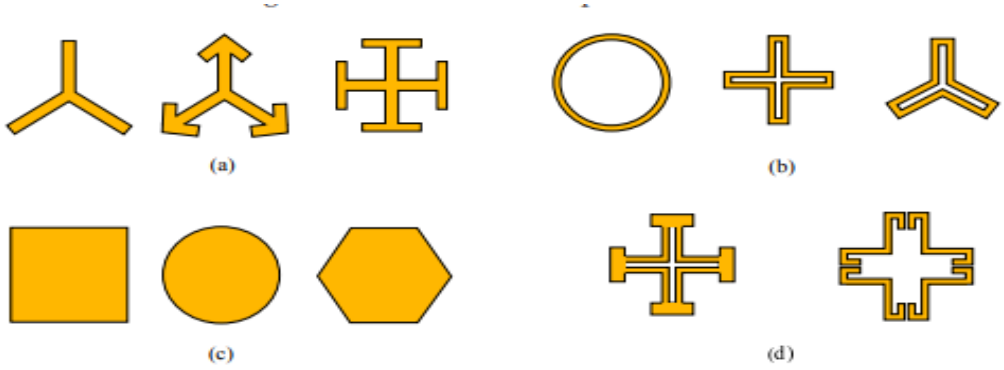

Fig 2.19 Typical FSS centre unit cell is categorized in four groups (a) centre connected N poles (b) loop type elements (c) Patch or plate type(d) combinations.

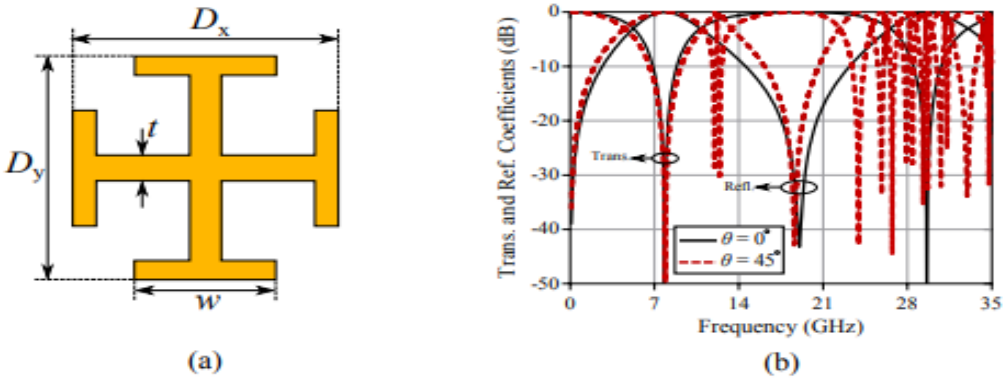

Fig 2.20 Frequency selective surfaces made of Jerusalem cross elements. (a) Jerusalem cross unit cell. (b) Simulated reflection and transmission coefficients under normal and oblique incidence angle of 45.

Some of the typical unit cell geometries that are commonly used in the design of conversional FSSS are demonstrated in Fig. 2.19. As an example of the resonant type FSSS, a structure made of Jerusalem cross unit cell has been simulated in CST microwave studio. Fig. 2.20(a) shows the considered Jerusalem cross unit cell together with its geometrical dimensions whereas the simulated transmission and reflection coefficients of the FSS are plotted in Fig. 2.20(b). As seen, the FSS shows a transmission null at the fundamental frequency of around 8 GHz with a harmonic response at 30 GHz under normal incidence. However, by changing the incidence angle to 45°, several higher or der harmonics are excited that deteriorate the frequency response. Another important issue in traditional FSSS is designing the FSSS with higher-order filtering responses. To this end, different layers of first-order FSS layer should be arranged with A/4 spacing. This results in bulky profiles that might not be desirable in many applications.

2.6.2 Miniaturized elements frequency selective surfaces (FSS)

In order to decrease the sensitivity of the FSS response to the oblique angles of the incident wave, the unit cell size should be miniaturised. This is especially important when the FSS is used in close proximity to the radiation source. In order t to address this issue, a new class of FSSS have been developed based on miniaturised elements. These types of FSSS operate based on a different principle that allows superior performance over the traditional structures. In this approach, instead of using fully resonant elements as the unit cell of the FSS, non-resonant unit cells with small dimensions are used. These miniaturised elements act as

lumped capacitors or inductors and are arranged in a way that they couple to the incident electromagnetic wave. In this way, the electrical size of the unit cells is decreased to less than A/4 and even in some cases smaller than A/10. They are also called metamaterial-inspired FSSs because of their extremely miniaturised unit cells.

The FSS is composed of metallic arrays printed on both sides of a thin dielectric spacer. The front layer is made of a large capacitive patch array whereas the back layer is an inductive wire grid. Since the FSS is made of miniaturised elements, its frequency response can be accurately modelled through a lumped element circuit model.

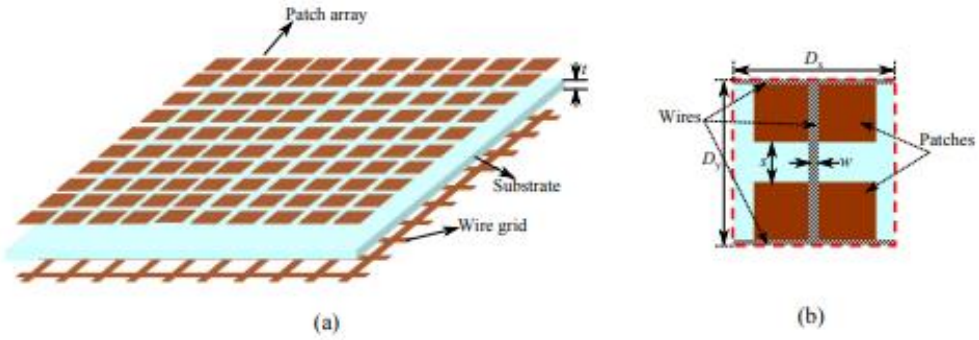

Fig 2.21 The first miniaturised elements FSS. (a) Three-dimensional view of the miniaturised elements FSS. (b) The unit cell of the structure.

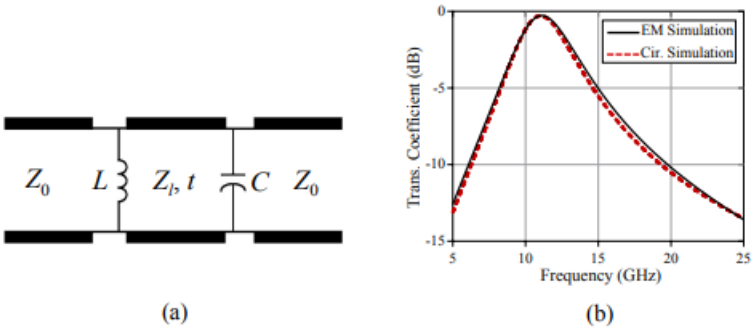

Fig 2.22 Lumped elements modelling of the miniaturised elements FSS. (a) Circuit model of the miniaturised elements FSS. (b) Comparison between the simulated transmission responses obtained from the EM and circuit model simulations. The circuit model parameters are: L = 1.08 nH. C = 0.15 pF. Z = 254 0,1=0.254 mm.

The circuit model of this FSS is given in , where the parallel capacitor mod els the capacitive patch array in the front layer and the L inductance stands for the wire grid in the back layer. The thin dielectric spacer is modelled with a short transmission line section with the characteristic impedance of $Z_1 = Zo/\sqrt{e}$, where Zo=3770 is the wave impedance in free space and e, is the relative permittivity of the dielectric spacer. A comparison between the simulated transmission coefficient of the FSS obtained from the circuit model simulations and the one from the full-wave EM simulations is presented. The FSS dimensions and the circuit model parameters are given in the captions of respectively. Fig. shows a good agree ment between the circuit model and full-wave EM simulation results over a wide frequency range. Fig. shows the scan angle performance of the FSS over wide range of 0°-60° for both of the TE and TM polarisations. As demonstrated, the FSS shows a reasonable stability of the transmission response for oblique incidence angles up to 45°

As mentioned before, an advantage of this type of FSS is that its frequency behaviour can be accurately modelled using lumped elements circuit model. So, FSSs with specified functionalities can be designed by the aid of standard circuit-based filter theory. This is a notable feature since the design and optimisation procedures can be significantly simplified by using circuit theory.

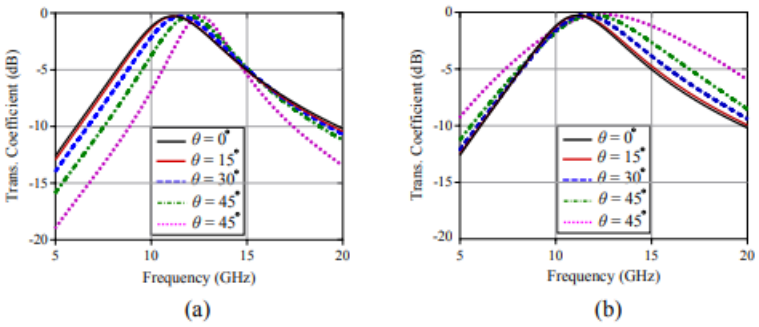

Fig 2.23 Scan angle performance of the miniaturised elements FSS. (a) Transmission responses for oblique incidences in the TE polarisation. (b) Transmission responses for oblique incidences in the TM polarisation.

After this first demonstration of the miniaturised elements FSS, several other FSSs with different improved functionalities have been designed and implemented.

CHAPTER 3

FREQUENCY SELECTIVE SURFACES

3.1 INTRODUCTION

The frequency selective surface (FSS) structure is an array of periodically arranged metallic patches on a dielectric substrate or slots in the metallic screen, which behaves as a spatial filter to the electromagnetic waves and offer selectivity in frequency, angle-of-incidence (AOI) and polarization of the incident waves. The FSS can be classified as high-pass, low-pass, bandpass and bandstop filter. These features make them suitable to control the propagation of electromagnetic energy and therefore, they can be employed in radomes, Cassegrain sub-reflector, diffraction gratings, frequency scanned antennas, microwave absorbers and recently in applications associated with security and efficiency of the wireless network communications. As, Sinclair has realized that the antennas placed on the aircraft provide significant scatterers, however, it is required to control the radar cross-section (RCS) of the antenna, which is significantly accomplished to an extent by using the FSS structure. The basic principle underlying the physics of FSS structure is directly been evolved from the investigation of diffraction gratings in optics, which is used to decompose a beam of non-monochromatic light into its spectral orders. However, the study of FSS structures and their interaction with electromagnetic waves received potential attention in the mid-1960s. In addition to this, there are many literatures, which had been reported from 1919 to the famous Marconi and Franklin reflector for use in wireless telegraphy and telephony. The patch- and slot-type FSS structures ideally exhibit total reflection and transmission, respectively, in the neighbourhood of the fundamental resonance frequency. The type of element geometry, size, inter-element spacing, dielectric substrate parameters and presence or absence of superstrate, which constitutes the unit-cell element, determines the overall resonance frequency, bandwidth and dependency on the AOI as well as polarization of the planar incoming wave. Therefore, in order to design a FSS structure for a desired frequency response, the appropriate selection of geometrical parameters is of prime importance because these parameters have potential to significantly vary the frequency response. The 2 unique characteristics and practical significances of FSS structures realized over many years have offered an extensivework both in academia and industrial

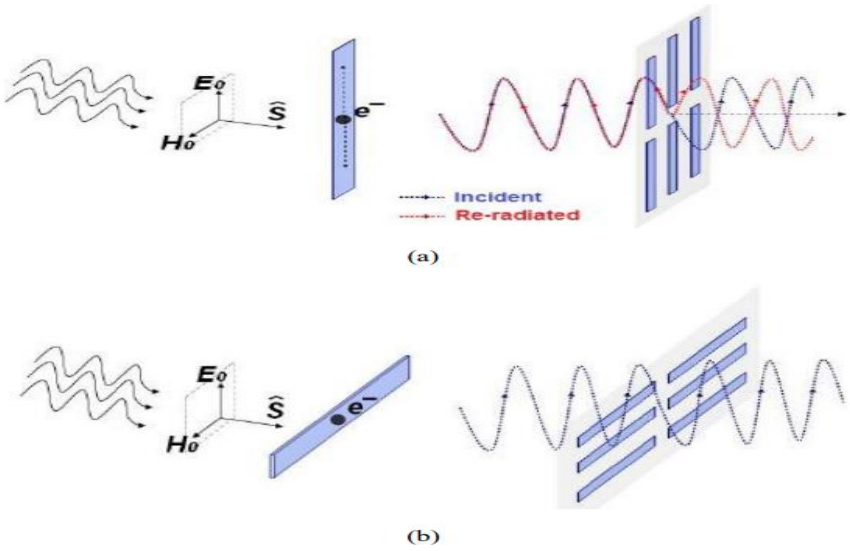

Fig 3.1 The basic filtering mechanism of FSS structure for E-vector (a) parallel and (b) orthogonal to the metallic dipole.

In order to understand the physical mechanism of the FSS filtering characteristics, two scenarios of the plane wave incidence on a metallic dipole FSS structure is presented as shown. In the first scenario, a plane wave impinges on a metallic dipole FSS structure in such a way that the FSS structure is orthogonal to the Poynting vector and electric field vector is oriented along the length of the dipole as shown in. The electric field vector oscillates the electrons due to which a portion of incidence plane wave energy is transformed into kinetic energy and gives rise to re-radiated waves/energy. These re-radiated waves on the right side of the FSS structure results in the cancellation of the incidence plane wave, which areon the left side of the FSS structure. In addition to this, the re-radiated waves on the left side of the FSS structure refer to as the reflected wave and this scenario result the low transmittance through the FSS filter. In the second scenario, the electric field vector is orthogonal to the parallel metallic dipole FSS, which is shown. In this case, the electrons do not re-radiate because of their inability to oscillate up and down. Therefore, the FSS structure remains invisible to the incidence plane wave and total transmission occurs or transmittance will be higher.

3.2 NUMERICAL TECHNIQUES FOR ANALYSIS OF FSS

In the computation of electromagnetic fields scattered by the FSS, several numerical methods are used. Various researchers have analyzed the reflection and transmission characteristics of different FSS structures through numerical techniques and validated the results through experimental measurements. However, all the numerical techniques are based on the well-

established Maxwell‟s equations and in general, these techniques are unable to provide exact solutions of the electromagnetic problem rather offer approximate solutions of sufficient accuracy. In the last five decades, various numerical techniques such as plane wave expansion method, spectraldomain Galerkin method method-of-moment (MoM) , finite methods (finite-difference-time-domain (FDTD) method /finite-element method (FEM) and equivalent circuit (EC) method have been discussed to investigate the scattering characteristics of different FSS structures. Among the above-mentioned numerical techniques, MoM, FDTD, FEM and EC technique are the most widely used numerical techniques. However, the MoM, FDTD and FEM are the computational intensive techniques and EC technique is comparatively simpler one. The selection of optimal technique for numerical modeling of FSS structure remains open. In this Section, we have discussed the state-of-the-art of different numerical techniques, which are available for the simulation of electromagnetic problems associated with the FSS structures.

The MoM technique investigated the scattering characteristics of the FSS structure in the frequency domain. The numerical modeling of FSS structure using FEM is initially discuss the evaluation of the current flowing on the metallic pattern by matching the tangential field at the surface of the unit-cell element and forms the integral equation for the unknown current. Further, the unknown electric field depends upon the unknown current near the metallic pattern, which is expanded into a set of Floquet modes and by satisfying the boundary conditions on the surface of the metallic pattern, an integral equation for the unknown current is obtained. At the final stage, the FEM is used to reduce the integral equation into a set of linear algebraic equations. The generalized steps to solve the scattering problem using MoM method are:

1)Expand the unknown function in terms of a set of N basis function with unknown coefficient

2) Enforce boundary conditions of the problems to generate a linear system of N equations, and

3) Solve the linear system of equations for unknown coefficients.

Thereafter, various researchers have discussed the different method to reduce its computational complexity. The FEM approach has the potential to evaluate the scattering characteristics over a wide range of AOIs, however it is usually restricted up to periodic FSS structures, which have supported homogeneous dielectric substrate.

In order to investigate the complex FSS structure, which are backed with inhomogeneous dielectric substrate, the FDTD and FEM approach comes out to be an effective numerical tool. These two methods come under the category of finite methods.

The FDTD technique investigates the scattering characteristics of FSS structure in time domain and covers a wide frequency range in a single simulation run. This technique is a direct solution of Maxwell's time dependent curl equations. The steps to solve the scattering problem using FDTD

are: 1) Breakdown the solution region into grid of nodes such as dividing the solution region into two different grids of nodes, one for the calculation of magnetic field and the other for the calculation of electric field,

2) Approximating the given differential equation by finite difference equivalent that relates the dependent variable at a point in the solution region to its values 5 at neighbouring point such as the value of magnetic field at an instant is calculated by the electric field at previous grid points, in other words, the electric field is solved at a given instant in time, then the magnetic field is solved at the next instant in time and so on and

3) Solving the difference equations subjected to the prescribed boundary/initial conditions . In addition to this, various other scientists have discussed the numerical modeling of different FSS structures using the FDTD as discussed in .

The FEM technique investigates the scattering characteristics of different FSS structures in frequency domain and initialize with the partial differential equation form of Maxwell‟s equation. The generalized steps for the scattering problem using FEM technique are:

1) Discretize the solution region into finite number of sub regions and corner of each sub-region is called as node. In the first step, this method determine the field quantities at these nodes,

2) Derive governing equations for a typical sub region,

3) Integrating all sub-regions over the entire geometry, and

4) Solving the system of equations obtained from above steps.

The technical advancements in the FEM are discussed by various researchers as discussed

. In comparison to the aforementioned numerical techniques, which are computationally intensive, the EC technique provides a simpler method to investigate the scattering characteristics of the different FSS structures. The EC technique is based on the transmission line analogy, where the EC parameters of a FSS structure is obtained due to the inductive and capacitive behavior of its geometrical parameters . This technique is a scalar technique due to which the modeling is limited upto linear polarizations and simple FSS geometries only. However, the dielectric substrates parameters and AOIs have been taken into account in the EC equations and the accuracy of the technique depends upon the assumptions made in the analysis. Various researchers have analyzed the different FSS structures such as square loops, circular ring, dipoles and Jerusalem cross using EC technique. However, the EC technique provides the less precise analysis as compared to that of the other numerical methods rather offer better physical understanding of the filtering behaviour of the FSS structures, therefore, the EC technique is chosen as the analysis tool for this research. In addition to this, the EC technique provides the significantly accurate analytical response for this research, and most importantly it instantaneously characterizes the FSS structures with varying geometrical dimensions of the unit-cell element. Moreover, for the modeling of an infinite periodic FSS structure, the numerical methods such as MoM, FDTD and FEM require considerable computer resources and results complex computation, rather the EC technique require little computer resources and still offer an significantly accurate response. Due to these significances, the different FSS structures have been analyzed using EC technique in this thesis. Earlier due to the lack of resources, a narrow range of electromagnetic problems associated with the FSS structures have been investigated by the researchers. However, the technical advancements in the computer techniques have revolutionized the way in which the electromagnetic problems have been analyzed. Therefore, majority of antenna and microwave engineers rely heavily on the computer methods to analyze and design the novel FSS structures. Various commercial electromagnetic simulators are available, out of which more commonly employed are CST Microwave Studio, Ansoft HFSS and Ansoft Designer, which are based on finite integral technique, FEM and MoM, respectively. In this thesis, the numerical frequency responses have been validated through the simulation responses.

CHAPTER 4

DESIGN OF I SHAPED FSS BASED POLARIZATION CONVERTOR

4.1 Introduction of unit cell design:

In this chapter the design of the single layer and multi-layer unit cells with I shaped metallic patch are discussed. The single layer unit cell has dielectric substrate as top layer and metallic sheet as bottom surfaces. An I shaped metallic patch using two circles is constructed on the top surface of the unit cell. Whereas in the double layer unit cell since it has an air gap, an air substrate is used. The top layer is similar to that of single layer unit cell whereas the middle layer has complementary slot and a bottom metallic layer. The results of both unit cells are discussed and surface currents analysis are observed for the frequencies at which maximum reflection magnitudes are observed for both the unit cells**.**

4.2 Single layer unit cell design with I shaped patch

4.2.1 Design Specifications:

The essential parameters for the design of any unit cell are:

1. Polytef Substrate: The relative permittivity of polytef dielectric substrate is 2.65 and dielectric loss is 0.002. The design patterns are printed on both sides of dielectric substrate.

2. Dimensions of dielectric substrate: The height of the polytef dielectric substrate selected here is 3.0mm, sides are taken as 10mm and constructed as square.

3. Dimensions of Copper substrate: The height of the copper substrate selected here is 0.035mm, sides are taken as 10mm and constructed as square which acts as ground for the design.

4.2.2 Design Procedure:

Design of a unit cell is done using HFSS. Here we create a box of material FR4 epoxy with substrate length of 10mm and substrate width of 3mm. Create a circle1 of radius 3.8 mm at the centre of the box. Create another circle 2 of radius 2.4 mm inside the circle of radius 4.4mm. By subtracting circle 2 from circle 1 it forms a ring. Now construct two squares from the centre of the circles of length 4.5mm and subtract the square from the ring. By substracting both the squares , two arcs are formed opposite to each other.Take a polyline of type rectangle and width

1.6mm placed along the axis and the edges of the polyline touches the arcs. Select the polyline and rotate along the z-axis with angle 135 degrees. By uniting both the arcs and rectangle it forms the I shaped cell. Select thicken sheet from sheet of thickness 0.035mm and the material of the sheet is copper. Create another box to provide ground of box width 0.035mm. Now select the box and provide the material of the box as copper. Create a region of region type as absolute offset and provide +Z padding as 10mm. A floquet port is provided on the upper side of region which is faced at the front part of the unit cell.Select analysis setup and mention the operating frequency as 8.34 GHZ (12.18GHz, 17.08GHz for corresponding values). After this add the frequency trace and do the validation check. All the cases pass significantly saying the design has no errors . After the validation check click the run button i.e analyse all option and the results will be observed.

4.2.3 Parameters table:-

NAME	VALUE	UNIT
SL1	10	mm
W1	3	mm
L1	3.8	mm
L2	2.4	mm
W	1.6	mm
W2	0.035	mm
Sthick	0.035	mm
Sheetwid	0.035	mm
β1	135	deg
θ	90	deg

4.2.4 Parametric Results: -

In the parametric sweep, we simulate the ant design of different values of a parameter. This is useful in selecting the desired parameter value for the design. By selecting the best results in a parametric sweep, with those parameters values, we will optimize for the best results.

L1 Sweep: -

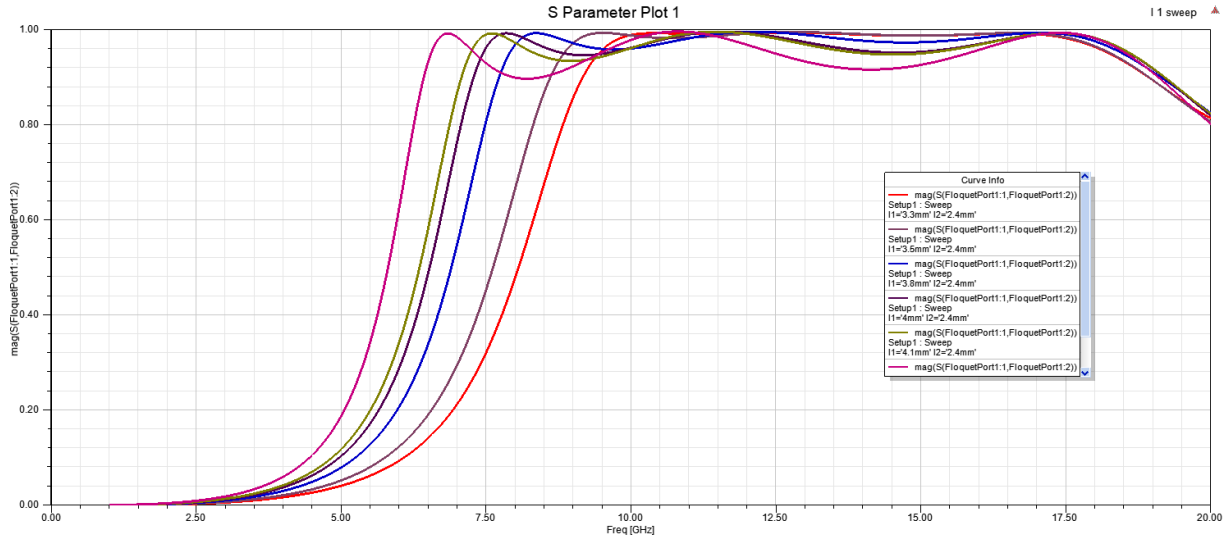

fig 4.1 Reflection magnitudes for different L1 values under normal x-polarized incident waves

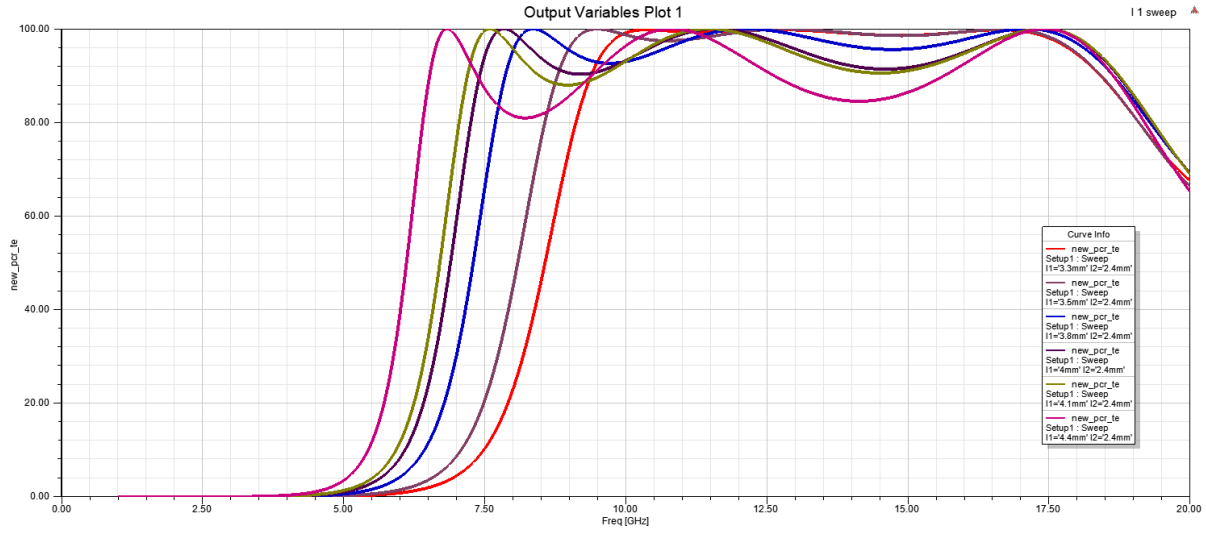

Fig 4.2 PCR for different L1 values under normal x-polarized incident waves.

By using Parametric Sweep for the variable L1 from 4.4mm to 3.5mm at a decrease of 0.3mm per step the required graphs are obtained for single-layer reference unit.

L2 sweep: -

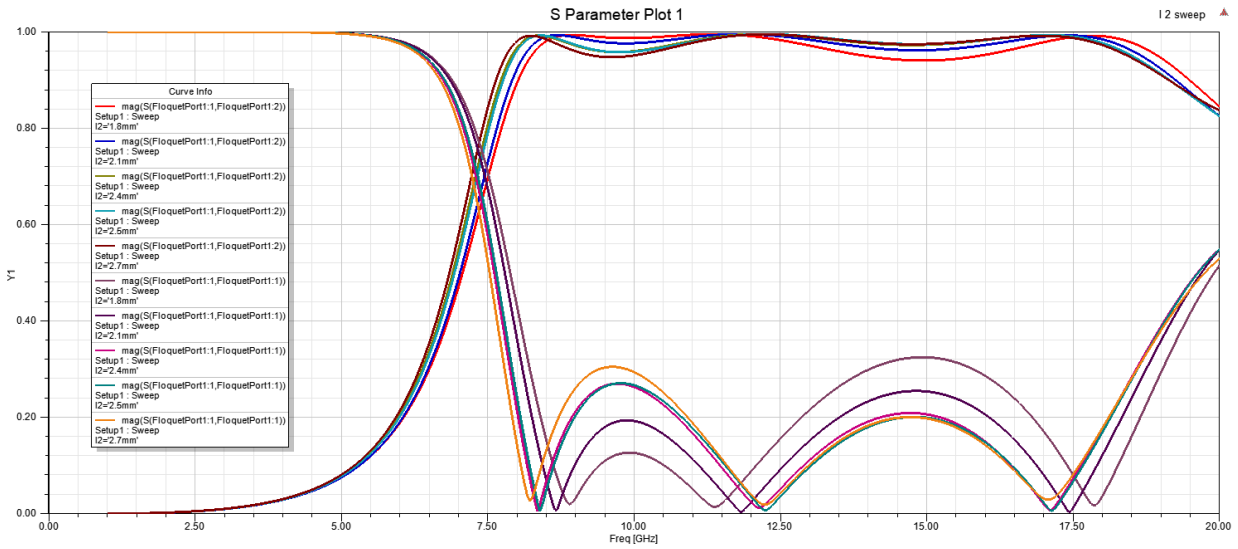

Fig 4.3 Reflection magnitudes for different L2 under normal x-polarized incident waves.

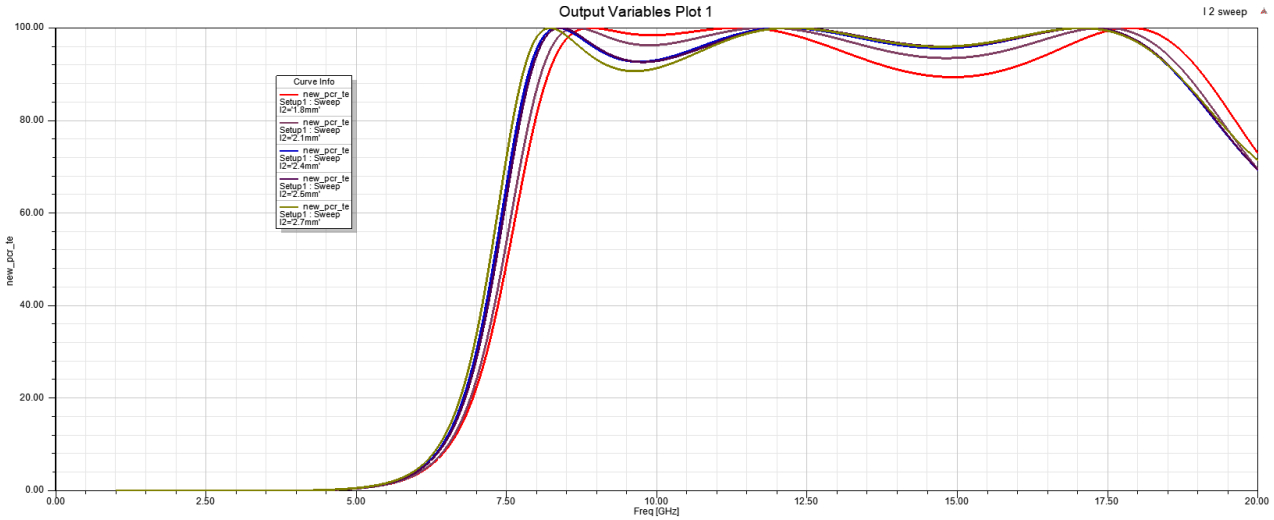

Fig 4.4 PCR for different L2 under normal x-polarized incident waves

By using Parametric Sweep for the variable L2 from 2.8mm to 1.9mm at a decrease of 0.3mm per step the required graph is obtained for single-layer reference unit.

With the decrease of L1 and L2, the peak values of cross-polarization at 8.34 GHz and 12.18 GHz shift toward high-frequency range while the peak value at 17.08 GHz is almost maintained because the peak values of cross-polarization at 17.08 GHz is caused by I-shaped patch itself, the interaction between the two structures of modified I-shaped patch becomes strong when

the length of two "|" structures are decreased. Thus, the peak value at 17.08 GHz is almost maintained. From above parameters investigations, the current distributions analysis of proposed structures is reasonable.

Theta scan: -

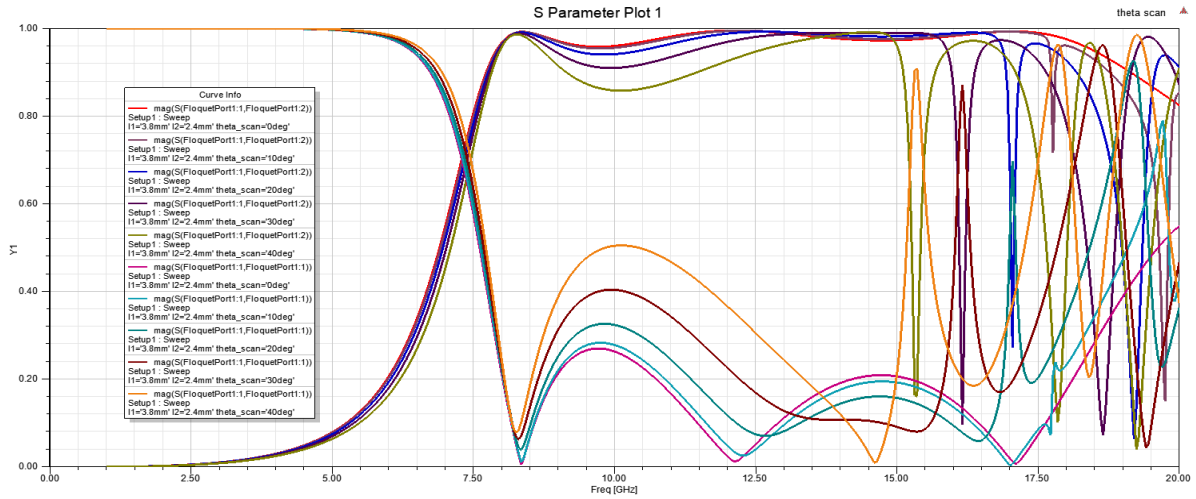

fig 4.5 Refection magnitudes of proposed units for different oblique incident angles.

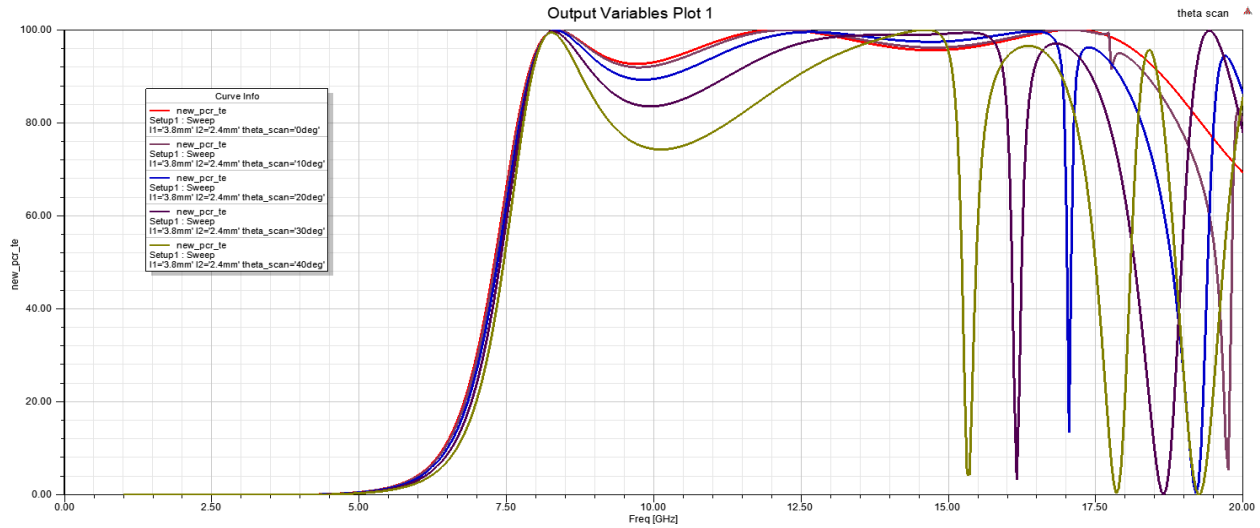

Fig 4.6 PCR of proposed units for different oblique incident angles.

With incident angles increase to 40°, the polarization conversion properties are almost maintained from 4.0 to 15.0 GHz. To further reveal operation mechanism of proposed unit, current distributions of proposed unit at 8.34, 12.18 and 17.08 GHz (peak reflection magnitude frequency) were investigated. Intense induced current is observed on the top and middle surfaces at three frequencies

Angle sweep: -

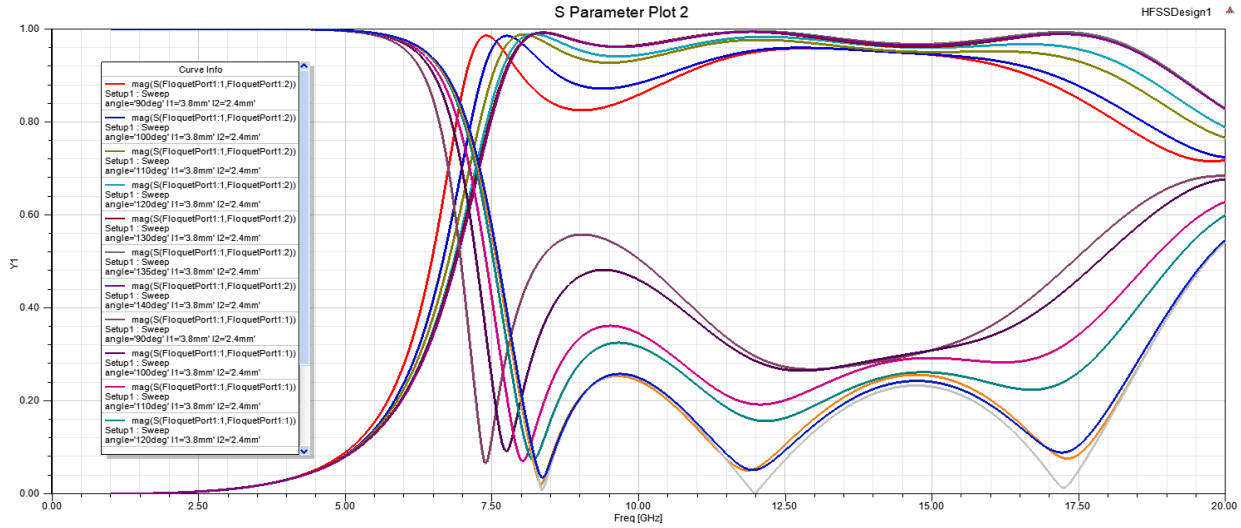

Fig 4.7 Reflection magnitudes for different angle of the square under normal x-polarized incident waves

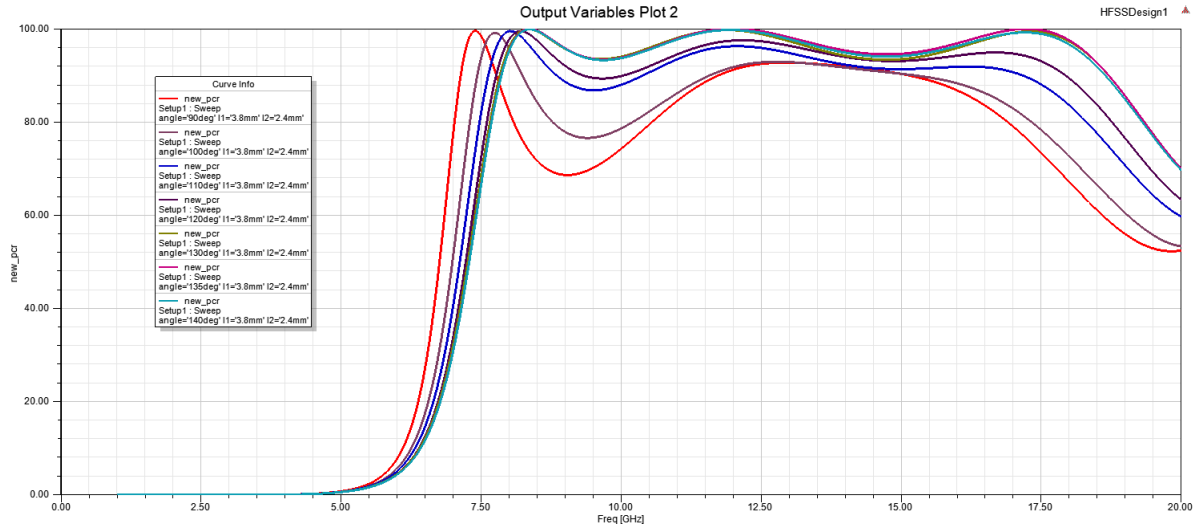

Fig 4.8 PCR for different angle of the square under normal x-polarized incident waves

The above graphs represent the Angle sweep for single-layer reference unit. With the increase of θ (the length of "–" of modified I-shaped patch is decreased), the peak values of cross-polarization at 8.34 GHz and 12.18 GHz shift toward high-frequency range, whereas the peak value at 17.08 GHz shift slightly toward low-frequency range. Moreover, the peak values of cross-polarization at 12.18 GHz and 17.08 GHz are overlapped when θ equal to 140°. That is to say, the peak value at 17.08 GHz disappears. The polarization efficiency decreases with increase in the oblique angle.

4.2.5 Final design

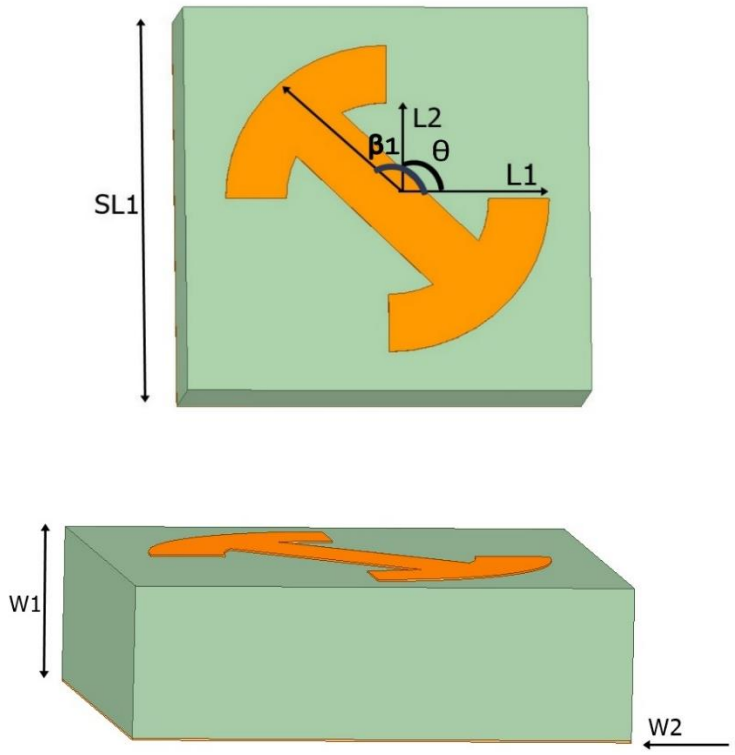

Fig 4.9 Single layer unit cell design with I shaped patch

4.2.6 Simulation Results of Unit cell design:

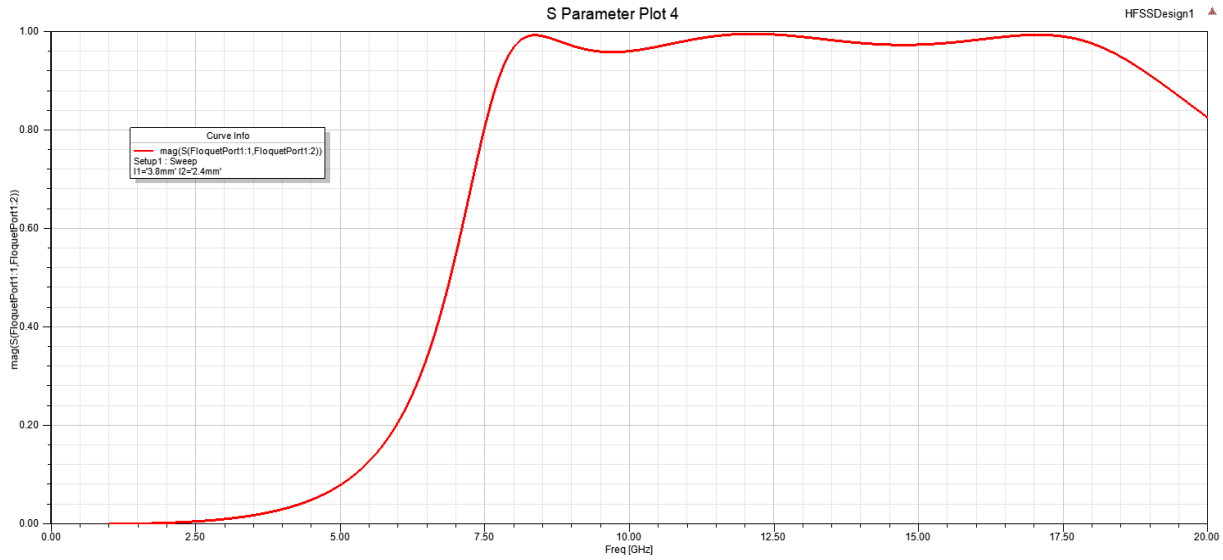

Fig 4.10 Refection magnitudes of single-layer reference unit

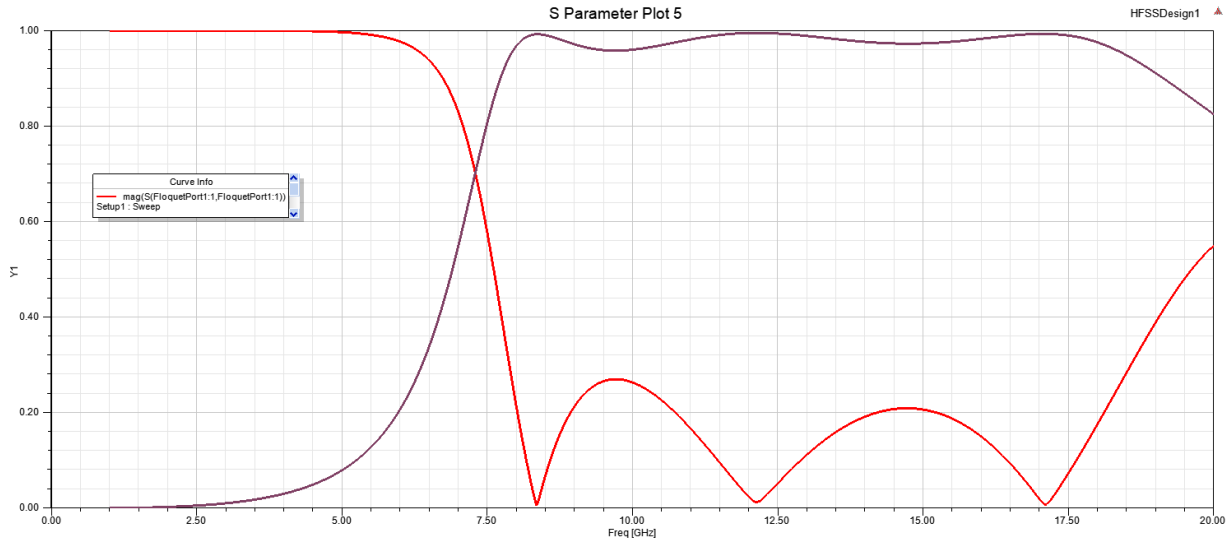

Fig4.11 Refection magnitudes of proposed units for different β1 and β2 under normal x-polarized incident waves.

The figures 4.10 represents the refection magnitudes of single-layer reference unit. Most incident waves are reflected to its orthogonal counterparts. Taking a further step, the reflection magnitudes of proposed unit and its mirror one (i.e., the proposed unit rotates 90°) are investigated in detail for normal incidence.

The reflection magnitudes of the mirror unit coincide well with the proposed one. The PCR plot shown inn figure 4.4 shows the efficiency of the converter in converting the incident waves to cross polarized waves, where the maximum conversions are observed at frequencies where reflection magnitudes are maximum.

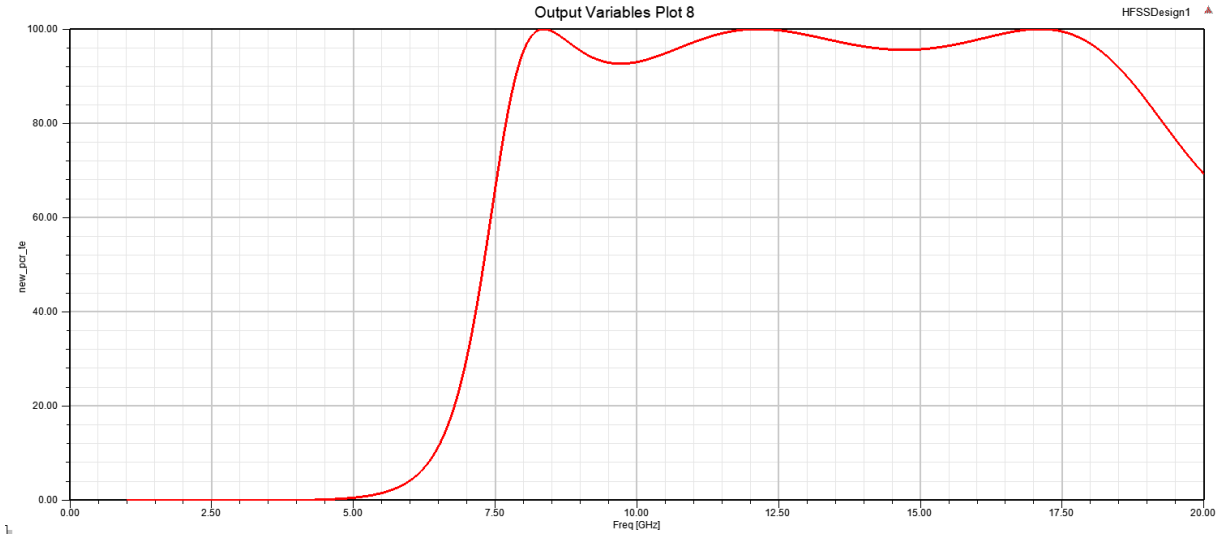

Fig 4.12 PCR for single layer reference unit.

The figure 4.11 represents reflection magnitudes of proposed units for different β1 and β2 under normal x-polarized incident waves for single-layer reference unit. The graph in red represents the cross-polarization reflection magnitude when β1 is 45° and β2 is 135° whereas the violet graph represents the co-polarization reflection magnitude when β1 is 135° and β2 is 45°. The values of reflection magnitudes are more than 0.85 from 5.1 to 19.5 GHz.

Surface currents:-

For 8.34ghz

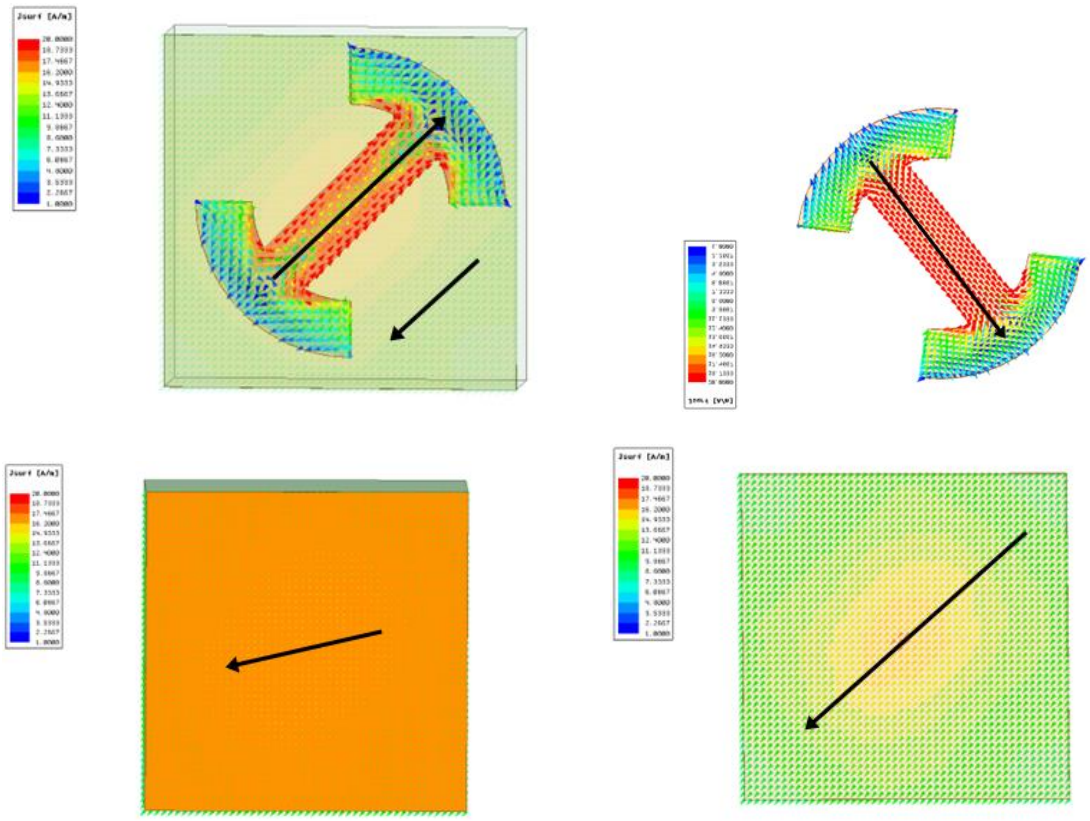

Fig 4.13 Current distributions of proposed units at 8.34GHZ.

For 12.18Ghz

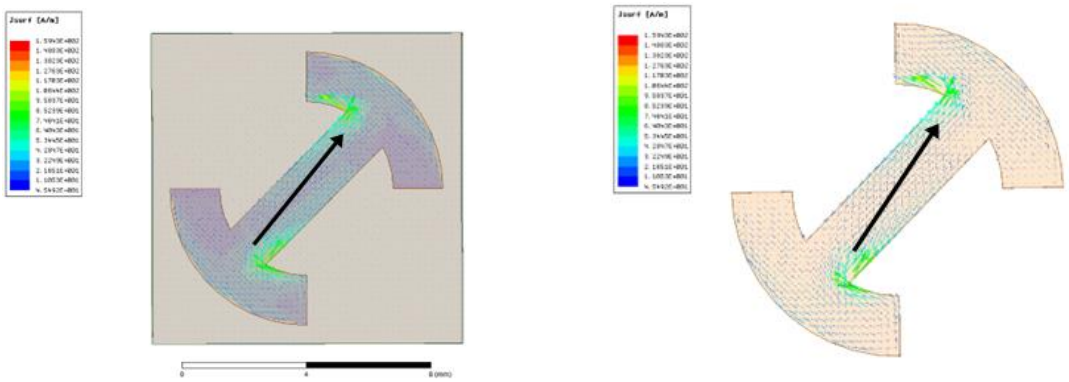

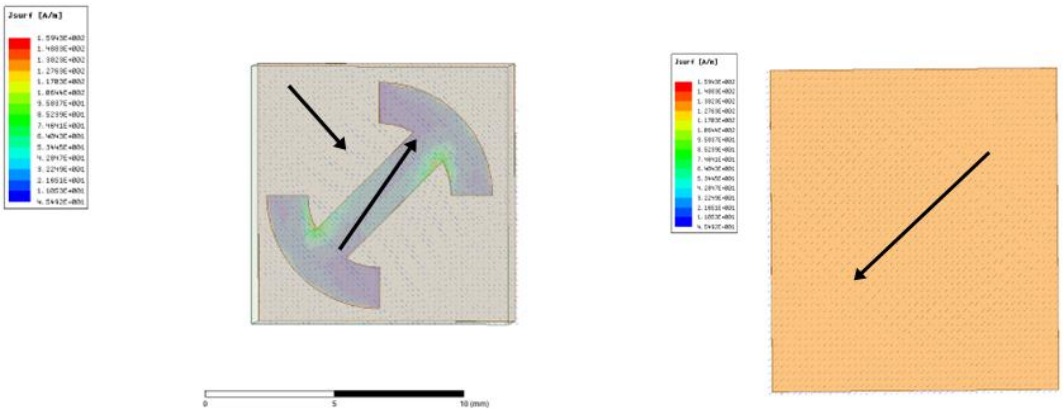

Fig 4.14 Current distributions for proposed units at 12.18 GHz.

For 17.08GHz

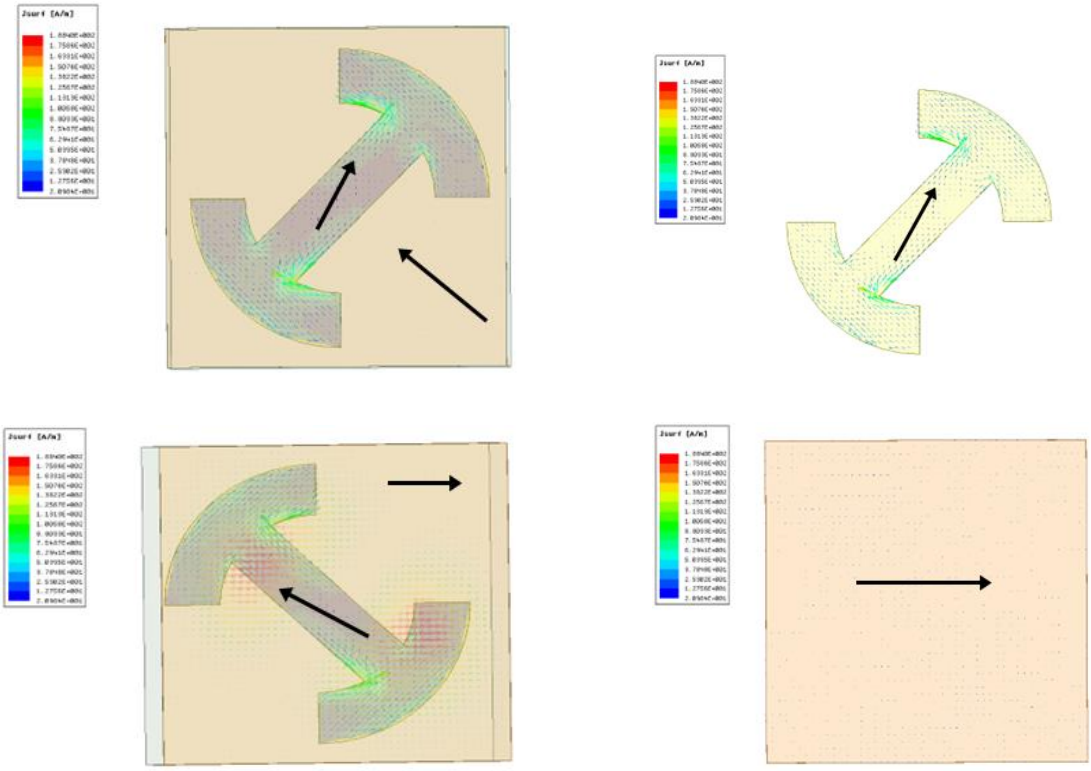

Fig 4.15 Current distributions of proposed units at 17.08GHZ.

The above figures represent the surface currents distribution for 8.34GHz, 12.18GHz and 17.08GHz frequencies of Single layer reference unit cell with I shaped patch. To further reveal operation mechanism of proposed unit, current distributions of proposed unit at 8.34, 12.18 and17.08 GHz (peak reflection magnitude frequency) were investigated. Intense induced current is observed on the top and bottom surfaces at three frequencies.

In 8.34Ghz frequency the current directions on the top surface are completely different from those on the bottom surface. Strong interaction is produced between the top and bottom surfaces.

However, the different current directions are mainly observed on the "–" of modified I-shaped patch are represented in 12.18 GHz. Strong interaction is produced between the "–" of modified I-shaped patch and bottom surface. But the levels of interaction between the top and bottom surfaces decreased when compared to that of the 8.34GHz frequency surface currents.

Furthermore, at 17.08GHz the different current directions are mainly observed the "–" of I-shaped patch itself. The interaction between the top and bottom surface becomes pale when compared to that of 8.34Ghz and 12.18GHz where 8.34GHz interactions stand high of the three compared.
It can be concluded that the interaction between the top and bottom surfaces becomes weak with the increase of frequency. Although the current directions are different between top and bottom surfaces at 8.34, 12.18 and 17.08 GHz, the strong interaction is mainly produced at 8.34 GHz.

Double layer unit cell design

4.3 Double layer unit cell design with I shaped patch

4.3.1 Design Specifications:

The essential parameters for the design of any unit cell are:
1.Polytef Substrate: Polytef dielectric substrate and air substrate are utilized to form the double-layer structure. The relative permittivity of polytef dielectric substrate is 2.65 and dielectric loss is 0.002. The design patterns are printed on both sides of dielectric substrate.
2. Dimensions of dielectric substrate: The height of the polytef dielectric substrate selected here is 3.0mm and sides are taken as 10mm and constructed as square.
3. Dimensions of Copper substrate: The height of the copper substrate selected here is 0.035mm, sides are taken as 10mm and constructed as square which acts as ground for the design.

4. Dimensions of Air substrate: The height of the air substrate selected here is 3.0mm and sides are taken as 10mm and constructed as square

4.3.2 Design Procedure:

Design of a multilayer unit cell is done using HFSS. Create a box of material FR4 epoxy of sublen 10mm and subwidth 3mm. Create a circle1 of radius 4.4mm at the centre of the box. Create another circle 2 of radius 2.8mm. By subtracting circle 2 from circle 1 it forms a ring.Construct two squares from the centre of the circles of length 4.5mm and subtract the square from the ring. By subtracting both the squares , two arcs are formed.

Take a polyline of type rectangle and width 1.6mm placed along the axis and the edges of the polyline touches the arcs. Select the polyline and rotate along the z-axis with angle 135 degrees. Now unite both the arcs and rectangle to form the I shaped cell.

Select the I shaped cell and select thicken sheet from sheet of thickness 0.035mm and the material of the sheet is copper.Create another box to provide ground of box width -0.035mm. Now select the box and provide the material of the box as copper.Create a circle 1 of radius 4.4mm and circle 2 of radius 2.8mm at the back side i.e on the ground. Select circle 1 and circle 2 and substract circle 2 from circle 1 .This forms a ring.Construct two squares from the centre of the circles of length 4.5mm and subtract the square from the ring. By substracting both the squares , two arcs are formed.

Take a polyline of type rectangle and width 1.6mm placed along the axis and the edges of the polyline touches the arcs. Now rotate the polyline with angle 45 degrees and select polyline and both the arcs . Now unite both of them. Select the I shaped cell and select thicken sheet from sheet of thickness 0.035mm and the material of the sheet is copper.Select ground and I shaped material and substract I material from the ground.Create another box of width 3.0mm upon the copper metal and assign air to it .

Create another box of width 0.035mm and assign copper to it. Create region of region type as absolute offset and provide +Z padding as 10mm.Create a floquet port on the upper side of region which is faced at the front part of the unit cell.Now click analysis and add solution setup and provide frequency as 7.29GHZ. Go to setup1 and add frequency sweep and provide range from 1 to 20GHZ. Now do validation check and analyse all further observe the results obtained.

4.3.3 Parameters Table:-

NAME	VALUE	UNIT
SL1	10	mm
W1	3	mm
L1	4.4	mm
L2	2.8	mm
W	1.6	mm
W2	0.035	mm
Sthick	0.035	mm
W3	3	mm
sheetwid	0.035	mm
β1	135	deg
θ	90	deg

4.3.4 Parametric Results: -

In the parametric sweep, we simulate the ant design of different values of a parameter. This is useful in selecting the desired parameter value for the design. By selecting the best results in a parametric sweep, with those parameters values, we will optimize for the best results.

L1 sweep: -

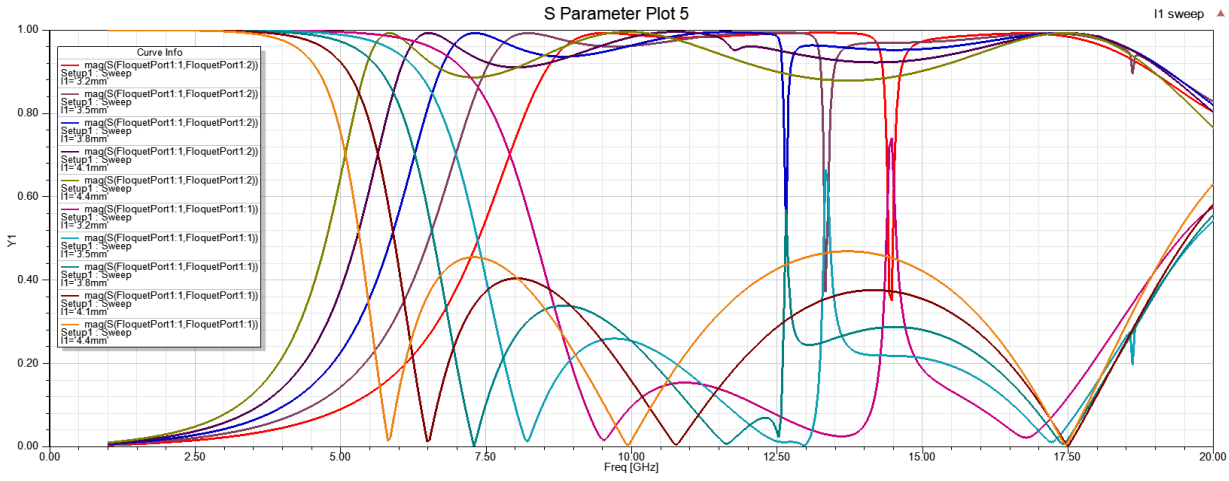

Fig 4.16 Reflection magnitudes for different L1 under normal x-polarized incident waves.

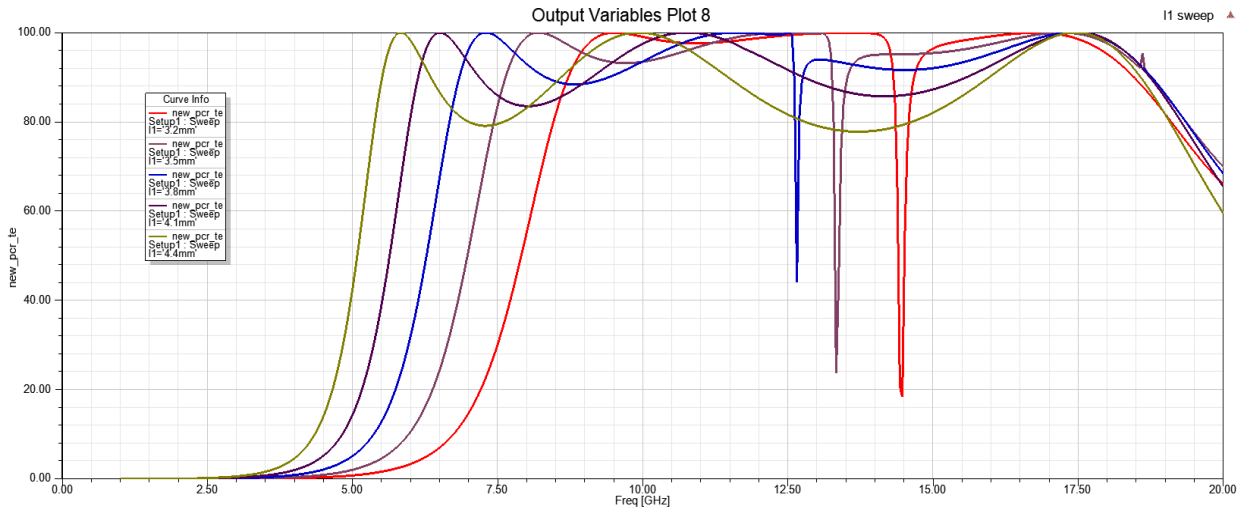

Fig 4.17 PCR for different L1 under normal x-polarized incident waves.

By using Parametric Sweep for the variable L1 from 4.4mm to 3.5mm at a decrease of 0.3mm per step the required graph is obtained for double-layer complementary MS unit.

L2 sweep:

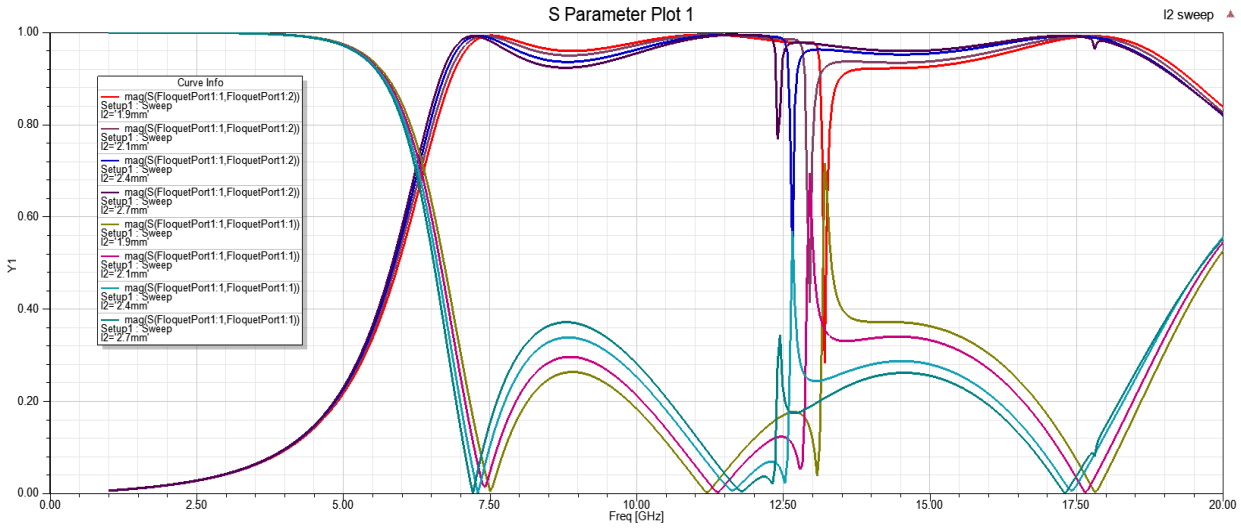

Fig 4.18 Reflection magnitudes for different L2 under normal x-polarized incident waves.

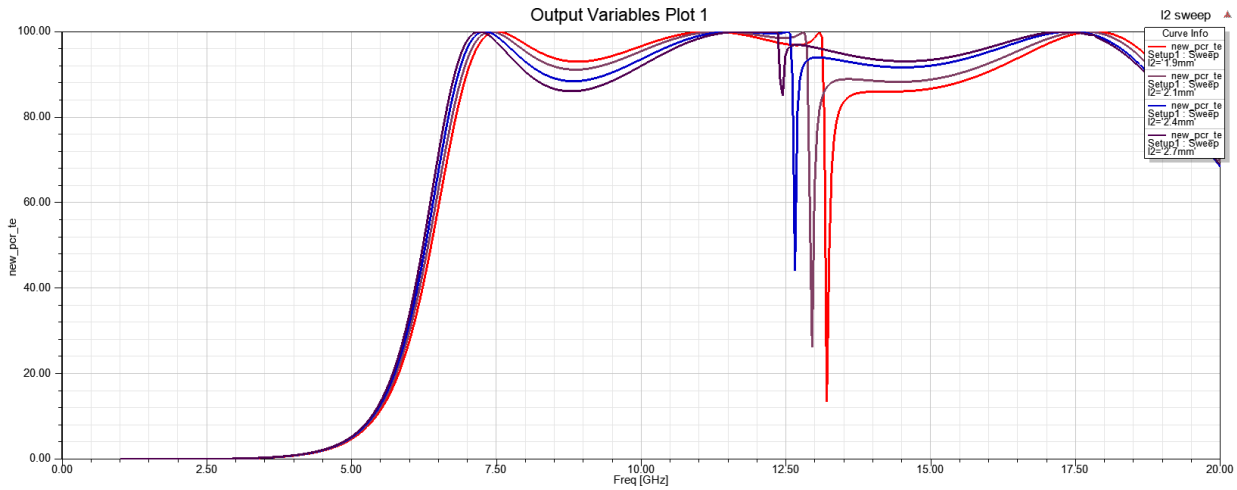

Fig 4.19 PCR for different L2 under normal x-polarized incident waves.

By using Parametric Sweep for the variable L2 from 2.8mm to 1.9mm at a decrease of 0.3mm per step the required graph is obtained for double-layer complementary MS unit.

With the decrease of L1 and L2, the peak values of cross-polarization at 7.29 GHz and 11.68 GHz shift toward high-frequency range while the peak value at 17.42 GHz is almost maintained because the peak values of cross-polarization at 17.42 GHz is caused by I-shaped patch itself, the interaction between the two structures of modified I-shaped patch becomes strong when the length of two "|" structures are decreased. Thus, the peak value at 17.42 GHz is almost maintained. From above parameters investigations, the current distributions analysis of proposed structures is reasonable.

Theta Scan:

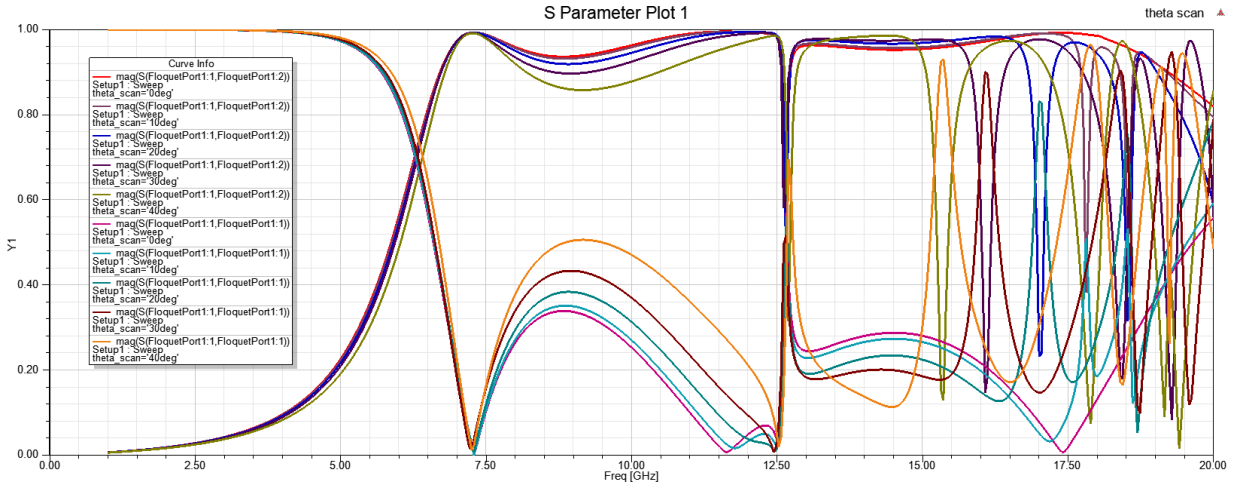

Fig 4.20 Refection magnitudes of proposed units for different oblique incident angles.

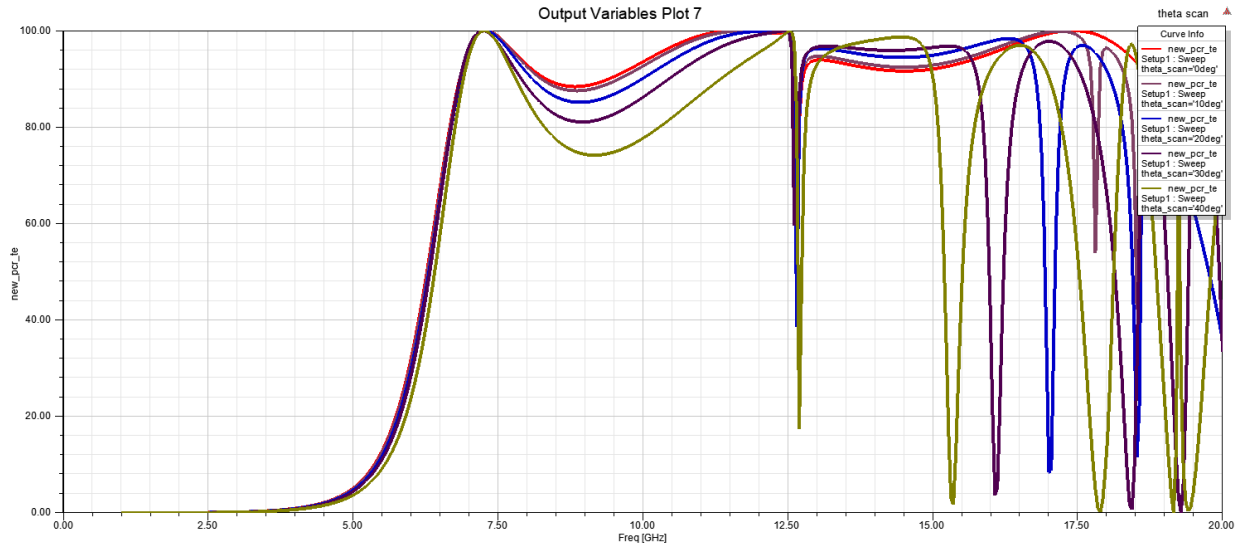

Fig 4.21 PCR of proposed units for different oblique incident angles.

With incident angles increase to 40°, the polarization conversion properties are almost maintained from 4.0 to 15.0 GHz. To further reveal operation mechanism of proposed unit, current distributions of proposed unit at 7.29, 11.68 and 17.42 GHz (peak reflection magnitude frequency) were investigated. The polarization efficiency in Figure 5.10 decreases with increase in the oblique angle

Angle Sweep:

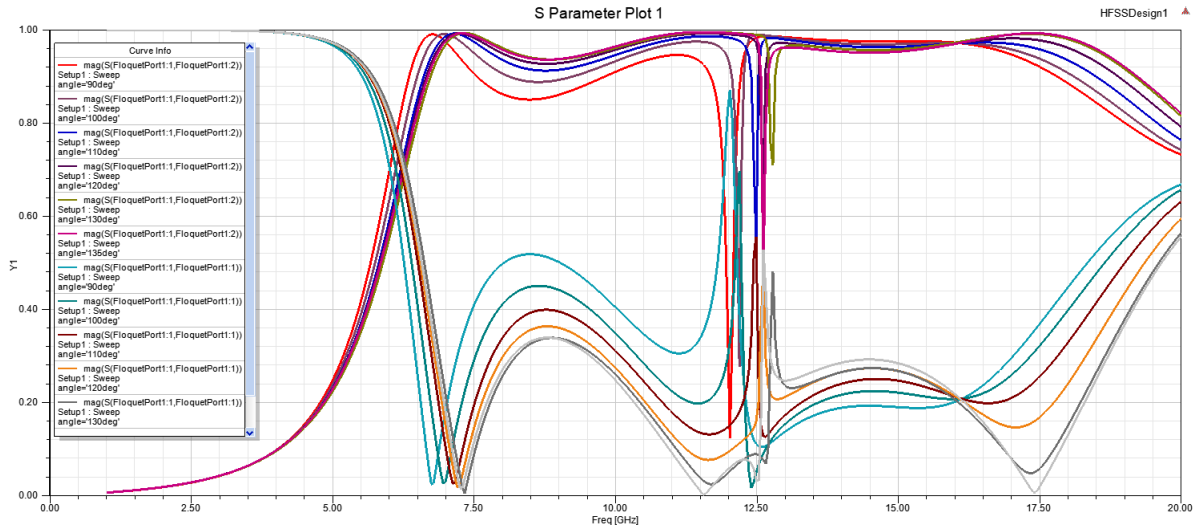

Fig 4.22 Reflection magnitudes for different theta under normal x-polarized incident waves

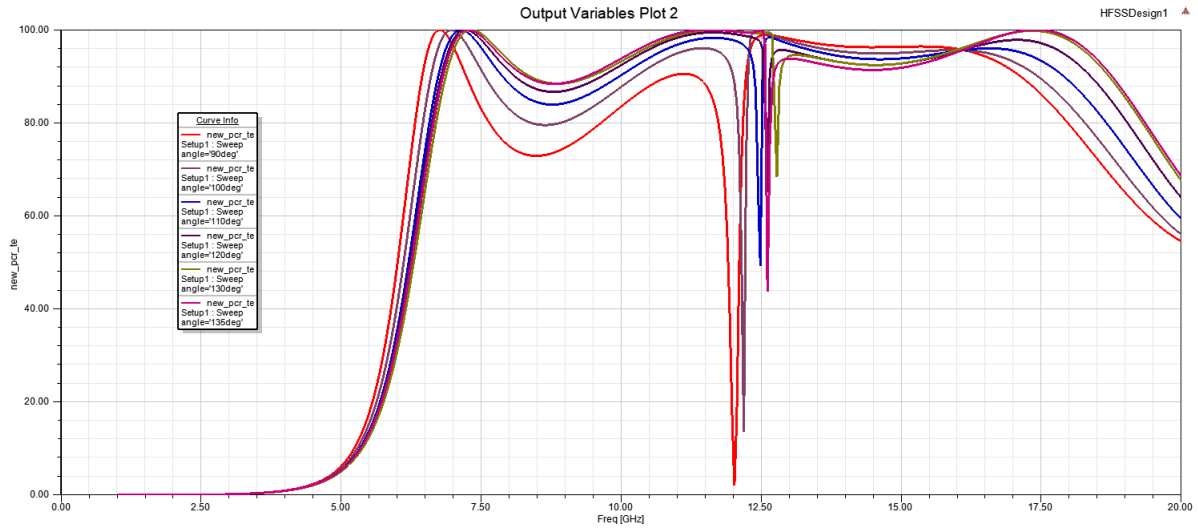

Fig 4.23 PCR for different theta under normal x-polarized incident waves.

The above graph represents the Angle sweep for double-layer complementary MS unit. With the increase of θ (the length of "–" of modified I-shaped patch is decreased), the peak values of cross-polarization at 7.29 GHz and 11.68 GHz shift toward high-frequency range, whereas the peak value at 17.42 GHz shift slightly toward low-frequency range. Moreover, the peak values of cross-polarization at 11.68 GHz and 17.42 GHz are overlapped when θ equal to 140°. That is to say, the peak value at 17.42 GHz disappears.

4.3.5 Final design

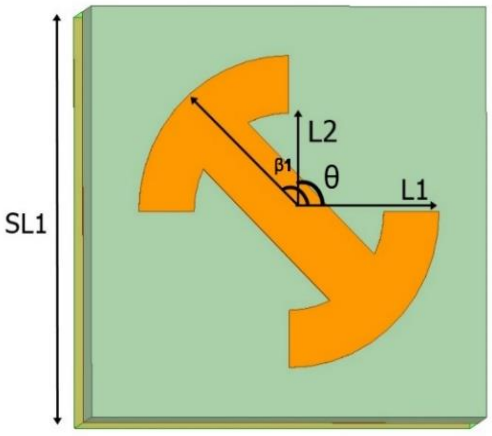

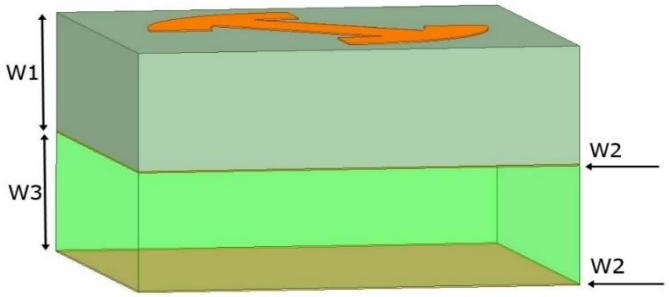

Fig 4.24 Double layer unit cell design with I shaped patch

4.3.6 Simulation and Results of Unit cell design: -

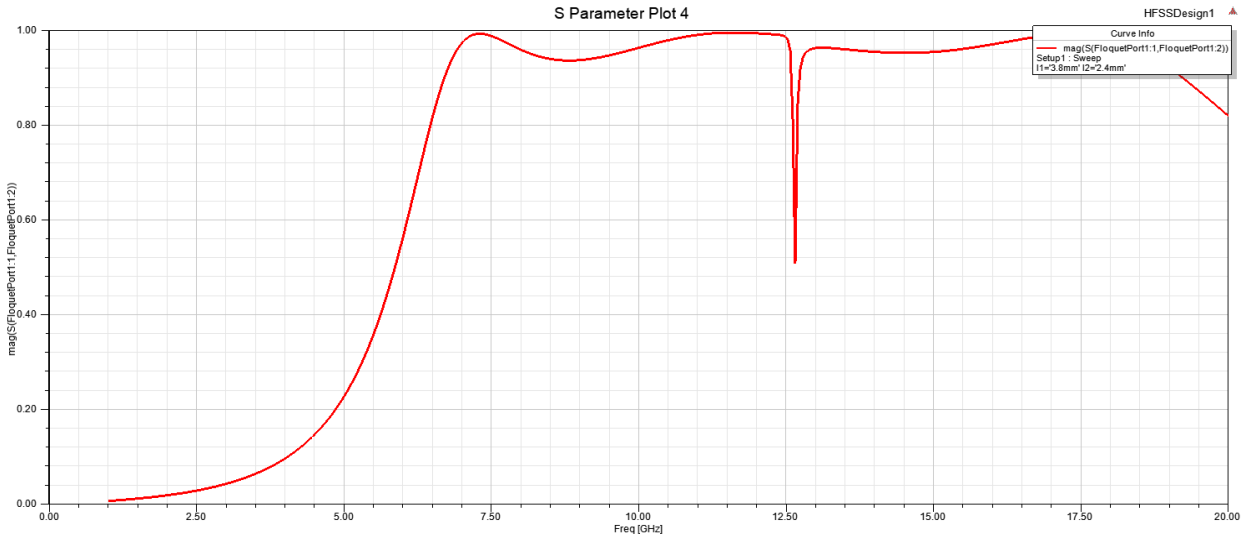

Fig 4.25 refection magnitudes of double-layer complementary MS reference unit.

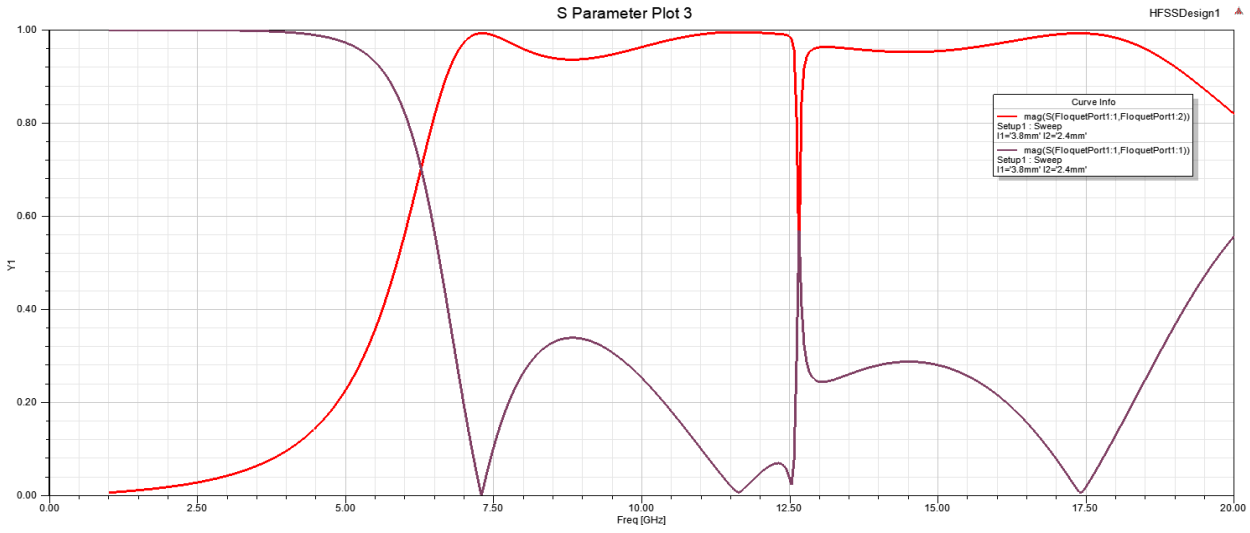

Fig 4.26 Reflection magnitudes of proposed units for different β1 and β2 under normal x-polarized incident waves.

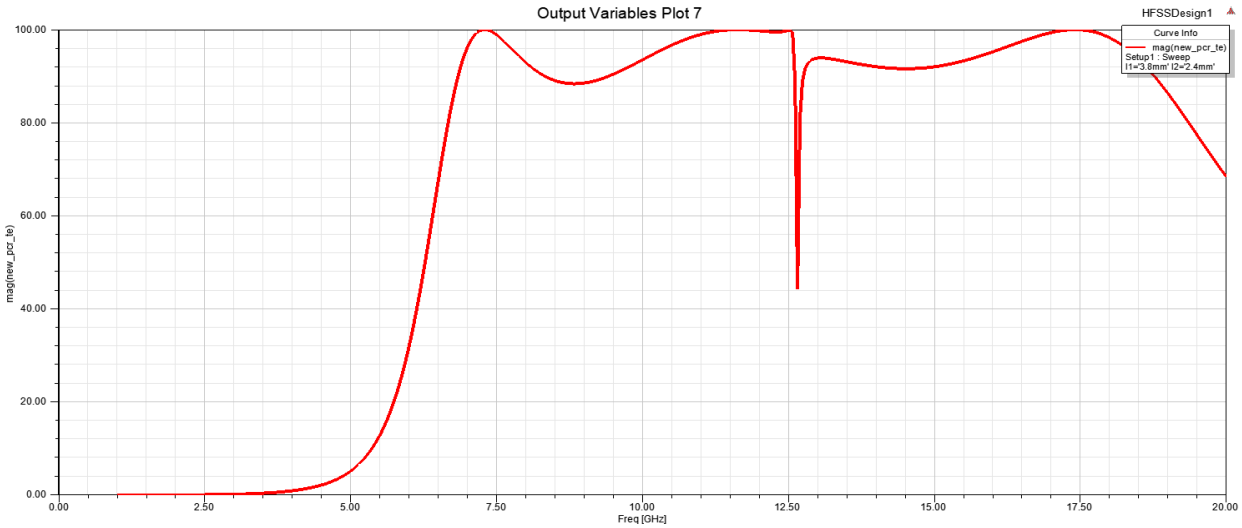

Fig 4.27 PCR of double-layer complementary MS reference unit.

The figure 4.25 represents the refection magnitudes and figure 4.27 represents PCR of double-layer complementary MS unit. Most incident waves are reflected to its orthogonal counterparts. Taking a further step, the reflection magnitudes of proposed unit and its mirror one (i.e., the proposed unit rotates 90°) are investigated in detail for normal incidence. The reflection magnitudes of the mirror unit coincide well with the proposed one. Figure 5.4 represents the efficiency of the design in converting the incident waves to required polarized waves and maintains a consistent efficiency through the frequencies 7.29GHz to 17.42GHz.

The figure 4.26 represents reflection magnitudes of proposed units' cell for different β1 and β2 under normal x-polarized incident waves for double-layer complementary MS reference unit. The graph in red represents the cross-polarization reflection magnitude when β1 is 45° and β2 is 135° whereas the violet graph represents the co-polarization reflection magnitude when β1 is 135° and β2 is 45°. The values of reflection magnitudes are more than 0.85 from 5.1 to 19.5 GHz.

Surface currents: -

For 7.29GHz:

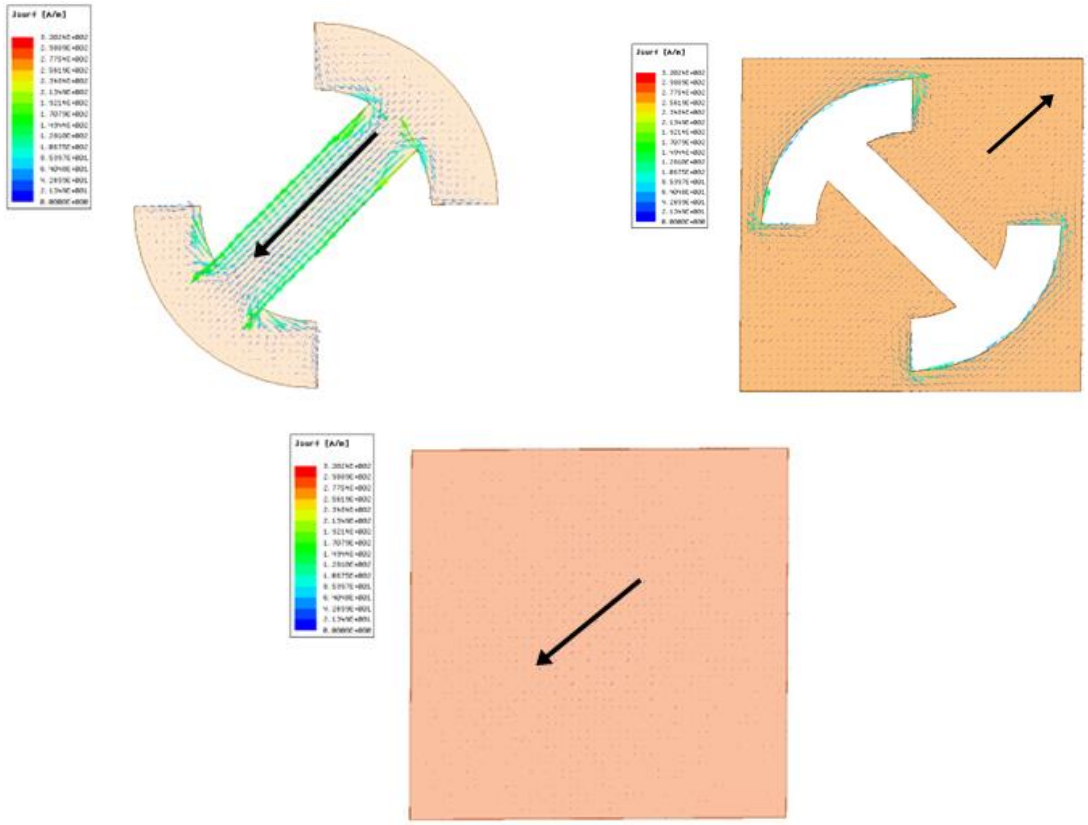

Fig 4.28 Current distributions of proposed units at 7.29GHz.

For 11.68GHz:

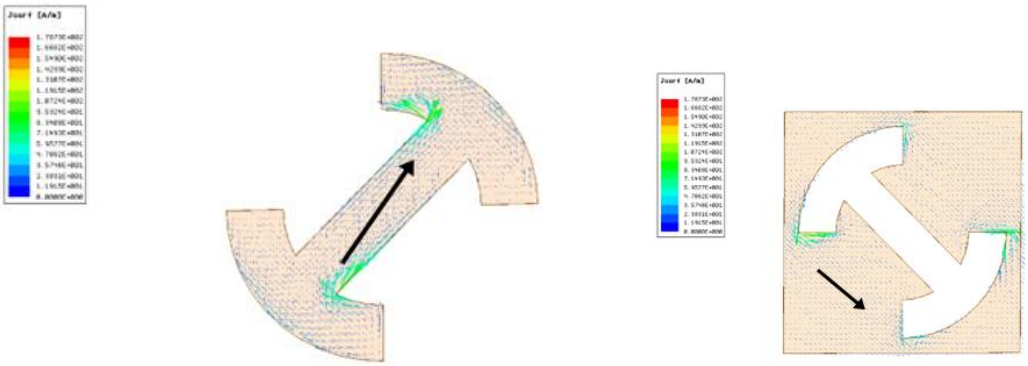

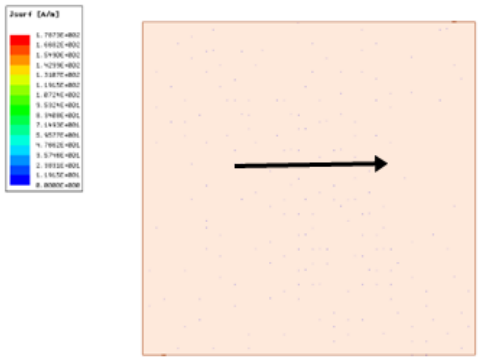

Fig 4.29 Current distributions of proposed units at 11.68GHz.

For 17.42GHz

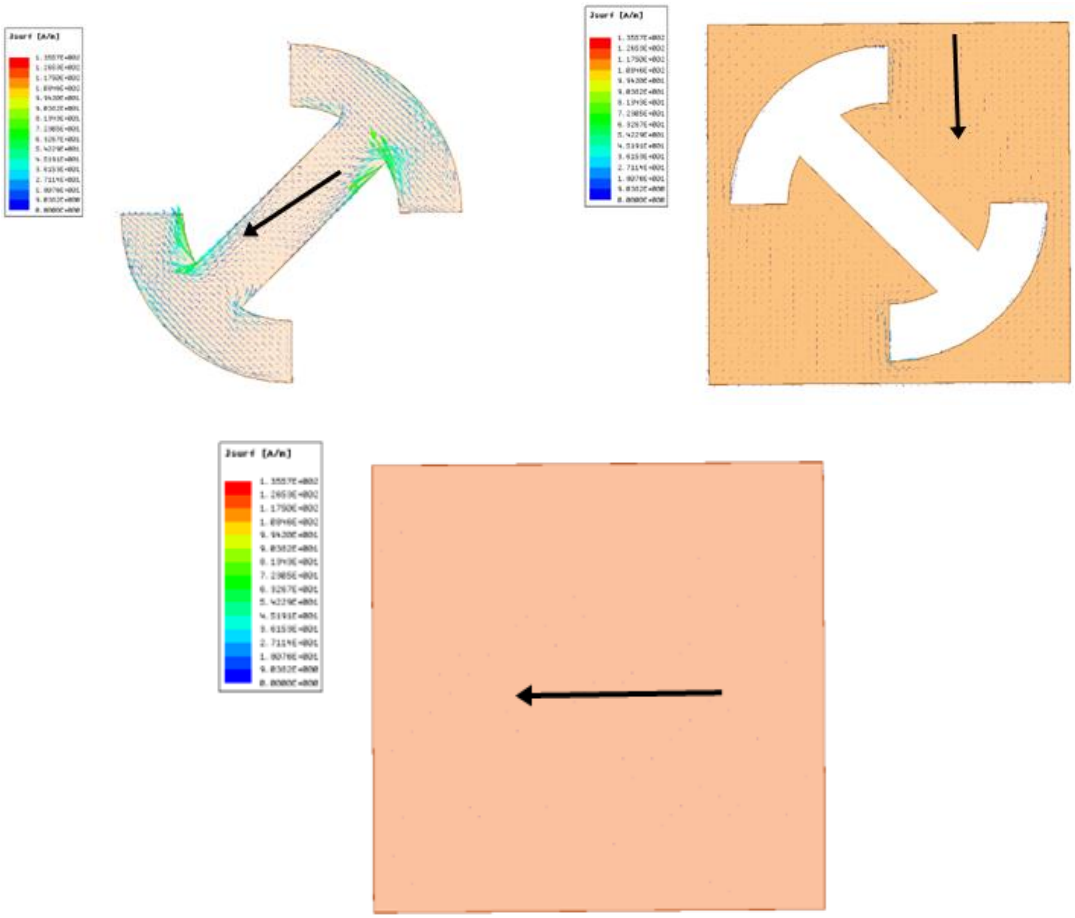

Fig 4.30 Current distributions of proposed units at 17.42GHz.

The above figures represent the surface currents distribution for 7.29GHz, 11.68GHz and 17.42GHz frequencies of double layer Complementary unit cell with I shaped patch. To further reveal operation mechanism of proposed unit, current distributions of proposed unit at 7.29,

11.68 and17.42 GHz (peak reflection magnitude frequency) were investigated. Intense induced current is observed on the top, middle and bottom surfaces at three frequencies,

In 7.29Ghz frequency the current directions on the top surface are completely different from those on the middle and bottom surface. Strong interaction is produced between the top and bottom surfaces whereas light interactions were produced with that of the bottom surface.

However, the different current directions are mainly observed on the "–" of modified I-shaped patch are represented in 11.68 GHz. Strong interaction is produced between the "–" of modified I-shaped patch and middle surface. But the levels of interaction between the top and middle surfaces decreased when compared to that of the 7.29GHz frequency surface currents.

Furthermore, at 17.42GHz the different current directions are mainly observed the "–" of I-shaped patch itself. The interaction between the top and middle surface becomes pale when compared to that of 7.29Ghz and 11.68GHz and the bottom surface interactions become minimal as frequency increases where 7.29GHz interactions stand high of the three compared.

It can be concluded that the interaction between the top and middle surfaces becomes weak with the increase of frequency. Although the current directions are different between top and middle surfaces at 7.29, 11.68 and 17.42 GHz, the strong interaction is mainly produced at 7.29 GHz.

CHAPTER-5

DESIGN OF DOUBLE ARROW SHAPED FSS BASED POLARIZATION CONVERTOR

5.1 Introduction:

In this chapter the design of the single layer and multi layer unit cells with Arrow shaped metallic patch are discussed. The single layer unit cell has dielectric substrate as top layer and metallic sheet as bottom surfaces . An arrow shaped metallic patch using two squares is constructed on the top surface of the unit cell. Whereas in the double layer unit cell since it has an air gap, an air substrate is used . The top layer is similar to that of single layer unit cell where as the middle layer has complementary slot and a bottom metallic layer . The results of both unit cells are discussed and surface currents analysis are observed for the frequencies at which maximum reflection magnitudes are observed for both the unit cells**.**

5.1.1 Design specifications:

The essential parameters for the design are:

1. Polytef Substrate: The relative permittivity of polytef dielectric substrate is 2.65 and dielectric loss is 0.002. The design patterns are printed on both sides of dielectric substrate.

2. Dimensions of dielectric substrate: The height of the polytef dielectric substrate selected here is 3.0mm, sides are taken as 10mm and constructed as square.

3. Dimensions of Copper substrate: The height of the copper substrate selected here is 0.035mm, sides are taken as 10mm and constructed as square which acts as ground for the design.

5.1.2 Design Procedure:

Design of an arrow cell is done using HFSS. Here we create a box of material FR4 epoxy with substrate length of 10mm and substrate width of 3mm. Create a square1 of radius 3.4mm at the centre of the box. Create another square 2 of radius 2.2mm inside the square of radius 4.4mm. By subtracting square 2 from square1 it forms a ring. Now construct two squares from the centre of the squares of length 4.5mm and subtract the square from the ring. By substracting both the squares , two arcs are formed opposite to each other.

Take a polyline of type rectangle and width 2 mm placed along the axis and the edges of the polyline touches the arcs. Select the polyline and rotate along the z-axis with angle 135 degrees. By uniting both the arcs and rectangle it forms the arrow shaped cell. Select thicken sheet from sheet of thickness 0.035mm and the material of the sheet is copper. Create another box to provide ground of box width 0.035mm. Now select the box and provide the material of the box

as copper. Create a region of region type as absolute offset and provide +Z padding as 10mm. A floquet port is provided on the upper side of region which is faced at the front part of the unit cell.

Select analysis setup and mention the operating frequency as 8.25 GHZ (11.75GHz, 17.7GHz for corresponding values). After this add the frequency trace and do the validation check. All the cases pass significantly saying the design has no errors . After the validation check click the run button i.e analyse all option and the results will be observed.

5.1.3 Parameters Table:-

NAME	VALUE	UNIT
SL1	10	mm
W1	3	mm
L1	3.4	mm
L2	2.2	mm
W	2	mm
W2	0.035	mm
Sthick	0.035	mm
Sheetwid	0.035	mm
β1	45	deg
θ	90	deg

5.1.4 Parametric Results: -

In the parametric sweep, we simulate the ant design of different values of a parameter. This is useful in selecting the desired parameter value for the design. By selecting the best results in a parametric sweep, with those parameters values, we will optimize for the best results.

L1 sweep: -

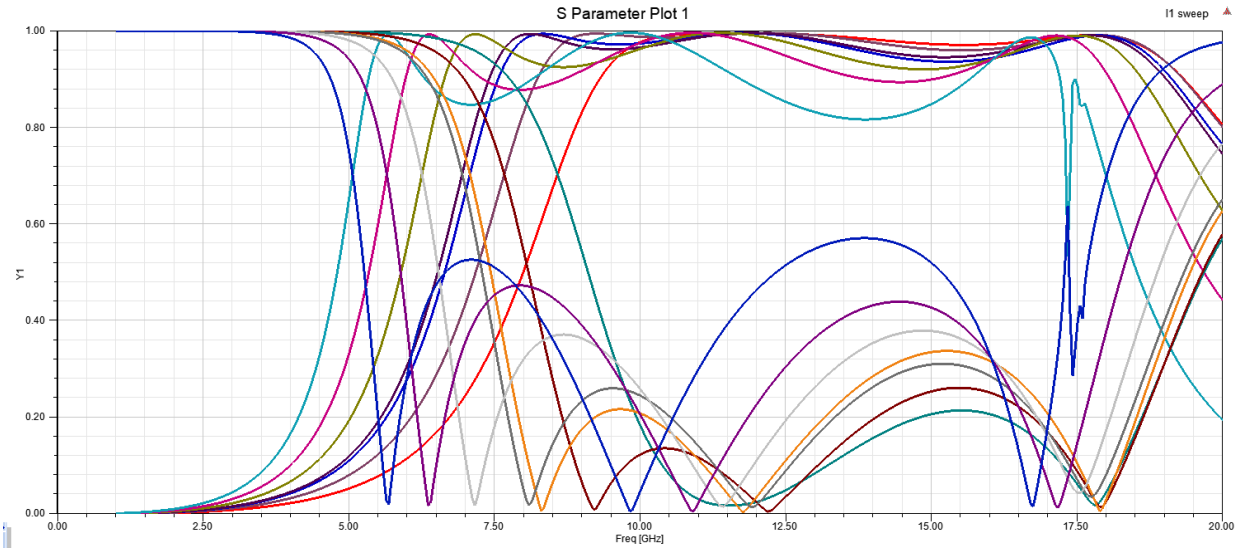

Fig 5.1 Reflection magnitudes for different L1 values under normal x-polarized incident waves.

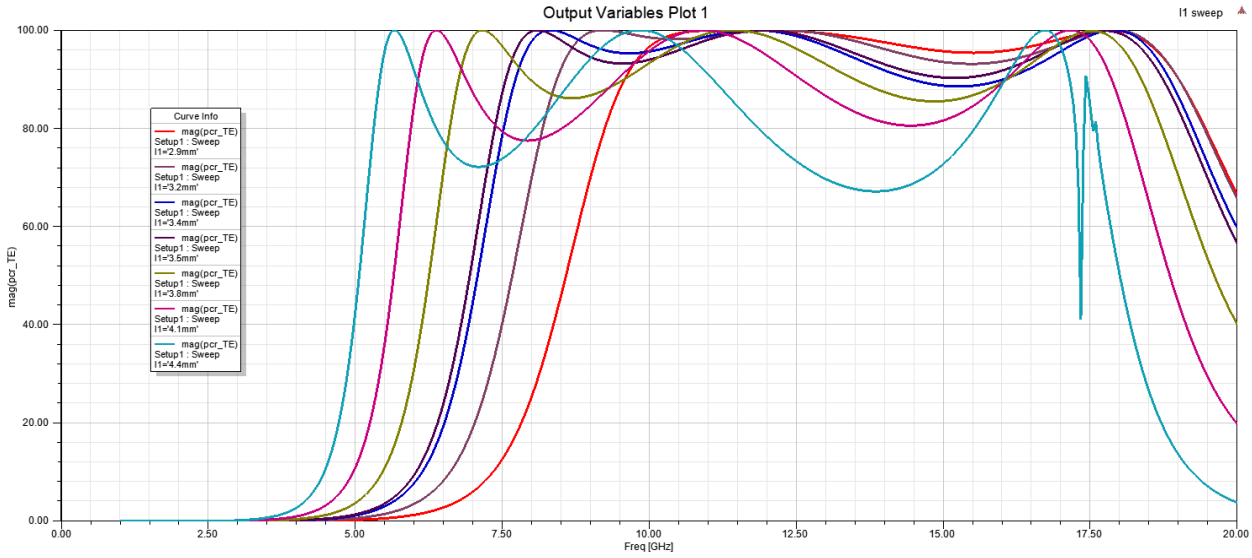

Fig 5.2 PCR for different L1 values under normal x-polarized incident waves.

By using Parametric Sweep for the variable L1 from 4.4mm to 2.9mm at a decrease of 0.3mm per step the required graph is obtained for single-layer reference unit

L2 sweep:

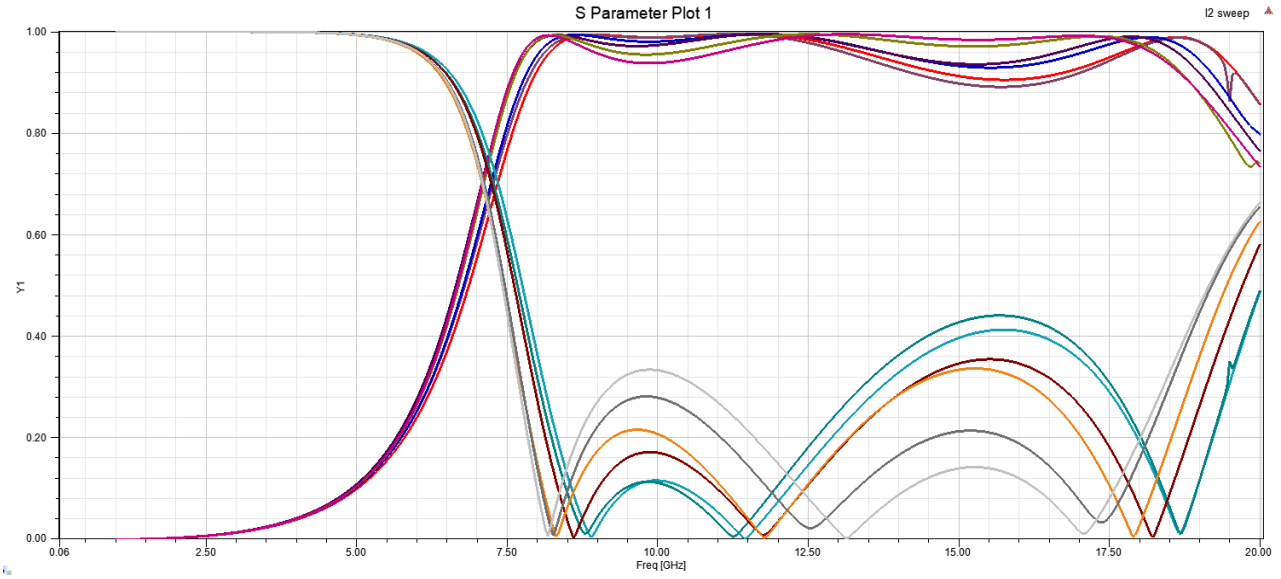

Fig 5.3 Reflection magnitudes for different L2 values under normal x-polarized incident waves.

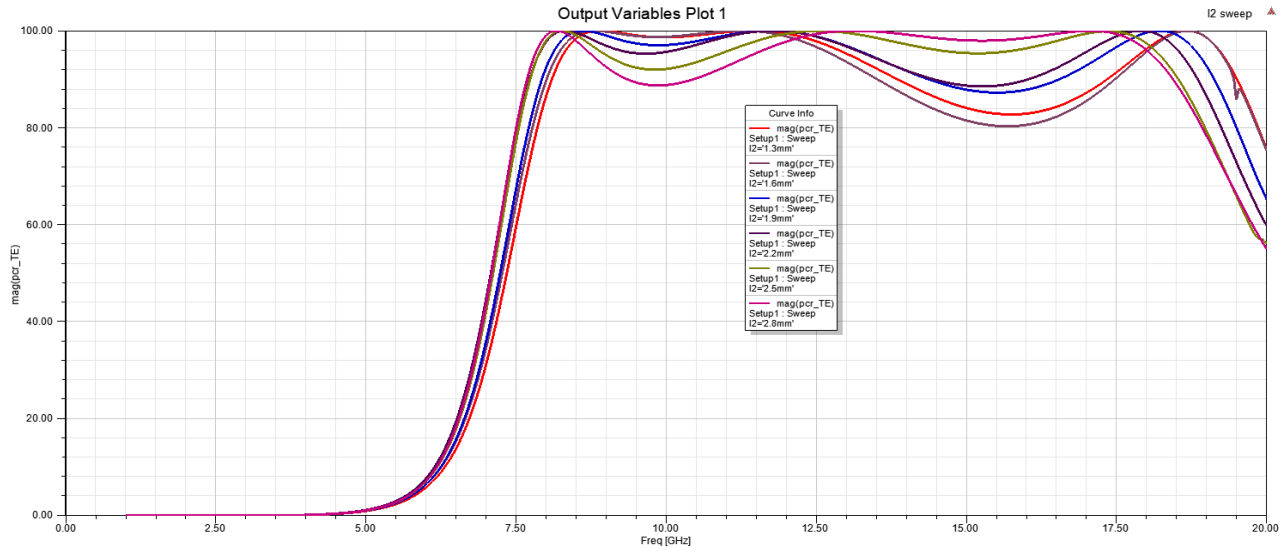

Fig 5.4 PCR for different L2 values under normal x-polarized incident waves.

By using Parametric Sweep for the variable L2 from 2.8mm to 1.3mm at a decrease of 0.3mm per step the required graphs are obtained for single-layer reference unit with arrow patch.

With the decrease of L1 and L2, the peak values of cross-polarization at 8.25 GHz and 11.75 GHz shift toward high-frequency range while the peak value at 17.7 GHz is almost maintained because the peak values of cross-polarization at 17.7 GHz is caused by Arrow-shaped patch itself, the interaction between the two structures of modified arrow-shaped patch becomes

strong when the length of two "|" structures are decreased. Thus, the peak value at 17.7 GHz is almost maintained.

Also, by changing the L1 values we can observe wide range of changes in the reflection magnitude when compared that to that of the L2 variable thus indicating that the outer square area plays major role in deciding the reflection magnitude and PCR ranges in the design. From above parameters investigations, the current distributions analysis of proposed structures is reasonable.

Width sweep: -

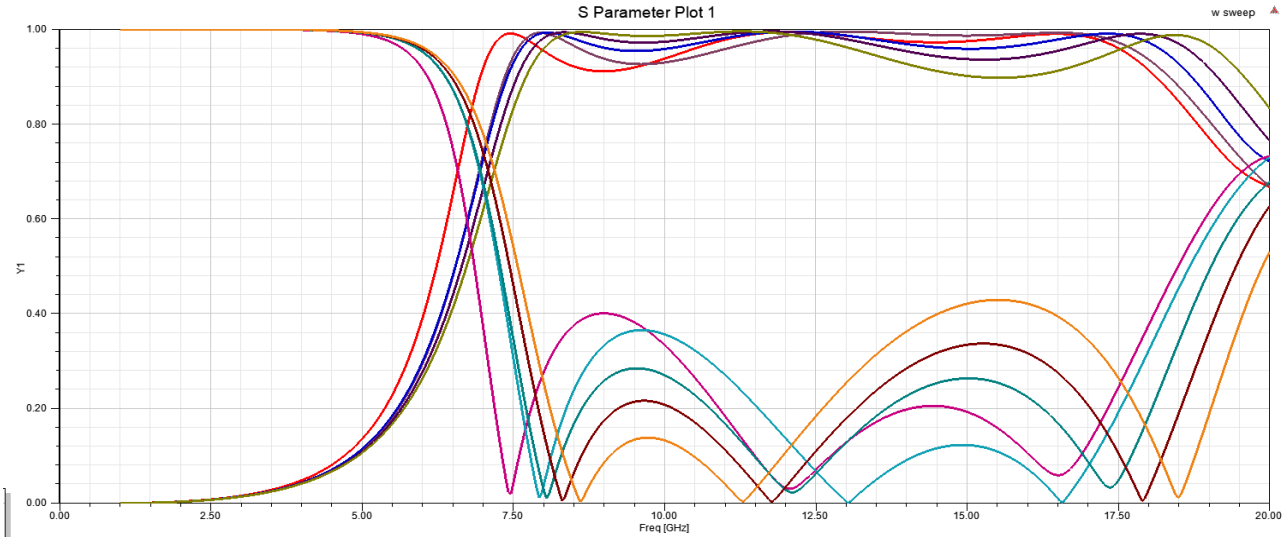

Fig 5.5 Reflection magnitudes for different W values under normal x-polarized incident waves.

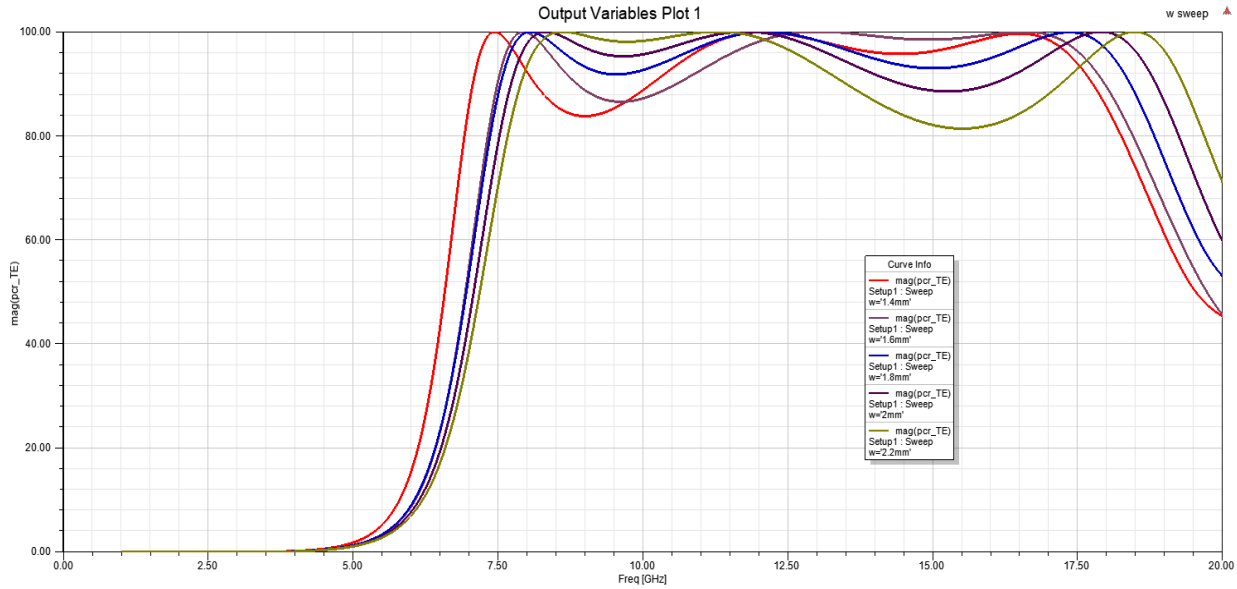

Fig 5.6 PCR for different W values under normal x-polarized incident waves.

By using Parametric Sweep for the width W that represents the width of the polyline used in between the arrow shaped arcs and united with them from 2.8mm to 1.3mm .

Also by changing the W values we can observe wide range of changes in the reflection magnitude and PCR efficiency, as the size of the width increases the reflection magnitude increases.

5.1.5 Final design

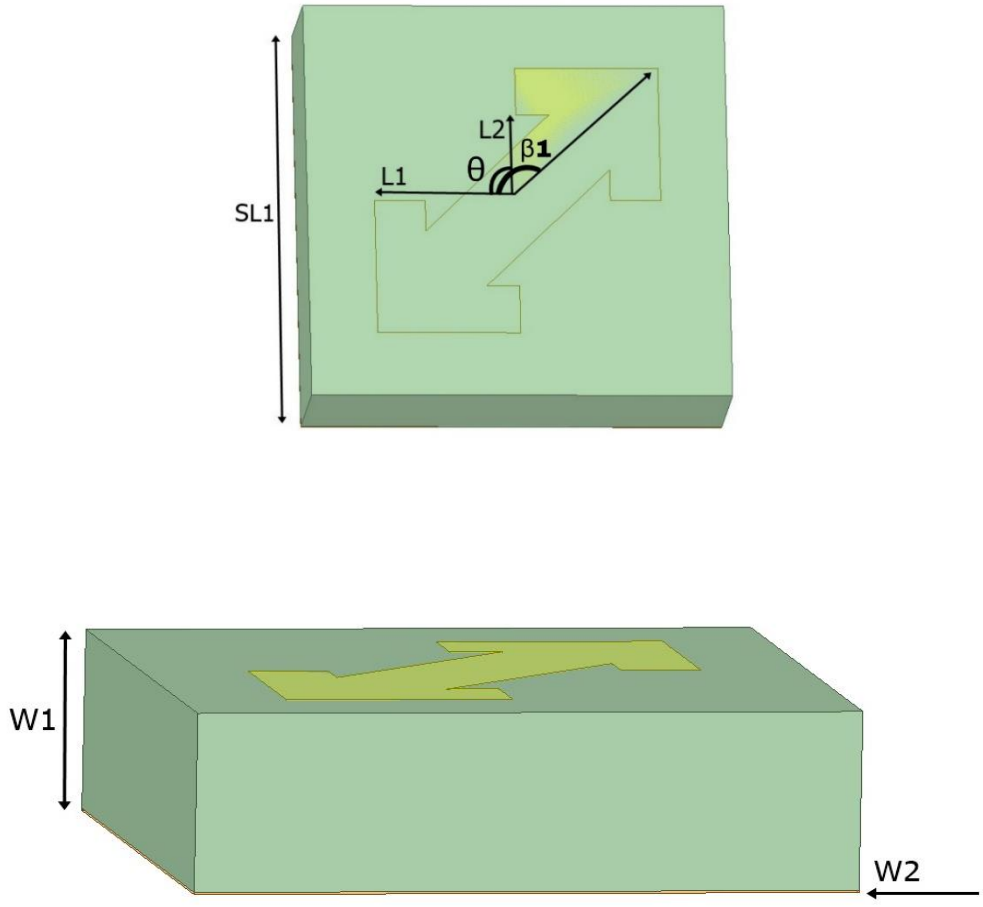

Fig 5.7 single Layer unit cell with Arrow shaped patch

5.1.6 Simulation and Results of Unit cell design:

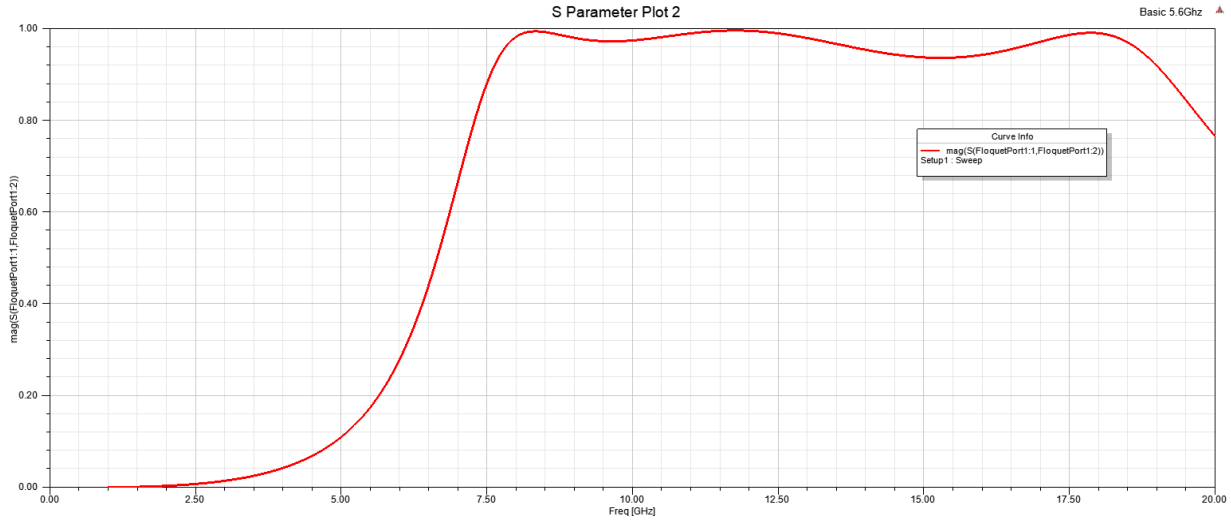

Fig 5.8 Refection magnitudes of single-layer reference unit

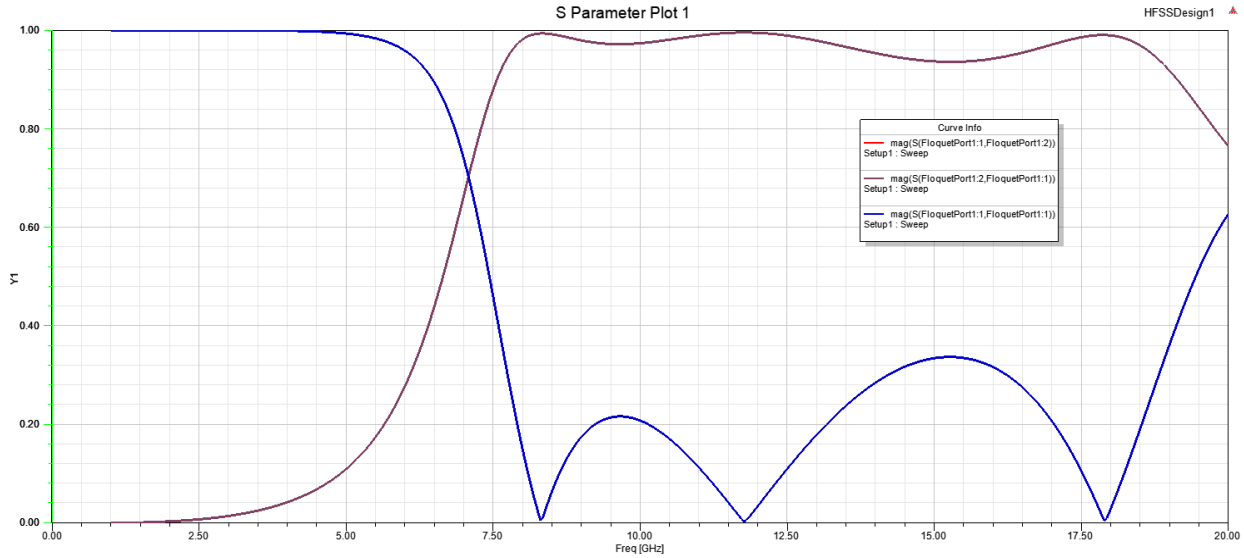

Fig 5.9 Refection magnitudes of proposed units for different β1 and β2 under normal x-polarized incident waves.

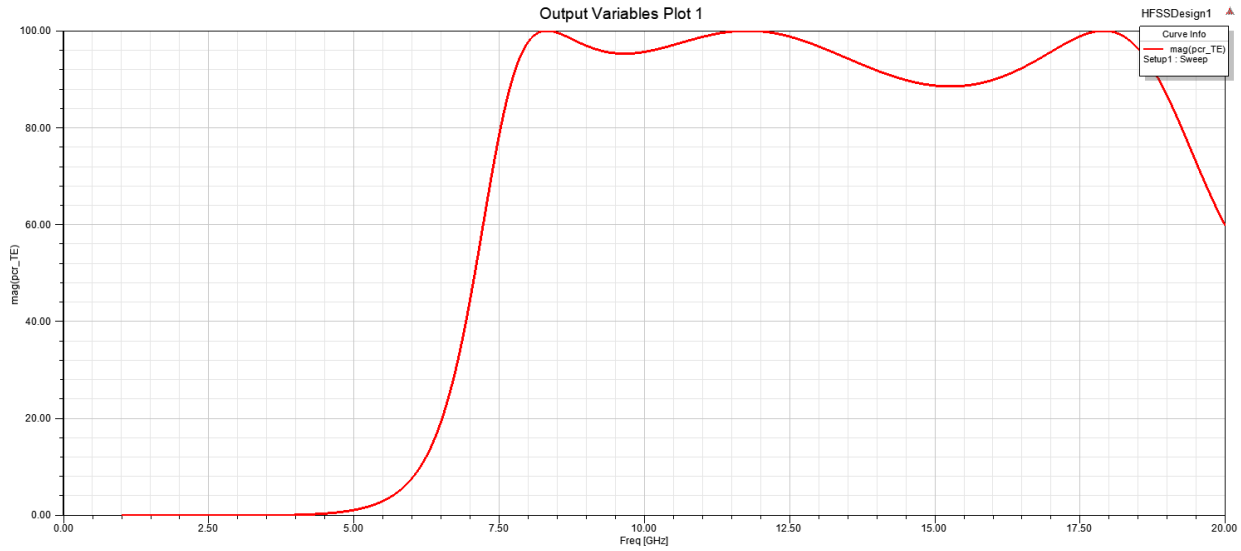

Fig 5.10 PCR of single-layer reference unit

The figure 5.8 represents the refection magnitudes of single-layer reference unit whereas Figure 5.10 represents the PCR plot. Most incident waves are reflected to its orthogonal counterparts. Taking a further step, the reflection magnitudes of proposed unit and its mirror one (i.e., the proposed unit rotates 90°) are investigated in detail for normal incidence. The reflection magnitudes of the mirror unit coincide well with the proposed one.

The figure 5.9 represents reflection magnitudes of proposed units for different β1 and β2 under normal x-polarized incident waves for single-layer reference unit. The graph in red represents the cross-polarization reflection magnitude when β1 is 45° and β2 is 135° whereas the violet graph represents the co-polarization reflection magnitude when β1 is 135° and β2 is 45°. The values of reflection magnitudes and PCR are more than 0.85 from 5.1 to 19.5 GHz.

The figure 5.10 represents PCR plot for single layer reference unit cell with arrow shaped patch. The PCR plot shows high efficiency potential of the designed unit cell as the value of the PCR remain more than 0.95 i.e., indicating 95% efficient in converting the incident waves to required cross polarized waves over a wide frequency range of 9.3 to 18 GHz.

Surface Currents: -

For 8.25GHz: -

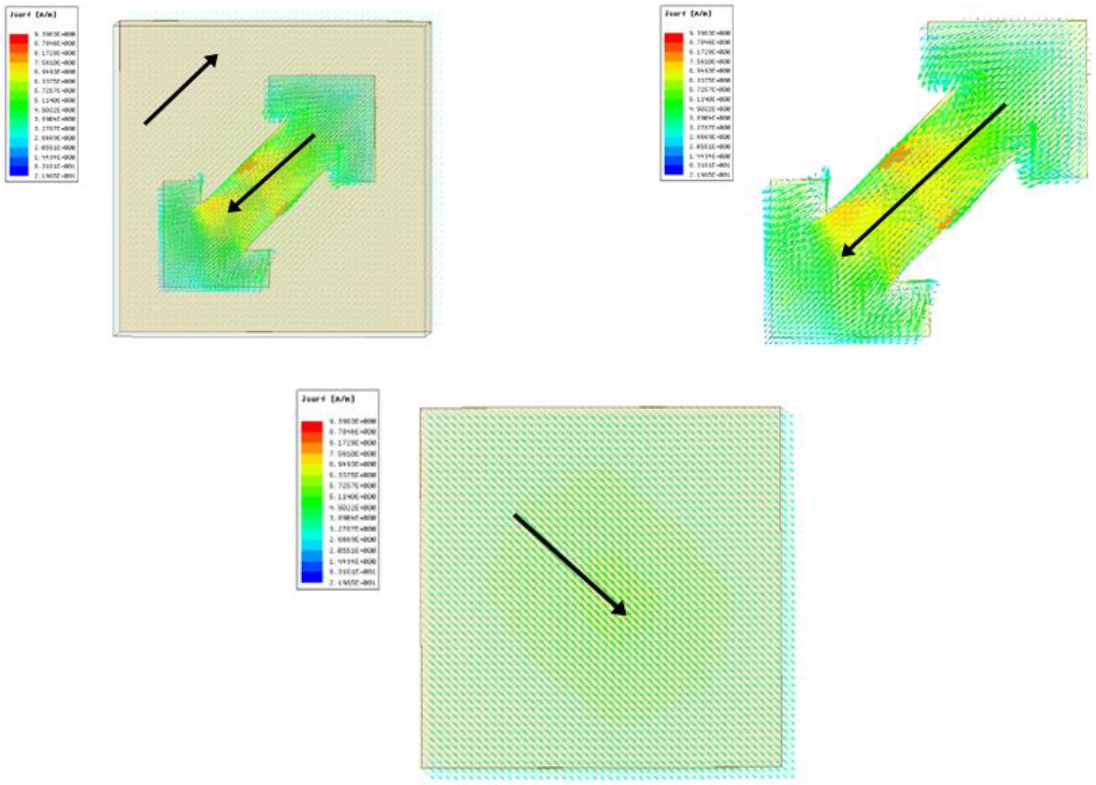

Fig 5.11 Current distributions for proposed units at 8.25 GHz.

For 11.75 GHz: -

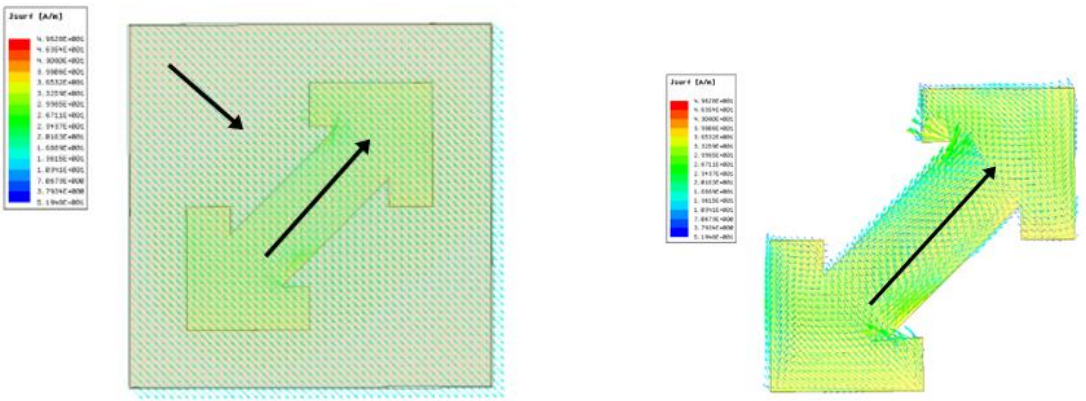

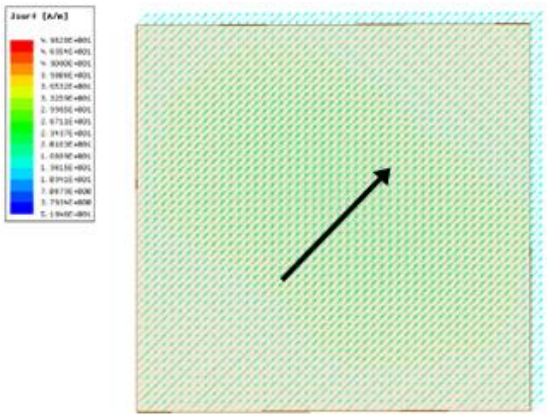

Fig 5.12 Current distributions for proposed units at 11.75 GHz.

For 17.7Ghz: -

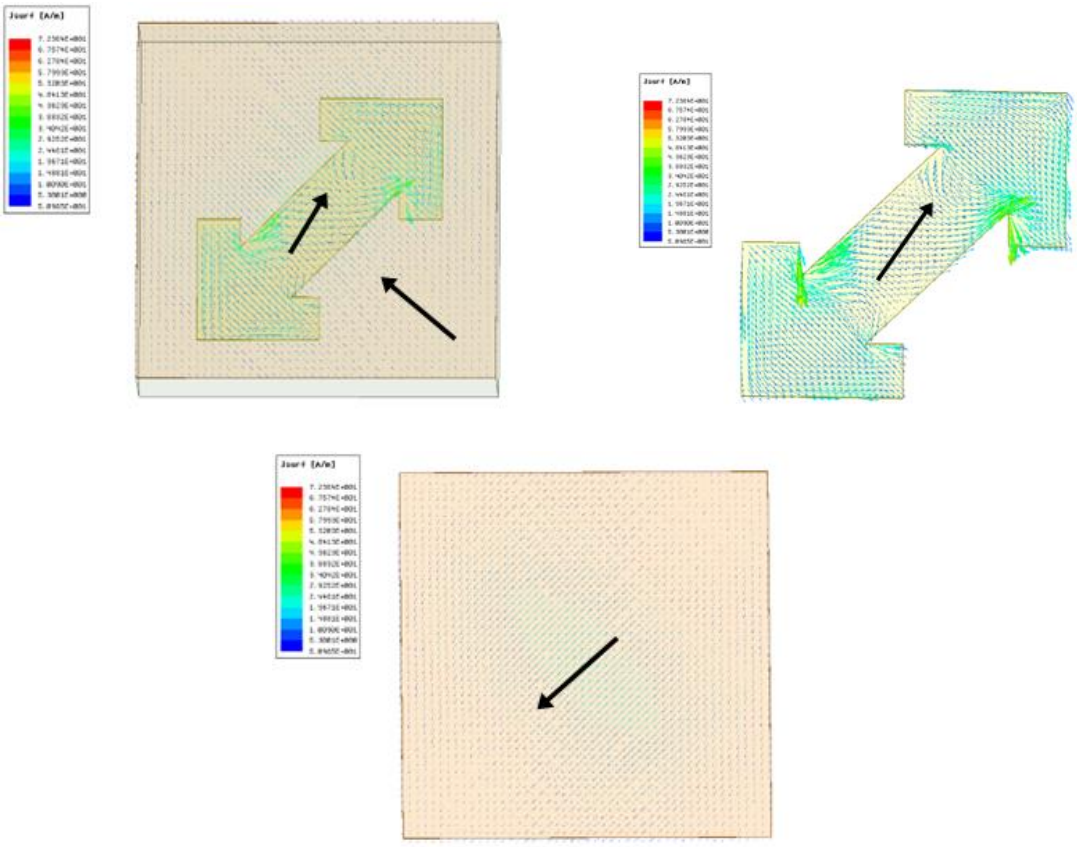

Fig 5.13 Current distributions for proposed units at 17.7 GHz.

The above figures represent the surface currents distribution for 8.25GHz, 11.75GHz and 17.7GHz frequencies of Single layer reference unit cell with Arrow shaped patch. To further reveal operation mechanism of proposed unit, current distributions of proposed unit at 8.25, 11.75 and17.7 GHz (peak reflection magnitude frequency) were investigated. Intense induced current is observed on the top and bottom surfaces at three frequencies, in 8.25Ghz frequency

the current directions on the top surface are completely different from those on the bottom surface. Strong interaction is produced between the top and bottom surfaces.

However, the different current directions are mainly observed on the "–" of modified arrow-shaped patch are represented in 11.75 GHz. Strong interaction is produced between the "–" of modified arrow-shaped patch and bottom surface. But the levels of interaction between the top and bottom surfaces decreased when compared to that of the 8.25GHz frequency surface currents. Furthermore, at 17.7GHz the different current directions are mainly observed the "–" of arrow-shaped patch itself. The interaction between the top and bottom surface becomes pale when compared to that of 8.25Ghz and 11.75GHz where 8.25GHz interactions stand high of the three compared.

It can be concluded that the interaction between the top and bottom surfaces becomes weak with the increase of frequency. Although the current directions are different between top and bottom surfaces at 8.25, 11.75 and 17.7 GHz, the strong interaction is mainly produced at 8.25 GHz.

5.2 Double-layer complementary unit cell with arrow shaped patch:

5.2.1 Design Specifications:

The essential parameters for the design are:

1.Polytef Substrate: Polytef dielectric substrate and air substrate are utilized to form the double-layer structure. The relative permittivity of polytef dielectric substrate is 2.65 and dielectric loss is 0.002. The design patterns are printed on both sides of dielectric substrate.

2. Dimensions of of dielectric substrate: The height of the polytef dielectric substrate selected here is 3.0mm and sides are taken as 10mm and constructed as square.

3. Dimensions of Copper substrate: The height of the copper substrate selected here is 0.035mm, sides are taken as 10mm and constructed as square which acts as ground for the design.

4. Dimensions of Air substrate: The height of the air substrate selected here is 3.0mm and sides are taken as 10mm and constructed as square

5.2.2 Design Procedure:

Design of a multilayer arrow is done using HFSS. Create a box of material FR4 epoxy of sublen 10mm and sub width 3mm. Create a square 1 of radius 4.5mm at the centre of the box. Create another square 2 of radius 2.8mm. By subtracting square 2 from square 1 it forms a square ring.Construct two squares from the centre of the squares of length 4.5mm and subtract the square from the square ring. By subtracting both the squares , two arrows are formed. Take a polyline of type rectangle and width 1.6mm placed along the axis and the edges of the polyline touches the arrows. Select the polyline and rotate along the z-axis with angle 135 degrees. Now unite both the arrows and rectangle to form the arrow shaped cell. Select the arrow shaped cell and select thicken sheet from sheet of thickness 0.035mm and the material of the sheet is copper.Create another box to provide ground of box width -0.035mm. Now select the box and provide the material of the box as copper.Create a square 1 of radius 4.4mm and square 2 of radius 2.8mm at the back side i.e on the ground. Select square and square 2 and substract square 2 from square 1 .This forms a square ring.Construct two squares from the centre of the squares of length 4.5mm and subtract the square from the square ring. By substracting both the squares , two arrows are formed. Take a polyline of type rectangle and width 1.6mm placed along the axis and the edges of the polyline touches the arrows. Now rotate the polyline with angle 45 degrees and select polyline and both the arrows . Now unite both of them. Select the arrow shaped cell and select thicken sheet from sheet of thickness 0.035mm and the material of the sheet is copper.Select ground and arrow shaped material and substract arrow material from the ground.Create another box of width 3.0mm upon the copper metal and assign air to it .Create another box of width 0.035mm and assign copper to it. Create region of region type as absolute offset and provide +Z padding as 10mm.Create a floquet port on the upper side of region which is faced at the front part of the unit cell.Now click analysis and add solution setup and provide frequency as 8.16GHZ. Go to setup1 and add frequency sweep and provide range from 1 to 20GHZ. Now do validation check and analyse all and observe the results obtained.

5.2.3 Parameters Table:-

NAME	VALUE	UNIT
SL1	10	mm
W1	3	mm
L1	3.4	mm

L2	2.2	mm
W	2	mm
W2	0.035	mm
Sthick	0.035	mm
Sheetwid	0.035	mm
β1	45	deg
θ	90	deg
W3	3	mm

5.2.4 Parametric Results: -

In the parametric sweep, we simulate the ant design of different values of a parameter. This is useful in selecting the desired parameter value for the design. By selecting the best results in a parametric sweep, with those parameters values, we will optimize for the best results.

L1 Sweep: -

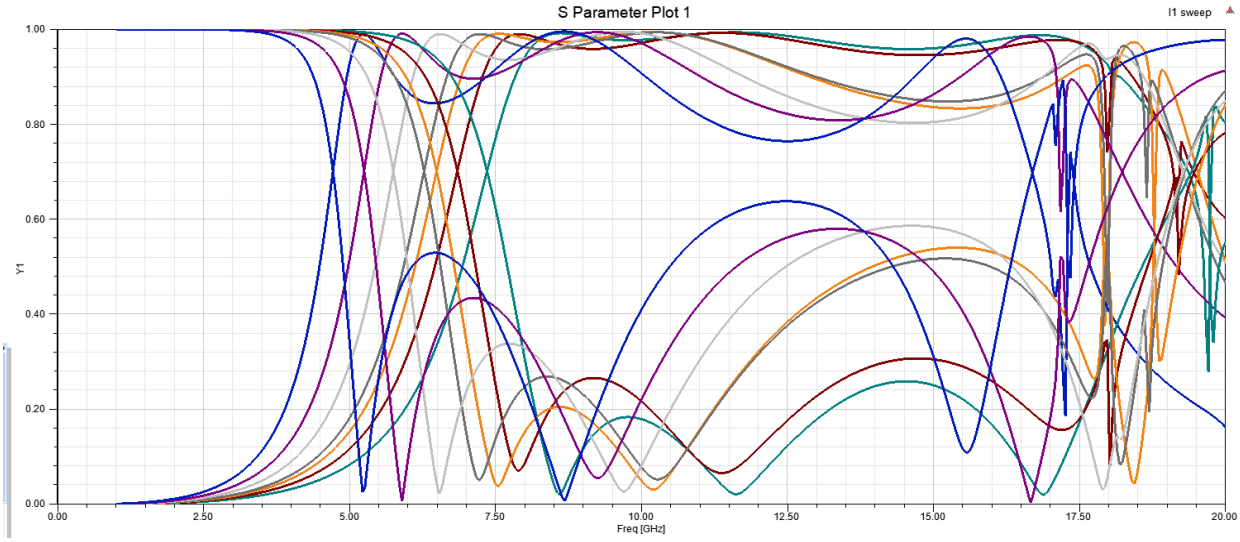

Fig 5.14 Reflection magnitudes for different L1 values under normal x-polarized incident waves

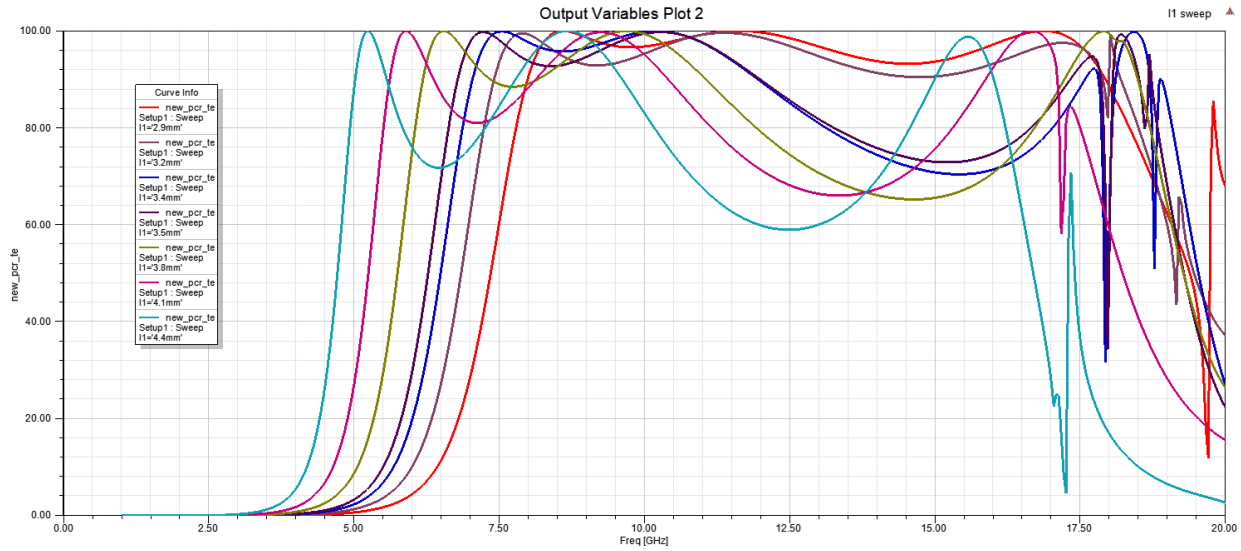

Fig 5.15 PCR for different L1 values under normal x-polarized incident waves.

By using Parametric Sweep for the variable L1 from 4.4mm to 2.9mm at a decrease of 0.3mm per step the required graph is obtained for double-layer proposed unit cell.

L2 Sweep: -

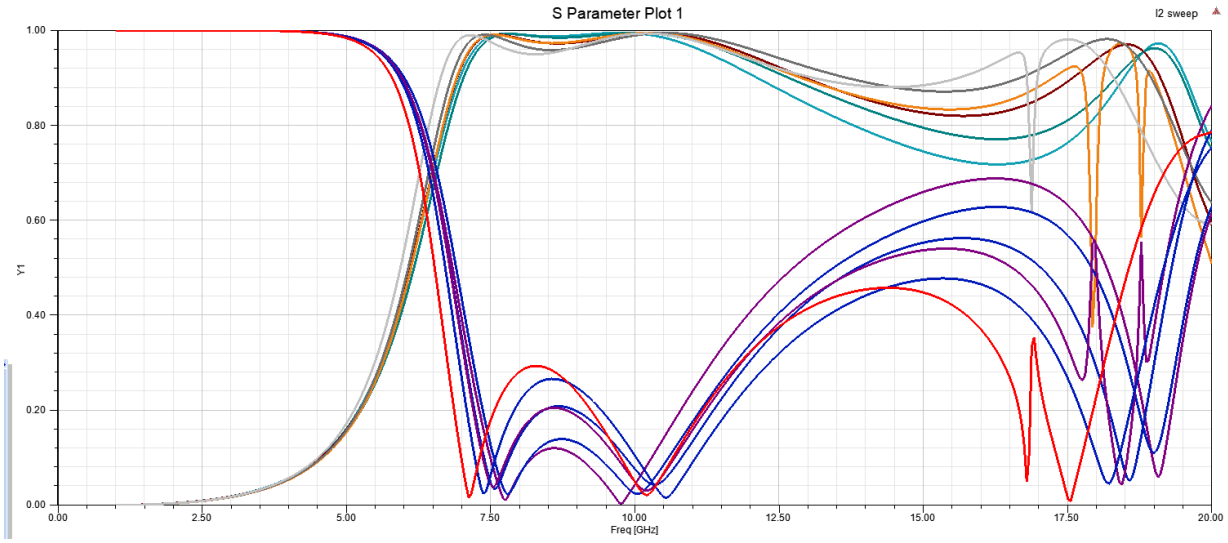

Fig 5.16 Reflection magnitudes for different L2 values under normal x-polarized incident waves.

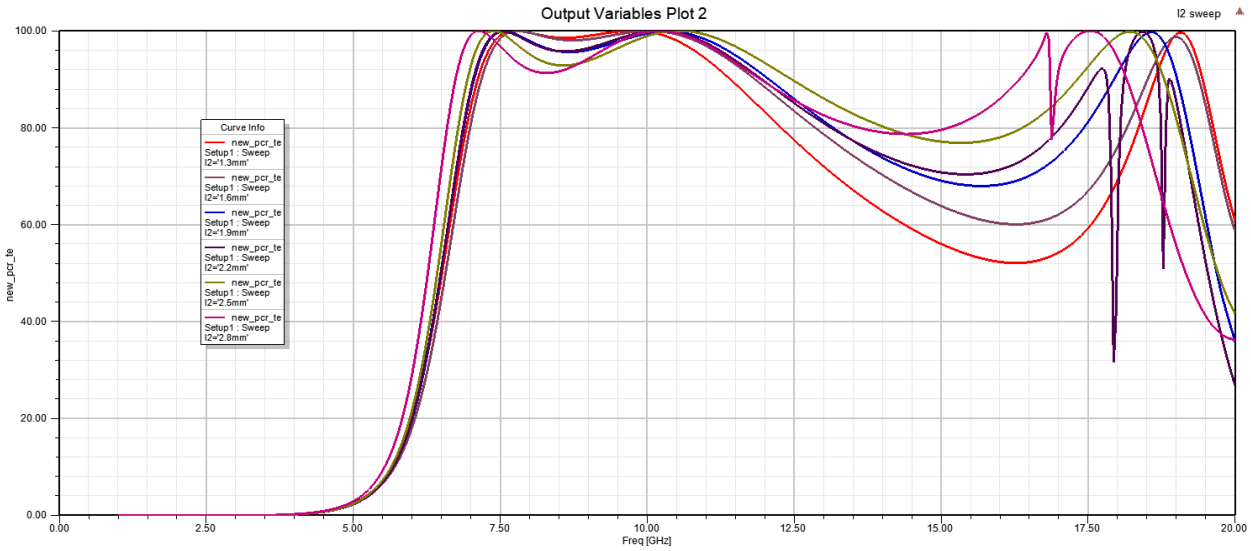

Fig 5.17 PCR for different L2 values under normal x-polarized incident waves.

By using Parametric Sweep for the variable L2 from 2.8mm to 1.3mm at a decrease of 0.3mm per step the required graph is obtained for double-layer proposed unit cell with arrow patch.

With the decrease of L1 and L2, the peak values of cross-polarization at 8.16 GHz and 11.58 GHz shift toward high-frequency range while the peak value at 17.52 GHz is almost maintained because the peak values of cross-polarization at 17.52 GHz is caused by Arrow-shaped patch itself, the interaction between the two structures of modified arrow-shaped patch becomes strong when the length of two "|" structures are decreased.

Also, by changing the L1 values we can observe wide range of changes in the reflection magnitude when compared that to that of the L2 variable thus indicating that the outer square area plays major role in deciding the reflection magnitude ranges in the design. From above parameters investigations, the current distributions analysis of proposed structures is reasonable

Width Sweep: -

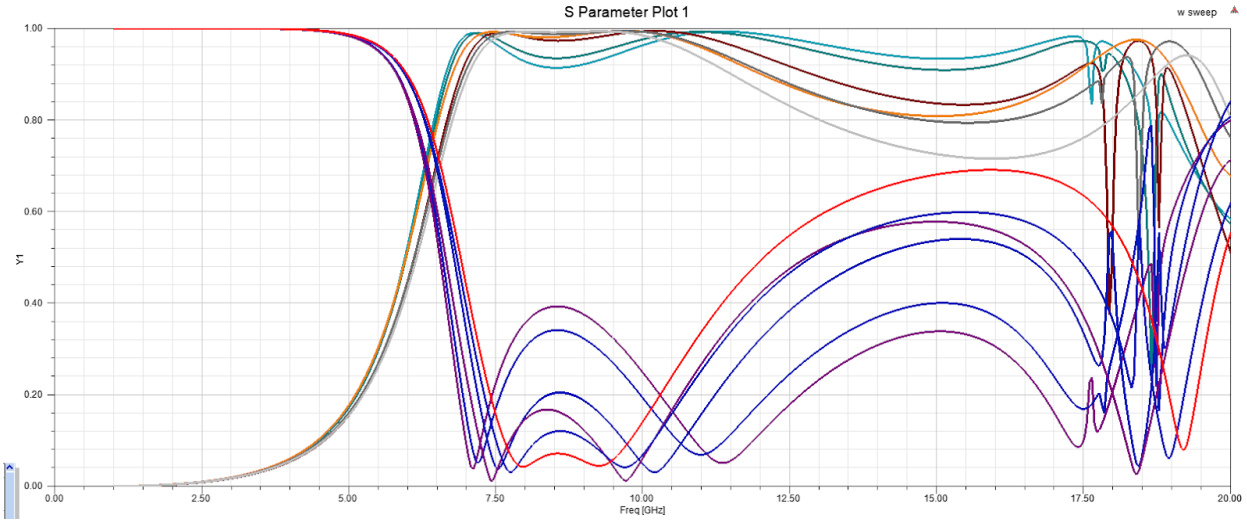

Fig 5.18 Reflection magnitudes for different W values under normal x-polarized incident waves.

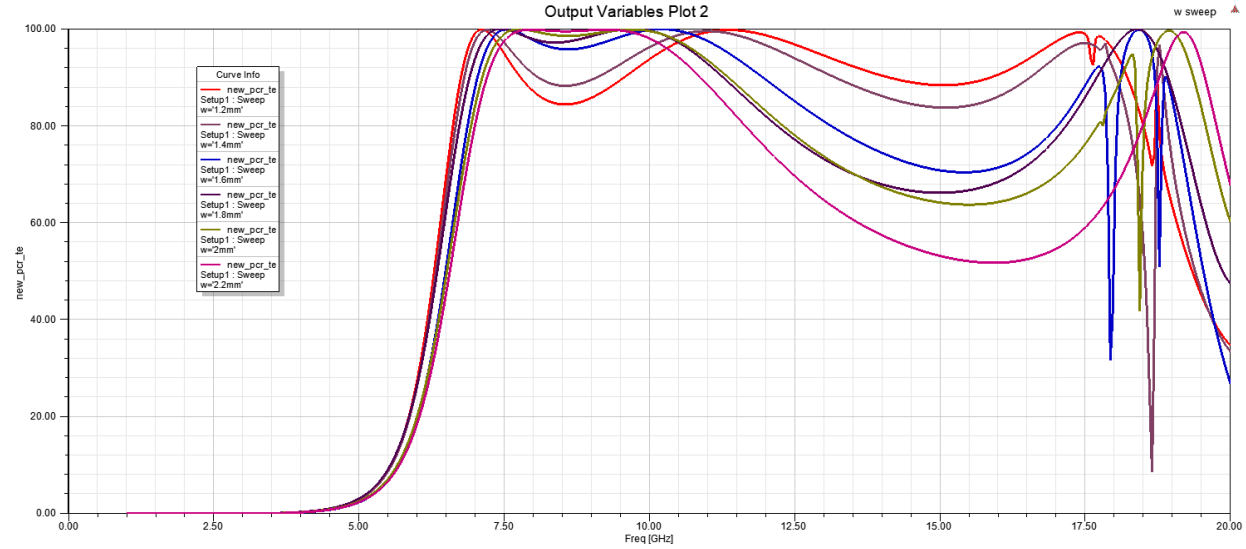

Fig 5.19 PCR for different W values under normal x-polarized incident waves.

By using Parametric Sweep for the width W that represents the width of the polyline used in between the arrow shaped arcs and united with them from 2.8mm to 1.3mm at a decrease of 0.3mm per step the required graph is obtained for double-layer proposed unit cell with arrow patch.

Also, by changing the W values we can observe wide range of changes in the reflection magnitude, as the size of the width increases the magnitude of the reflection magnitude increases thus indicating strong surface currents induced indicating that the width of the

polyline used to unite both the arrow shaped arcs plays a major role. From above parameters investigations, the current distributions analysis of proposed structures is reasonable.

5.2.5 Final design

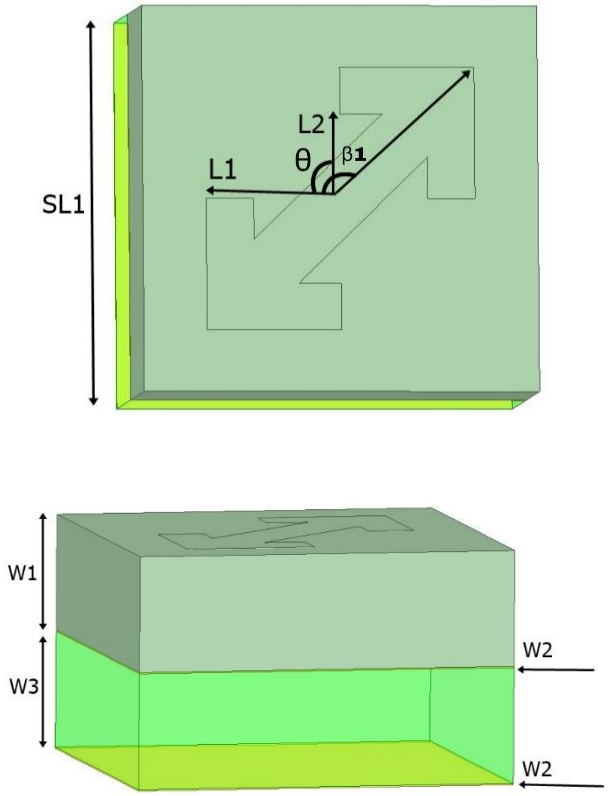

Fig 5.20 Double-layer complementary unit cell with arrow shaped patch

5.2.6 Simulation and Results of Unit cell design:

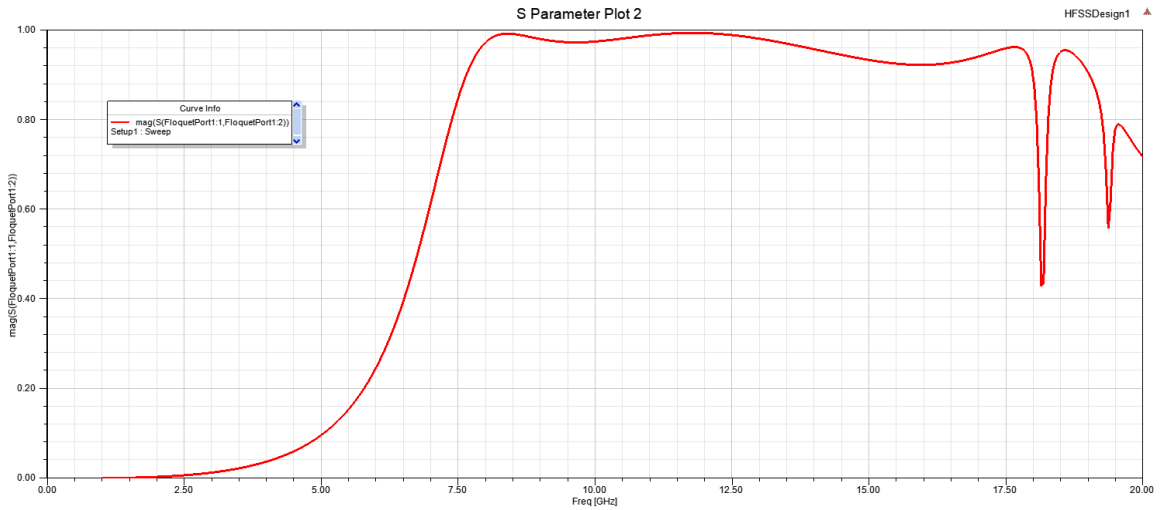

Fig 5.21 Refection magnitudes of double-layer proposed unit cell

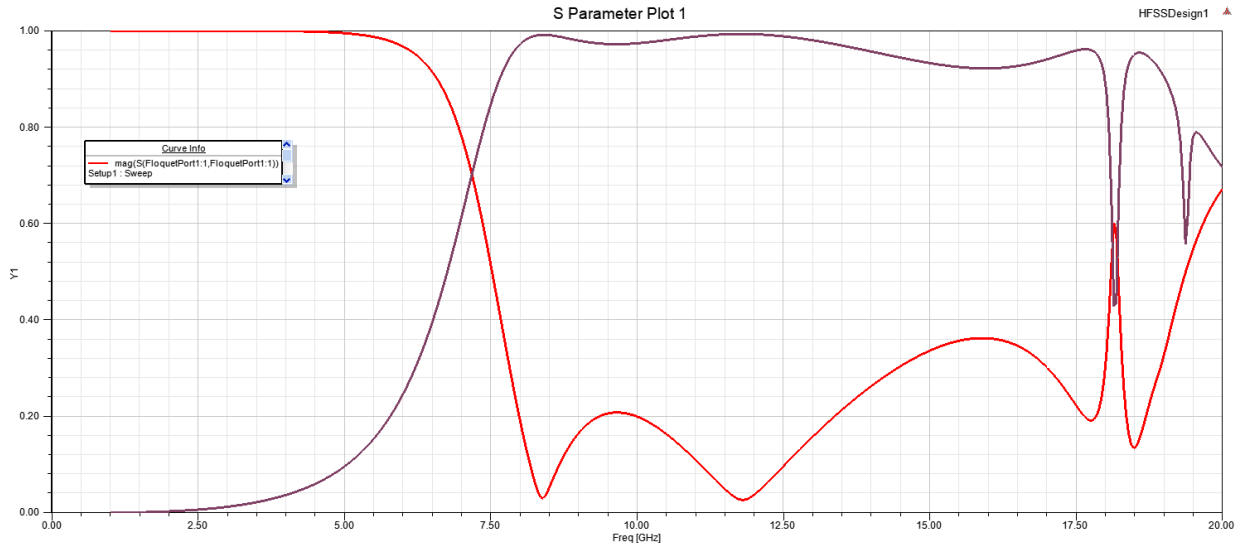

Fig 5.22 Refection magnitudes of proposed units for different β1 and β2 under x-polarized incident waves

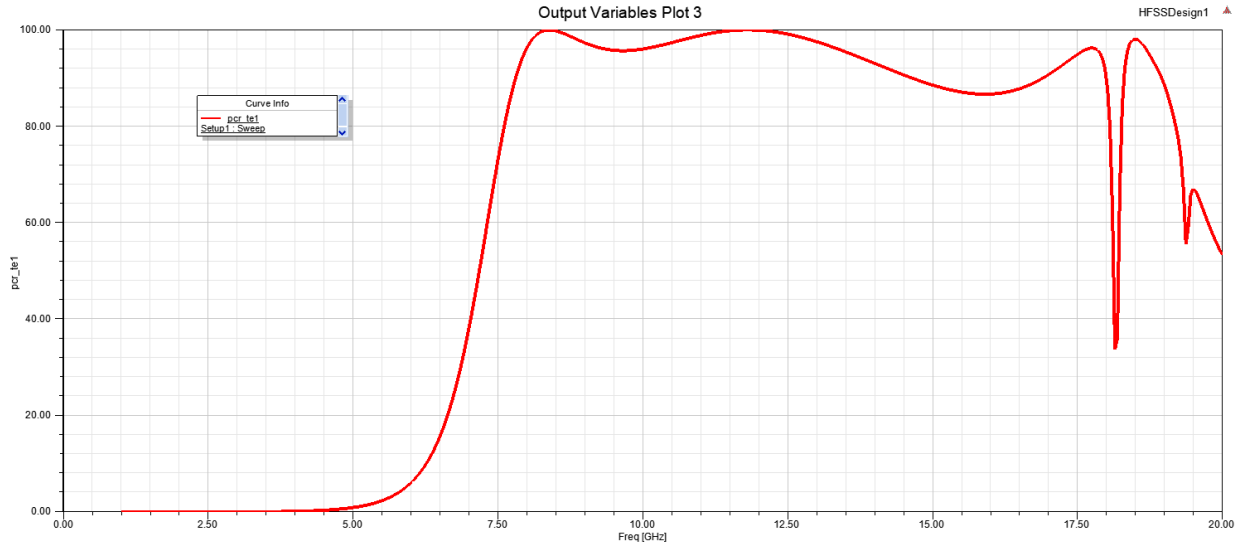

Fig 5.23 PCR of double-layer proposed unit cell.

The above graph represents the refection magnitudes of double-layer proposed unit cell. Most incident waves are reflected to its orthogonal counterparts. Taking a further step, the reflection magnitudes of proposed unit and its mirror one (i.e., the proposed unit rotates 90°) are investigated in detail for normal incidence. The reflection magnitudes of the mirror unit coincide well with the proposed one. Figure 5.23 shows PCR plots of the design where an efficiency of over

The above graph represents reflection magnitudes of proposed units for different β1 and β2 under normal x-polarized incident waves for double-layer proposed unit cell. The graph in red represents the cross-polarization reflection magnitude when β1 is 45° and β2 is 135°

whereas the violet graph represents the co-polarization reflection magnitude when β1 is 135° and β2 is 45°. The values of reflection magnitudes are more than 0.85 from 5.1 to 19.5 GHz.

Multilayer arrow surface currents:

For 8.16GHz: -

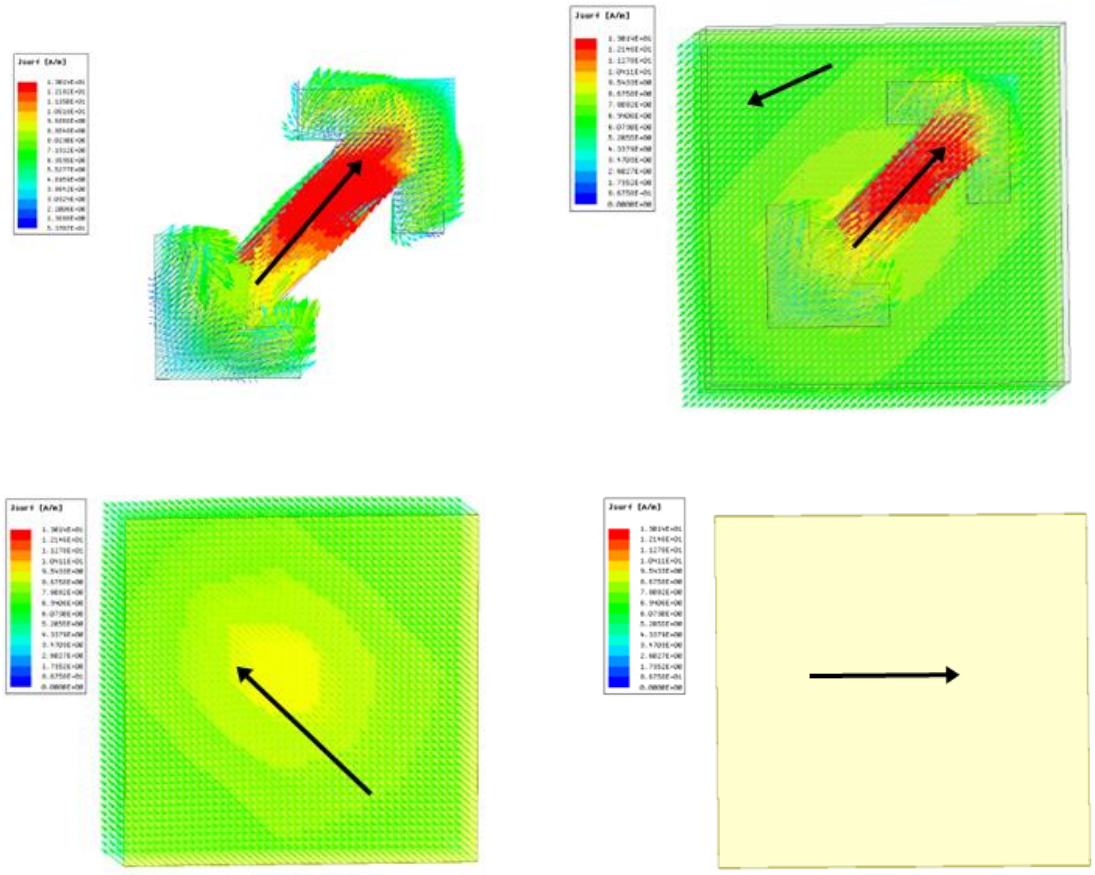

Fig 5.24 Current distributions for proposed units at 8.16 GHz.

For 11.58GHz: -

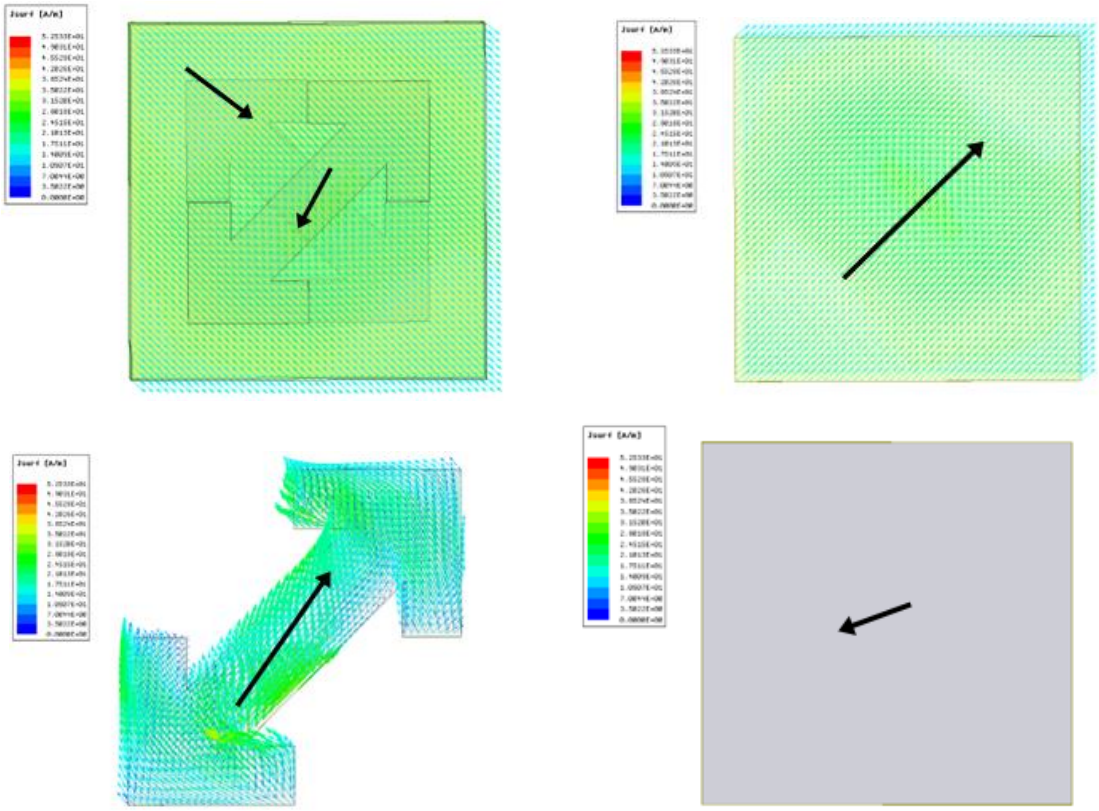

Fig 5.25 Current distributions for proposed units at 11.58 GHz

For 17.52GHz: -

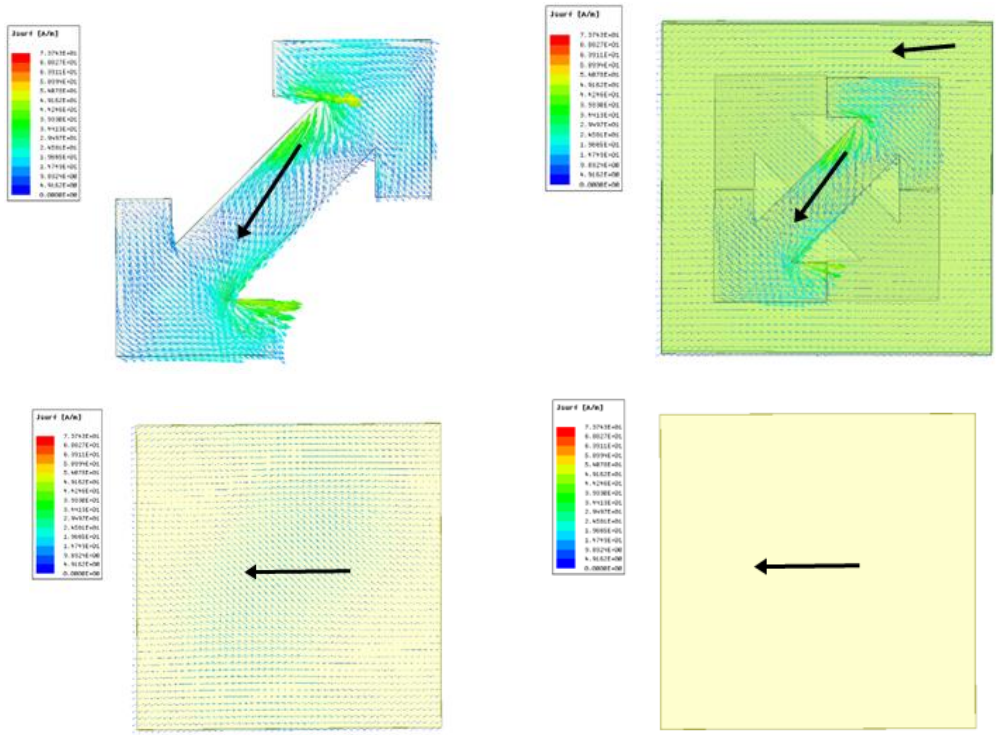

Fig 5.26 Current distributions for proposed units at 17.52 GHz.

The above figures represent the surface currents distribution for 8.16GHz, 11.58GHz and 17.52GHz frequencies of double layer Complementary unit cell with arrow shaped patch. To further reveal operation mechanism of proposed unit, current distributions of proposed unit at 8.16, 11.58 and17.52 GHz (peak reflection magnitude frequency) were investigated. Intense induced current is observed on the top, middle and bottom surfaces at three frequencies,

In 8.16Ghz frequency the current directions on the top surface are completely different from those on the middle and bottom surface. Strong interaction is produced between the top and bottom surfaces whereas light interactions were produced with that of the bottom surface.

However, the different current directions are mainly observed on the "–" of modified arrow-shaped patch is represented in 11.58 GHz. Strong interaction is produced between the "–" of modified arrow-shaped patch and middle surface. But the levels of interaction between the top and middle surfaces decreased when compared to that of the 8.16GHz frequency surface currents.

Furthermore, at 17.52GHz the different current directions are mainly observed the "–" of arrow-shaped patch itself. The interaction between the top and middle surface becomes pale when compared to that of 8.16Ghz and 11.58GHz and the bottom surface interactions become minimal as frequency increases where 8.16GHz interactions stand high of the three compared.

It can be concluded that the interaction between the top and middle surfaces becomes weak with the increase of frequency. Although the current directions are different between top and middle surfaces at 8.16, 11.58 and 17.52 GHz, the strong interaction is mainly produced at 8.16 GHz.

CONCLUSION

The reference single layer unit cell and the proposed double layer complementary unit cell for both I-shaped patch and arrow shaped patch are designed and simulated using HFSS version 19.0.0. We proposed an ultra-wideband, highly efficient, wide angle cross polarization converter reflective meta surface. A broadband cross-polarization converter was achieved for a wide frequency of 5.1 to 17 GHz. Numerical simulations were performed to validate the performance and justify the claim of a large operational bandwidth.

To demonstrate the physical mechanism behind the polarization conversion, the reflected amplitude and surface current distribution plots were presented for different resonance frequencies at the top and bottom metallic layers for single layer unit cells and top, middle and bottom metallic layers for double layer complementary unit cells. In addition, the polarization converter showed a stable performance over a wide range of oblique incidence angles. Resultantly, the proposed meta surface behaved like a high impedance surface and reflected the incidence wave in its orthogonal counterpart. In the low−frequency spectrum, the conversion efficiency was also above 90%. The proposed converters have many potential applications, including satellite communication, radar cross−section reduction, and navigation systems.

REFERENCES

1. Yuejun Zheng, Yulong Zhou, Jun Gao, Xiangyu Cao, Huanhuan Yang, Sijia Li , Liming Xu, Junxiang Lan & Liaori Jidi ; Ultra-wideband polarization conversion metasurface and its application cases for antenna radiation enhancement and scattering suppression. Springer (2017)

2. Tauqir Ahmad Arbab Abdur Rahim , Rana Muhammad Hasan Bilal, Adnan Noor, Husnul Maab ,Muhammad Ashar Naveed , Abdullah Madni , Muhammad Mahmood Ali and Muhammad Ahsan Saeed; Ultrawideband Cross-Polarization Converter Using Anisotropic Reflective Metasurface. Electronics (2022), 11, 487.

3. Cui, T. J., Smith, D. R. & Liu, R. P. Metamaterials: theory, design, and applications, Springer Science & Business Media, New York (2009).

4. Yuan, Y. Y., Ding, X. M., Zhang, K. & Wu, Q. Planar efficient meta surface for vortex beam generating and converging in microwave region. IEEE T. Magn. **53**, 2500204 (2017).

5. Wan, X., Qi, M., Chen, T. & Cui, T. J. Field-programmable beam reconfiguring based on digitally-controlled coding metasurface. Sci.Rep. **6**, 20663 (2016).

6. Li, Y. et al. Transmission-type 2-bit programmable meta surface for single-Sensor and single-frequency microwave imaging. Sci. Rep.**6**, 23731 (2016).

7. Cui, T. J., Qi, M., Wan, X., Zhao, J. & Cheng, Q. Coding metamaterials, digital metamaterials and programmable metamaterials. Light: Sci. Appl. **3**, 1–8 (2014).

8. Aieta, F. et al. Out-of-plane reflection and refraction of light by anisotropic optical antenna meta surfaces with phase discontinuities. Nano Lett. **12**, 1702–1706 (2012).

9. Landy, N. I., Sajuyigbe, S., Mock, J. J., Smith, D. R. & Padilla, W. J. Perfect metamaterial absorber. Phys. Rev. Lett. **100**, 207402 (2008).

10. Wang, H. B. & Cheng, Y. J. Frequency selective surface with miniaturized elements based on quarter-mode substrate integrated waveguide cavity with two poles. IEEE Trans. Antennas Propag. **64**, 914–922 (2016).

11. Zhu, B., Zhao, J. & Feng, Y. J. Active impedance metasurface with full 360 deg reflection phase tuning. Sci. Rep. **3**, 3059 (2013).

12. Lipworth, G., Caira, N. W., Larouche, S. & Smith, D. R. Phase and magnitude constrained metasurface holography at W-band frequencies. Opt. Express **24**, 267603 (2016).

13. Pfeiffer, C.; Grbic, A. A printed, broadband Luneburg lens antenna. IEEE Trans. Antennas Propag. **2010**, 58, 3055–3059.

14. Bilal, R.; Baqir, M.; Iftikhar, A.; Ali, M.; Rahim, A.; Akhtar, M.N.; Mughal, M.; Naqvi, S. A Novel Omega Shaped Microwave Absorber with Wideband Negative Refractive Index for C-Band Applications. Optik **2021**, 242, 167278.

15. Kim, I.; Kim, W.-S.; Kim, K.; Ansari, M.A.; Mehmood, M.Q.; Badloe, T.; Kim, Y.; Gwak, J.; Lee, H.; Kim, Y.-K. Holographic meta surface gas sensors for instantaneous visual alarms. Sci. Adv. **2021**, 7, eabe9943.